

AD-A164 468

A THREE-DIMENSIONAL MESOSCALE MODEL FOR THE SIMULATION  
OF CLOUDS PRECIPIT. (U) NATIONAL OCEANIC AND  
ATMOSPHERIC ADMINISTRATION BOULDER CO GE.

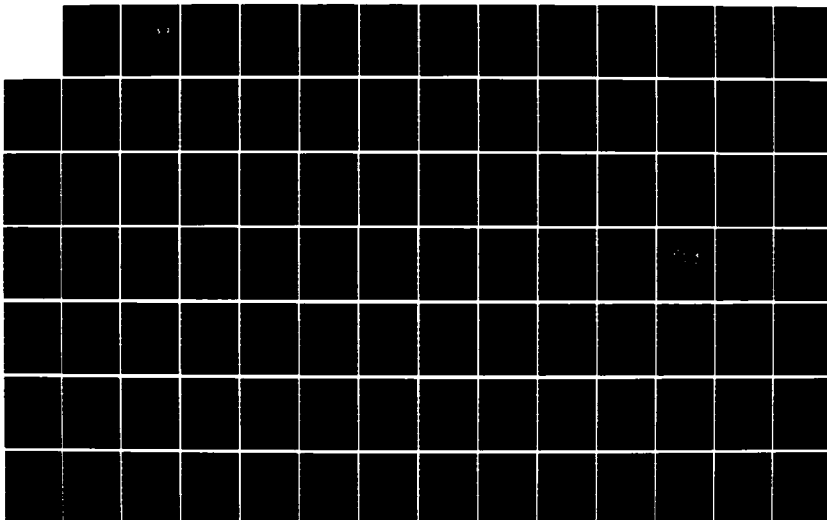
1/2

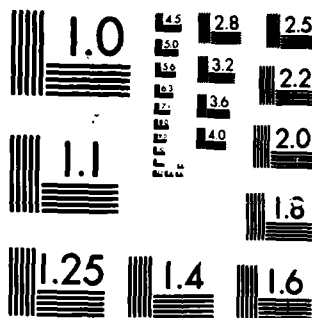
UNCLASSIFIED

E C NICKERSON 31 OCT 85 AFGL-TR-85-8307

F/G 4/2

NL





MICROCOPY RESOLUTION TEST CHART  
NATIONAL BUREAU OF STANDARDS-1963-A

12

AFGL-TR-85-0307

A THREE-DIMENSIONAL MESOSCALE MODEL FOR THE  
SIMULATION OF CLOUDS, PRECIPITATION AND AIRFLOW

Everett C. Nickerson

Geophysical Monitoring for Climatic Change  
Air Resources Laboratory, ERL  
National Oceanic & Atmospheric Administration  
Boulder, Colorado 80303

DTIC  
ELECTE  
FEB 21 1986  
S D  
D

AD-A164 468

31 October 1985

Final Report  
1 October 1983 - 31 September 1985

APPROVED FOR PUBLIC RELEASE; DISTRIBUTION UNLIMITED

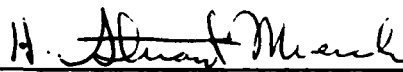
DTIC FILE COPY

AIR FORCE GEOPHYSICS LABORATORY  
AIR FORCE SYSTEMS COMMAND  
UNITED STATES AIR FORCE  
HANSCOM AIR FORCE BASE, MASSACHUSETTS 01731

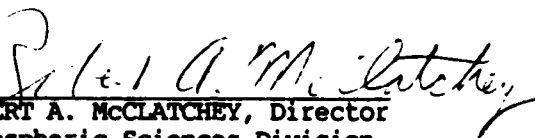
86 2 21 013

This technical report has been reviewed and is approved for publication.

  
\_\_\_\_\_  
GEORGE D. MODICA  
Contract Manager

  
\_\_\_\_\_  
H. STUART MUENCH, Acting Chief  
Atmospheric Prediction Branch

FOR THE COMMANDER

  
\_\_\_\_\_  
ROBERT A. McCLATCHEY, Director  
Atmospheric Sciences Division

This report has been reviewed by the ESD Public Affairs Office (PA) and is releasable to the National Technical Information Service (NTIS).

Qualified requestors may obtain additional copies from the Defense Technical Information Center. All others should apply to the National Technical Information Service.

If your address has changed, or if you wish to be removed from the mailing list, or if the addressee is no longer employed by your organization, please notify AFGL/DAA, Hanscom AFB, MA 01731. This will assist us in maintaining a current mailing list.

AD-A164 468

REPORT DOCUMENTATION PAGE

1a. REPORT SECURITY CLASSIFICATION <b>Unclassified</b>		1b. RESTRICTIVE MARKINGS	
2a. SECURITY CLASSIFICATION AUTHORITY		3. DISTRIBUTION/AVAILABILITY OF REPORT Approved for public release; Distribution unlimited.	
2b. DECLASSIFICATION/DOWNGRADING SCHEDULE		4. PERFORMING ORGANIZATION REPORT NUMBER(S)	
4. PERFORMING ORGANIZATION REPORT NUMBER(S)		5. MONITORING ORGANIZATION REPORT NUMBER(S) AFGL-TR-85-0307	
6a. NAME OF PERFORMING ORGANIZATION Geophysical Monitoring for Climatic Change	6b. OFFICE SYMBOL (If applicable)	7a. NAME OF MONITORING ORGANIZATION Air Force Geophysics Laboratory	
6c. ADDRESS (City, State and ZIP Code) Air Resources Laboratory, ERL National Oceanic & Atmospheric Administration Boulder, Colorado 80303		7b. ADDRESS (City, State and ZIP Code) Hanscom AFB Massachusetts 01731	
8a. NAME OF FUNDING/SPONSORING ORGANIZATION	8b. OFFICE SYMBOL (If applicable)	9. PROCUREMENT INSTRUMENT IDENTIFICATION NUMBER ESD-85-609	
8c. ADDRESS (City, State and ZIP Code)		10. SOURCE OF FUNDING NOS.	
		PROGRAM ELEMENT NO. 62101F	PROJECT NO. 6670
		TASK NO. 10	WORK UNIT NO. BE
11. TITLE (Include Security Classification): A Three-Dimensional Mesoscale Model for the Simulation of Clouds, Precipitation and Airflow			
12. PERSONAL AUTHOR(S) Everett C. Nickerson			
13a. TYPE OF REPORT FINAL REPORT	13b. TIME COVERED FROM 10/1/83 TO 9/31/85	14. DATE OF REPORT (Yr., Mo., Day) 1985 October 31	15. PAGE COUNT 136
16. SUPPLEMENTARY NOTATION			
17. COSATI CODES		18. SUBJECT TERMS (Continue on reverse if necessary and identify by block number)	
FIELD	GROUP	SUB GR.	Numerical weather prediction; > NOAA; Mesoscale models; Atmospheric Clouds; <
			Precipitation;
19. ABSTRACT (Continue on reverse if necessary and identify by block number) A simulation of a heavy rainfall event has been carried out over southern France using 3-D Neph data to initialize a meso-alpha model. That model was subsequently run for a period of three hours and the resulting meteorological fields were then interpolated to a smaller grid to provide balanced initial conditions for a meso-beta model with parameterized microphysics. The meso-beta model is shown to be capable of simulating many features of an orographically forced precipitation event, including the temporal and spatial evolution of liquid water, as well as the number concentration (and hence size distribution) of raindrops. The model is especially suited for the simulation of clouds, precipitation, and airflow over complex terrain.			
20. DISTRIBUTION AVAILABILITY OF ABSTRACT UNCLASSIFIED/UNLIMITED <input checked="" type="checkbox"/> SAME AS RPT <input type="checkbox"/> DTIC USERS <input type="checkbox"/>		21. ABSTRACT SECURITY CLASSIFICATION Unclassified	
22a. NAME OF RESPONSIBLE INDIVIDUAL George Modica		22b. TELEPHONE NUMBER (Include Area Code) (617) 861-2956	22c. OFFICE SYMBOL AFGL/LYP

## TABLE OF CONTENTS

	Page
1. Introduction	1
2. Task I: Real Data Initialization	2
3. Task II: Lateral Boundary Conditions	119
4. Task III: Integration Procedures	120
5. Task IV: Aerosol Model	121
6. Conclusions	122
7. Suggestions for Further Work	123
8. Acknowledgements	124
9. References	124



Accession For	
NTIS CRA&I	<input checked="" type="checkbox"/>
DTIC TAB	<input type="checkbox"/>
Unannounced	<input type="checkbox"/>
Justification	
By _____	
Distribution / _____	
Availability Codes	
Dist	Avail and/or Special
<b>A-1</b>	

## LIST OF ILLUSTRATIONS

<u>FIGURE</u>		<u>PAGE</u>
1.1	Grid area: region of 3-D Neph data. Inset box: model domain for meso-beta simulation. "NW-SE" shows location of cross sections in Figures 1.2 and 1.3	11
1.2	Vertical distribution of cloud along line in Figure 1.1 deduced from 3-D Neph data	12
1.3	Original 3-D Neph data used to construct Figure 1.2	13
2	Meso-beta model terrain shown in Figure 1.1	14
3.1	Initial horizontal wind field for sigma level 13 obtained from meso-alpha simulation. Minimum and maximum values of wind speed are also given	15
3.2	Same as Figure 3.1, but after 1 hour	16
3.3	Same as Figure 3.1, but after 2 hours	17
3.4	Same as Figure 3.1, but after 3 hours	18
3.5	Same as Figure 3.1, but after 4 hours	19
3.6	Same as Figure 3.1, but after 5 hours	20
3.7	Same as Figure 3.1, but after 6 hours	21
4.1	Initial horizontal wind speed corresponding to Figure 3.1	22
4.2	Same as Figure 4.1, but after 1 hour	23
4.3	Same as Figure 4.1, but after 2 hours	24
4.4	Same as Figure 4.1, but after 3 hours	25
4.5	Same as Figure 4.1, but after 4 hours	26
4.6	Same as Figure 4.1, but after 5 hours	27
4.7	Same as Figure 4.1, but after 6 hours	28
5.1	Vertical velocity for level 13 after 1 hour	29
5.2	Vertical velocity for level 13 after 2 hours	30

<u>FIGURE</u>		<u>PAGE</u>
5.3	Vertical velocity for level 13 after 3 hours	31
5.4	Vertical velocity for level 13 after 4 hours	32
5.5	Vertical velocity for level 13 after 5 hours	33
5.6	Vertical velocity for level 13 after 6 hours	34
6.1	Initial vertically integrated cloud water	35
6.2	Vertically integrated cloud water after 1 hour	36
6.3	Vertically integrated cloud water after 2 hours	37
6.4	Vertically integrated cloud water after 3 hours	38
6.5	Vertically integrated cloud water after 4 hours	39
6.6	Vertically integrated cloud water after 5 hours	40
6.7	Vertically integrated cloud water after 6 hours	41
7.1	Initial cloud water mixing ratio for level 13	42
7.2	Cloud water mixing ratio for level 13 after 1 hour	43
7.3	Cloud water mixing ratio for level 13 after 2 hours	44
7.4	Cloud water mixing ratio for level 13 after 3 hours	45
7.5	Cloud water mixing ratio for level 13 after 4 hours	46
7.6	Cloud water mixing ratio for level 13 after 5 hours	47
7.7	Cloud water mixing ratio for level 13 after 6 hours	48
8.1	Rain water mixing ratio for level 13 after 1 hour	49
8.2	Rain water mixing ratio for level 13 after 2 hours	50
8.3	Rain water mixing ratio for level 13 after 3 hours	51
8.4	Rain water mixing ratio for level 13 after 4 hours	52
8.5	Rain water mixing ratio for level 13 after 5 hours	53
8.6	Rain water mixing ratio for level 13 after 6 hours	54



<u>FIGURE</u>		<u>PAGE</u>
9.1	Forecast rainfall after 1 hour	55
9.2	Forecast rainfall after 2 hours	56
9.3	Forecast rainfall after 3 hours	57
9.4	Forecast rainfall after 4 hours	58
9.5	Forecast rainfall after 5 hours	59
9.6	Forecast rainfall after 6 hours	60
10.1	Surface pressure after 4 hours	61
10.2	Surface pressure after 5 hours	62
10.3	Surface pressure after 6 hours	63
11.1	West-East vertical cross section of U, 170 km from Southern boundary at time 0	64
11.2	Same as Figure 11.1, but after 1 hour	65
11.3	Same as Figure 11.1, but after 2 hours	66
11.4	Same as Figure 11.1, but after 3 hours	67
11.5	Same as Figure 11.1, but after 4 hours	68
11.6	Same as Figure 11.1, but after 5 hours	69
11.7	Same as Figure 11.1, but after 6 hours	70
12.1	West-East vertical cross section of V, 170 km from southern boundary at time 0	71
12.2	Same as Figure 12.1, but after 1 hour	72
12.3	Same as Figure 12.1, but after 2 hours	73
12.4	Same as Figure 12.1, but after 3 hours	74
12.5	Same as Figure 12.1, but after 4 hours	75
12.6	Same as Figure 12.1, but after 5 hours	76
12.7	Same as Figure 12.1, but after 6 hours	77

<u>FIGURE</u>		<u>PAGE</u>
13.1	West-East vertical boundary section of W, 170 km from southern boundary after 1 hour	78
13.2	Same as Figure 13.1, but after 2 hours	79
13.3	Same as Figure 13.1, but after 3 hours	80
13.4	Same as Figure 13.1, but after 4 hours	81
13.5	Same as Figure 13.1, but after 5 hours	82
13.6	Same as Figure 13.1, but after 6 hours	83
14.1	West-East vertical cross section of cloud water mixing ratio, 170 km from southern boundary at time 0	84
14.2	Same as Figure 14.1, but after 1 hour	85
14.3	Same as Figure 14.1, but after 2 hours	86
14.4	Same as Figure 14.1, but after 3 hours	87
14.5	Same as Figure 14.1, but after 4 hours	88
14.6	Same as Figure 14.1, but after 5 hours	89
14.7	Same as Figure 14.1, but after 6 hours	90
15.1	West-East vertical cross section of rain water mixing ratio, 170 km from southern boundary after 1 hour	91
15.2	Same as Figure 15.1, but after 2 hours	92
15.3	Same as Figure 15.1, but after 3 hours	93
15.4	Same as Figure 15.1, but after 4 hours	94
15.5	Same as Figure 15.1, but after 5 hours	95
15.6	Same as Figure 15.1, but after 6 hours	96
16.1	West-East vertical cross section of rain concentration, 170 km from southern boundary after 1 hour	97
16.2	Same as Figure 16.1, but after 2 hours	98
16.3	Same as Figure 16.1, but after 3 hours	99
16.4	Same as Figure 16.1, but after 4 hours	100
16.5	Same as Figure 16.1, but after 5 hours	101
16.6	Same as Figure 16.1, but after 6 hours	102

<u>FIGURE</u>		<u>PAGE</u>
17.1	West-East vertical cross section of U, 100 km from southern boundary after 3 hours	103
17.2	Same as Figure 17.1, but for V	104
17.3	Same as Figure 17.1, but for cloud water mixing ratio	105
17.4	Same as Figure 17.1, but for rain water mixing ratio	106
18.1	West-East vertical cross section of U, 150 km from southern boundary after 3 hours	107
18.2	Same as Figure 18.1, but for V	108
18.3	Same as Figure 18.1, but for cloud water mixing ratio	109
18.4	Same as Figure 18.1, but for rain water mixing ratio	110
19.1	West-East vertical cross section of U, 200 km from southern boundary after 3 hours	111
19.2	Same as Figure 19.1, but for V	112
19.3	Same as Figure 19.1, but for cloud water mixing ratio	113
19.4	Same as Figure 19.1, but for rain water mixing ratio	114

LIST OF TABLES

<u>TABLE</u>		<u>PAGE</u>
1	Program Flow Chart for the Medal Initialization Procedure	115
2	Contents of Tape Number 9245	116
3	Contents of Tape Number 9223	117
4	Contents of LANL Tape	117
5	Initial Large-Scale Sounding	118

## 1. INTRODUCTION

This presentation constitutes the final report to the Air Force Geophysical Laboratory, LYP under Contract No. ESD 85-609. In this report we present a description of the three-dimensional NOAA/LAMP mesoscale prediction model which contains explicit predictions of the evolving fields of cloud and rain water. We show some examples of numerical simulations made using the model, and discuss the success and limitations of the present version. We then outline the status of other efforts designed to overcome deficiencies in the model. The organization of this report will follow the task structure contained in the original proposal.

During the course of the work carried out in cooperation with the AFGL, there were several concurrent developments which served to significantly advance the mesoscale modeling program. The first of these events was the completion of a thesis by D. Medal (1985), which takes standard surface and upper air observations, interpolates them to a uniform grid, and then uses those data to initialize a three-dimensional, time-dependent meso-alpha model with a 40 kilometer mesh size covering an area 1600 kilometers on a side. This model is then run for a period of 3 hours to provide initial conditions for a meso-beta model with a 10 kilometer grid size covering an area 250 kilometers on a side. The thesis thus contains a real data initialization procedure and a comparison of model-predicted rainfall with observed data from a severe precipitation event in the south of France.

The main contribution of Medal's thesis was the development of a complete set of procedures to initialize the model of Nickerson and Richard (1981) with real data. A second and concurrent development consisted of the implementation of a new time integration procedure, the incorporation of an upper wave absorbing layer, and the testing of improved lateral boundary

conditions. There is now a new version of the model (Nickerson, et al., 1986) which will replace the version of the meso-beta model used by Medal.

The nine-track magnetic tapes whose contents are described in Tables 2-4 have already been delivered to AFGL, together with a copy of Medal's thesis, an English translation of a part of that thesis, and a listing (in Fortran) of all the programs in Medal's code. The model was installed at the computing center at Los Alamos National Laboratory and required little in the way of modification to the existing code. All of the subroutines were run and the output then compared with the calculations carried out in France. Installing the model code at AFGL should only require a change in the I/O procedures.

## 2. TASK I: Real Data Initialization

A systematic investigation of a heavy rainfall event has been carried out in order to compare model predictions with observations. A thesis by Medal (1985) contains a detailed description of a procedure which uses standard radiosonde and surface observations to generate a balanced set of initial conditions on a regular grid suitable for initializing the meso-alpha version of the meteorological prediction model. The meso-alpha model is similar to the meso-beta model, except that the equations are modified to include a map factor, and the precipitation processes have been eliminated. The model has been integrated over a  $41 \times 41$  horizontal grid using a grid length of 40 kilometers. There are 15 vertical levels in both the meso-alpha and meso-beta versions of the model. An English translation of the introductory section is included with Medal's thesis submitted as part of this final report.

The area under investigation is a mountainous region in the Cevennes, a part of France's Massif Central where an extensive rain-gauge network has been

installed in order to provide warnings of flash flooding. This region has historically been subjected to heavy rainfall events with attendant loss of life and extensive property damage. Hourly rainfall data are available to provide not only an evaluation of the total rainfall predicted by the model, but also to provide some insight on the ability of the model to depict the temporal evolution of the storm.

The following two paragraphs contain a translation of the conclusions from Medal's thesis:

The rainfall episodes in the Cevennes are characterized by a transgression of hot and humid Mediterranean air. The synoptic configuration and the orographic effects seem to be the main ingredients giving rise to rainfall; this was the case on 29 August 1976, a period we have chosen to simulate. For this purpose, we have developed and tested different initialization procedures for the Nickerson and Richard model (1981). The procedure of dynamic adaptation of the meteorological fields to the sub-synoptic scale, followed by a spatial nesting of the mesoscale model, produced the most encouraging results: the rainfall field calculated in this manner displays a spatial distribution which corresponds to the observations. As far as the simulated quantities are concerned, they appear to be underestimated.

Following various tests, the rainfall calculation appeared to be particularly sensitive to the initialization of the mass field, especially temperature and humidity.

Perky (1979) had already stressed the influence of these two fields on the amount of simulated rainfall. Anthes and Haagensen (1983) have explained, during the simulation of catastrophic rainfall in Sichuan (July 12-15, 1979) the deficit of calculated versus observed rainfall by an underevaluation of the initial humidity field (Nickerson et al., 1984). Our own conclusions confirm these results on a smaller scale (10 km). The temperature and humidity fields sensitive to local factors have characteristic scales which are probably not very well represented by the mesh of the available recording network. In order to increase the resolution of these initial fields in the surface layer, a possible solution consists of introducing the climatological network data (pressure, temperature, humidity) in the initialization procedure on numerical models. This is the subject of Appendix III which remains to be applied.

Medal's code has been installed and run on a Cray 1 at Los Alamos National Laboratory. Table 1 contains a simplified flow chart showing the organization of the twelve separate programs. A listing of each program, together with a translation of the comment lines is included with this report. The codes are written in modular form, and should be easily adapted to any machine having a Fortran compiler. Other than minor modifications required by a different operating system, it was not difficult to make the codes operational on the Los Alamos computing system. Magnetic tape numbers 9245 and 9223 contain the original codes and sample output from Medal's thesis. The third tape contains the codes modified to run at Los Alamos. The contents of all three tapes are given in Tables 2-4.



During the period 6-9 November 1982, the Cevennes was once again visited by an exceptionally severe storm, with heavy rains accompanied by surface winds in excess of 50 m/sec. Captain D. V. Ridge of AFGL provided us with 3-D Neph data for the period enabling us to construct cloud cross-sections through the region. Figure 1.1 shows the location of the 3-D Neph gridded data (the larger grid), and also the inset grid showing the domain covered by the meso-beta model. The line labeled NW - SE indicates the location of the schematic vertical cloud cross section shown in Figure 1.2. Figure 1.3 shows the original working drawing, together with the hand-written data garnered from the 3-D Neph data. Of particular interest is the vertical extent of the cloud and the presence of rainfall upwind of the mountain barrier indicated by a surface present weather code of "6."

Originally it was our intention to directly utilize the satellite data to initialize the meso-beta moisture fields in the manner described in an earlier quarterly progress report. However, experience gained from Medal's thesis led us to conclude that without a proper balance and initialization of the mass and momentum fields, the addition of satellite data would do little to improve the forecast. We, therefore, decided to use a radiosonde located in the southeast of France (43.5°N, 5°E) together with cloud data constructed from 12 satellite derived cross-sections similar to Figure 1.2 to initialize the meso-alpha model.

The meso-alpha model was initialized with a single sounding corresponding to 1200 GMT on 11 November 1982 and run for a period of 3 hours. Medal's interpolation program was then used to construct an initial data field for the meso-beta model, which was subsequently run for a period of 6 hours. The following section describes the results of the numerical simulation.

## 2.1 Model simulation of 7 November 1982

The initial soundings of temperature, vapor mixing ratio, cloud water, and wind are given in Table 5. In order to determine the structure of the cloud system over the meso-beta domain, 12 vertical cross sections were constructed using the 3-D Neph data. These showed that cloud bases were at approximately 500 meters, and that cloud tops were generally 5000 meters, except over the higher mountain elevations where tops were at approximately 12000 meters.

Two runs were made with the meso-alpha model ( $dx = 40$  km). In the first simulation the cloud water mixing ratio was set to 2.0 g/kgm in the height range from 500 to 5,000 meters. However, when the surface elevation was more than 1000 meters, the initial cloud extended to a height of 12,000 meters. For heights between 5,000 and 12,000 meters, the cloud water mixing ratio was set to 1.0 g/kgm. Whenever cloud water was initially present in the model, the vapor mixing ratio was set to the saturated value at that temperature. A second control run was then made in which everywhere in the model the cloud water mixing ratio was set to zero.

A comparison of the two simulations showed that after a period of 3 hours of model integration, the two simulations were essentially identical. That is, the presence of cloud water at the start of the simulation had little influence on the final predicted values.

The model terrain used in the meso-beta calculation is shown in Figure 2, and is the same found in the thesis by Medal. Surface elevations vary from sea level to a height of 1,700 meters. The Rhone valley separates the Cevennes in the northwest from the Alps in the east.

Figures 3.1 through 3.7 show the evolution of the wind field at level 13 during the course of the 6-hour simulation. One must remember that the model

makes use of a terrain-following coordinate system and that this, therefore, represents the flow on a surface which varies with altitude. Also, the terrain used in the meso-beta simulation with 10 kilometer grid resolution is not the same as that used in the meso-alpha simulation with a 40 kilometer grid resolution. It takes several hours, therefore, for the airflow to reach a quasi-steady state adjustment to the new underlying terrain. Horizontal plots of wind speed at the same level (Figures 4.1 through 4.7) show that the average speed changes very slowly at the end of the 6-hour period of integration. The adjustment of the horizontal wind field to a quasi-steady state is also evident in the plots of vertical velocity at level 13 shown in Figures 5.1 through 5.6.

The initial cloud field entirely covers the model domain. However, Figures 6.1 through 6.7 show that the higher clouds are located over the Cevennes and the Alps, in remarkable agreement with the conditions reported in the 3-D Neph data. Nevertheless, during the course of the meso-beta simulation, the vertical extent of the clouds decreases substantially.

Figures 7.1 through 7.7 show the cloud water mixing ratio at level 13. There is a very rapid adjustment in the cloud field giving way to maximum values of cloud water of approximately 0.3 g/kgm. It should be recalled that the meso-alpha model does not contain any mechanism for a conversion of cloud water to rain water, and that by the end of the simulation it produces large amounts of cloud water. During the first hour of the meso-beta simulation, rain drops formed and grew very quickly, thereby depleting the initial cloud water. The corresponding plots of rain-water mixing ratio are shown in Figures 8.1 through 8.6. The average grid point value decreases from .84 to .29 g/kgm during the first hour and then decreases at a much slower rate. One especially encouraging aspect of this simulation is that clouds and

precipitation are produced over the relatively flat terrain upwind of the major terrain forcing. Previous runs with the meso-beta model using a single sounding initialization procedure yielded only orographically forced clouds over the elevated terrain.

In some locations, observed precipitation rates amounted to nearly 10 mm/hr for the 3-day storm. Maximum precipitation rates predicted by the model were in excess of 7.5 mm/hr, although a detailed analysis of the observed rainfall is not available for inclusion in this report. The 3-D Neph data indicated a present weather code of "6" over most of the model domain, thereby indicating the presence of rain and lending support for the general rainy conditions in the numerical simulation (Figures 9.1 through 9.6).

One of the major problems experienced by AFGL users of the meso-beta model has been the appearance of significant noise in the pressure field. Figures 10.1 through 10.3 show the surface pressure during the last 3 hours of the simulation. It is seen that they essentially mirror the terrain shown in Figure 2, and do not give any indication of pronounced oscillations at the boundaries.

In order to examine the three-dimensional structure of the simulation, we now show several vertical cross sections. Figures 11.1 through 11.7 show the "U" component of the horizontal wind, and Figures 12.1 through 12.7 the "V" component along a west-east cross section at a distance of 170 kilometers from the southern boundary. These figures confirm that the winds at upper levels also reach a quasi-steady state by the end of the period of integration. The same also holds for the vertical velocity shown in Figures 13.1 through 13.6, although the zero-contour line shows more variability.

The previously mentioned large initial values of cloud water coupled with zero rain water lead to a rapid change in the cloud water mixing ratio as

shown in Figures 14.1 through 14.7. It takes approximately 1 hour for the clouds to reach a state which subsequently changes by rather small amounts. It should be kept in mind, however, that the smallest contour is 0.1 g/kgm, and that the actual cloud boundaries extend beyond that shown by the 0.1 contour.

The evolution of the rain water mixing ratio shown in Figures 15.1 through 15.6 provides further evidence of the microphysical chain of events. Whereas the rain water was initially zero, at the end of 1 hour the maximum value is in excess of 3.0 g/kgm. Here again the minimum contour value is 0.1 g/kgm, and the extent of the rain "cloud" is actually larger than that shown by the 0.1 contour. The persistence of the tall cloud along the eastern boundary where the model domain extends to the Alps is probably due in part to the constancy of the thermodynamic variables on the inflow boundary. The relatively small values of rain-drop concentration obtained during the initial phase of the simulation are due to the unrealistic initialization of the cloud and rain parameters (Figures 16.1 through 16.6). The initial cloud field resulted in an almost explosive growth of large rain drops during the first few minutes, followed by a change to a more normal growth regime.

Figures 17 through 19 show selected vertical cross sections after 3 hours of model time for distances of 100 km, 150 km, and 200km from the southern boundary. Figure 17.4 is especially noteworthy in that it shows the presence of rain at the low elevations of the Rhone Valley at this cross section 100 km from the southern boundary.

There will likely be a follow-up simulation of this storm by the modeling group in Clermont-Ferrand, France, where they are attempting to improve the initialization procedure for mass and momentum in order to more accurately relate the satellite-observed moisture fields and the initial model

parameters. The determination of vertical-velocity fields which are consistent with the cloud fields, seems especially important. Any forthcoming reports on this subject by the Laboratoire Associé de Météorologie Physique (LAMP) in Clermont-Ferrand will be forwarded to AFGL.

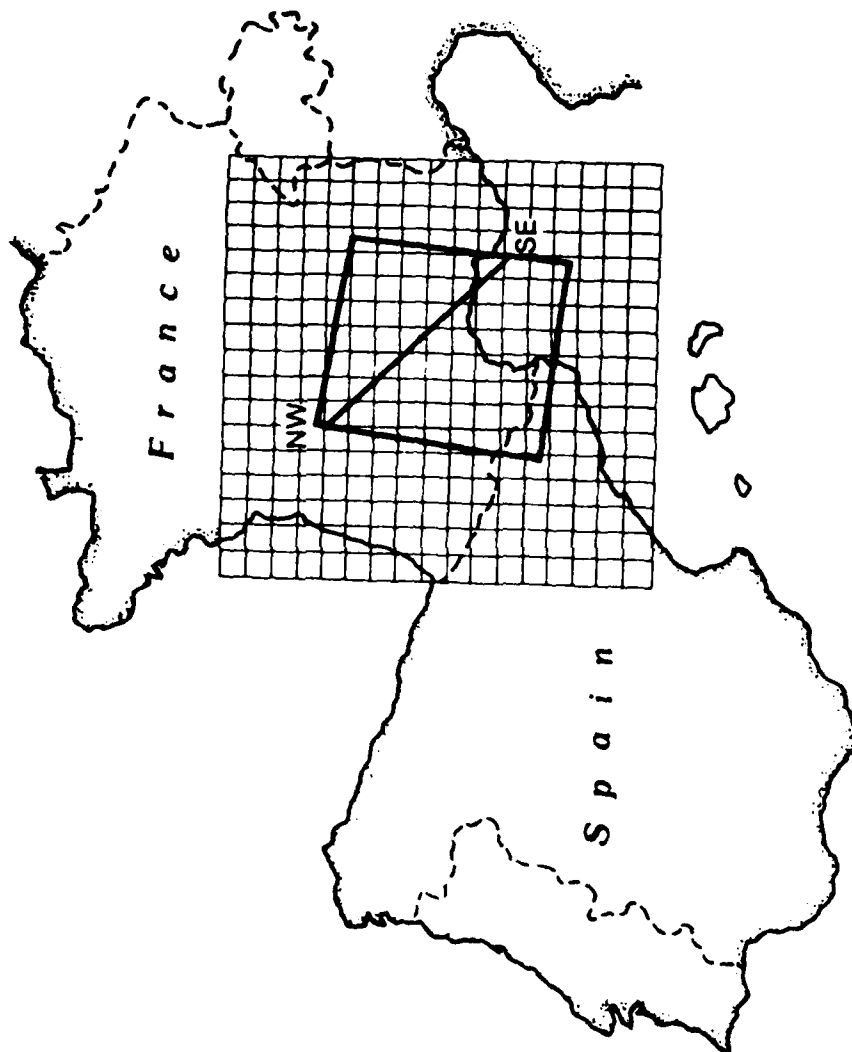


Figure 1.1

The grid area represents the region of 3-D Neph data. The inset box is the model domain for the meso-beta simulation, and the line "NW-SE" shows the location of cross sections in Figures 1.2 and 1.3.

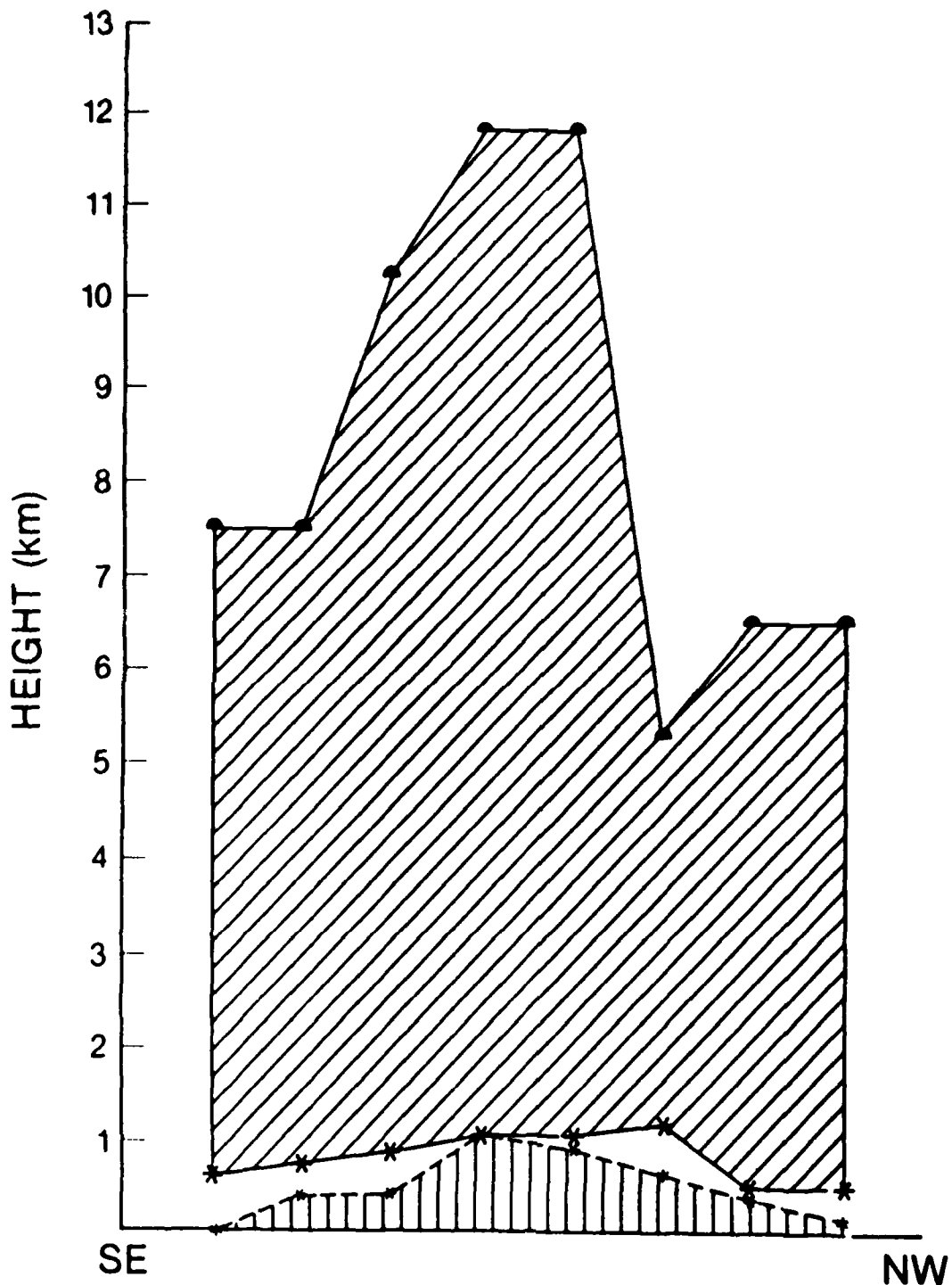
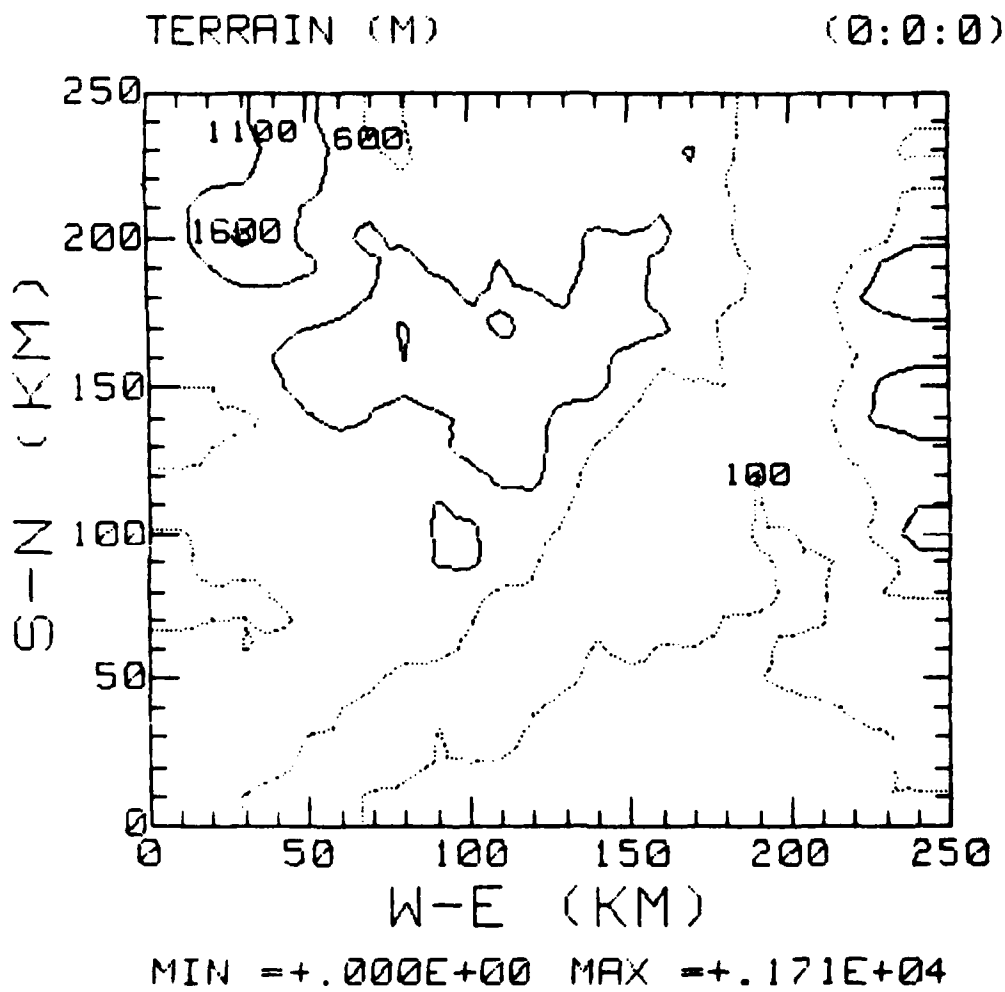


Figure 1.2

Vertical distribution of cloud along line in Figure 1.1 deduced from 3-D Neph data. (Note that the orientation of this figure is SE-NW.)





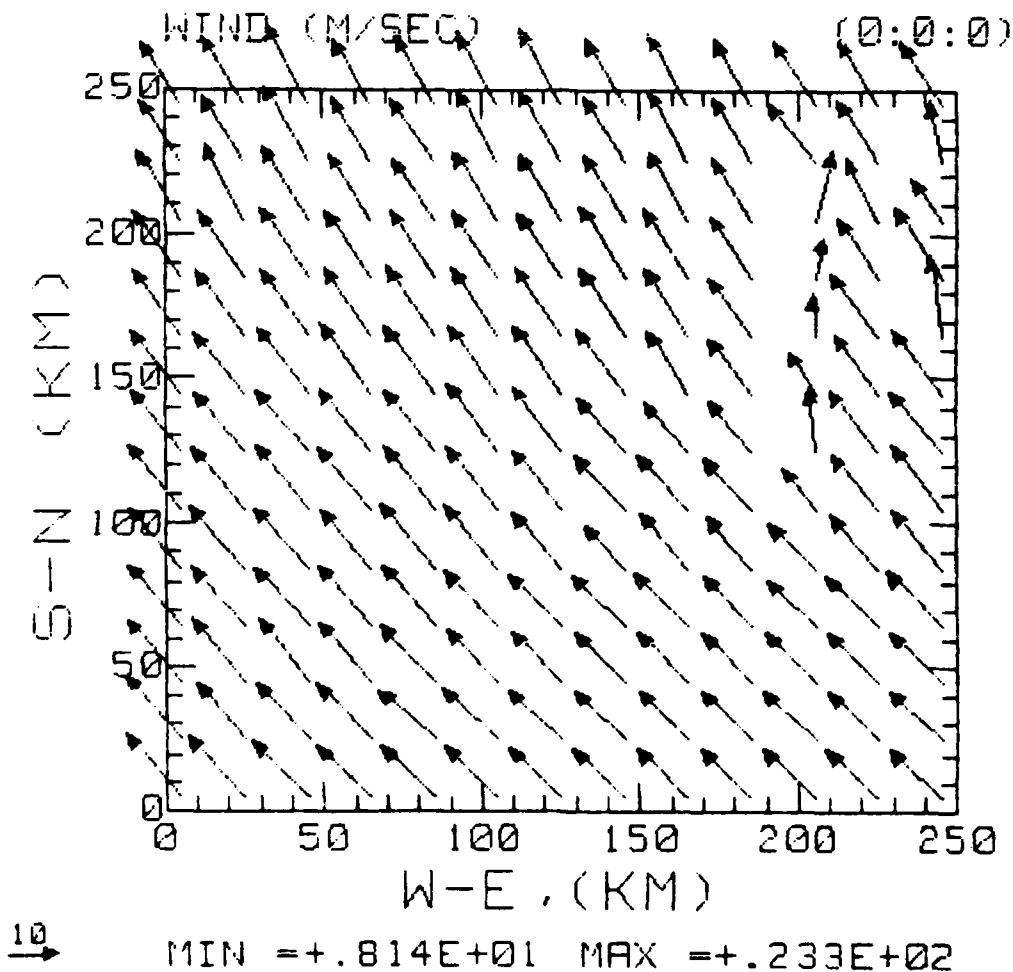


MAX =	1712.5523	XMAX =	30	YMAX =	200
MIN =	0	XMIN =	170	YMIN =	0
AVERAGE VALUE =	654.388040533				

Figure 2  
Meso-beta model terrain shown in Figure 1.1.

DATE= 15 Oct 1985 TIME= 11:53:40

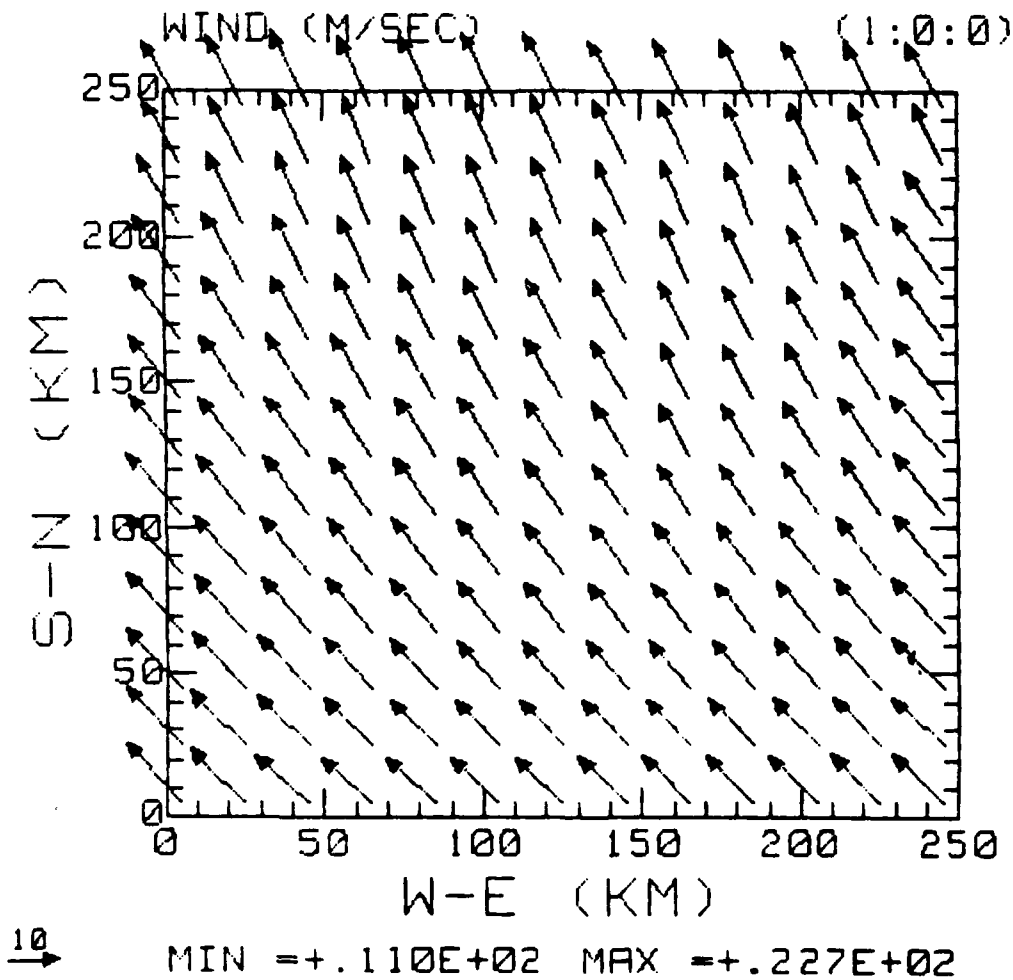
PLOTTING ON A SIGMA SURFACE= 13



MAX=	23.3237896655	XMAX=	50	YMAX=	250
MIN=	8.1372182452	XMIN=	210	YMIN=	190
AVERAGE VALUE=	19.236852895				

Figure 3.1  
Initial horizontal wind field for sigma level 13  
obtained from meso-alpha simulation. Minimum and  
maximum values of wind speed are also given.

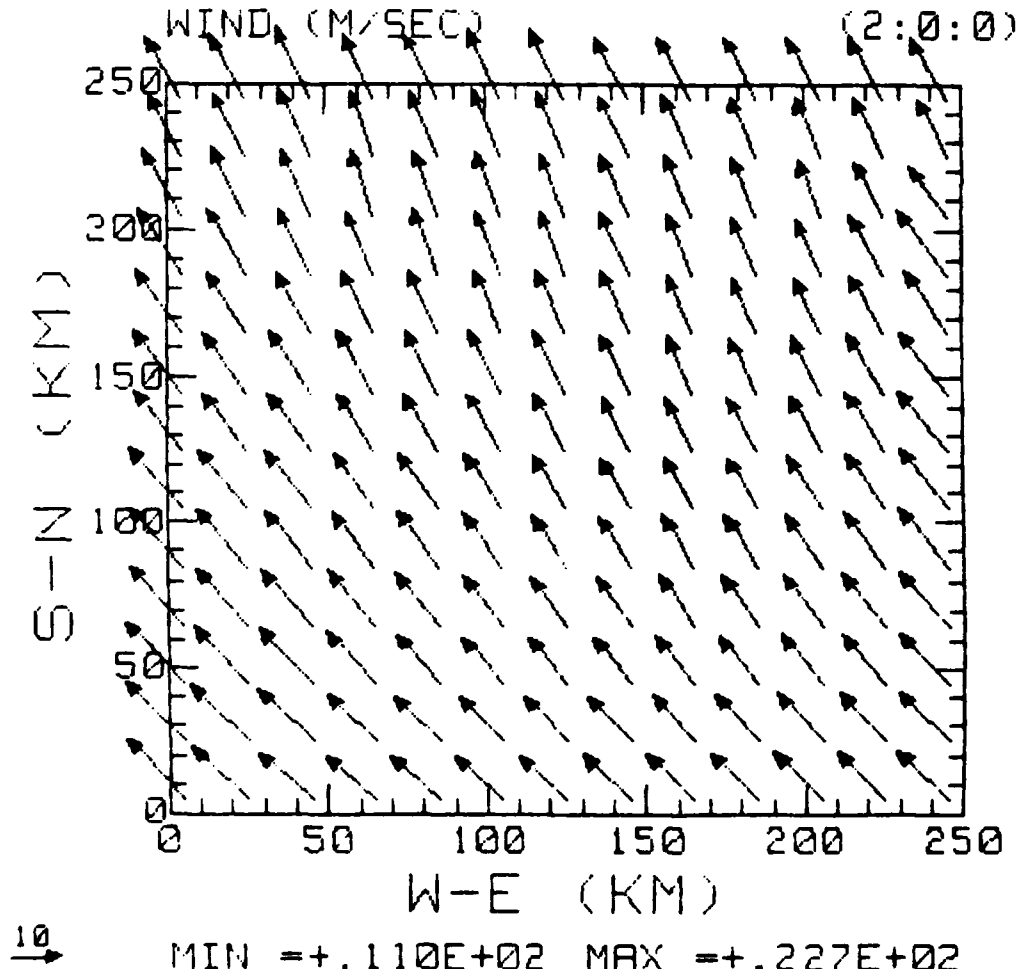
PLOTTING ON A SIGMA SURFACE= 13



MAX=	22.7133428627	XMAX=	260	YMAX=	190
MIN=	10.9635811686	XMIN=	260	YMIN=	210
AVERAGE VALUE=	17.241867686				

Figure 3.2  
Same as Figure 3.1 but after 1 hour.

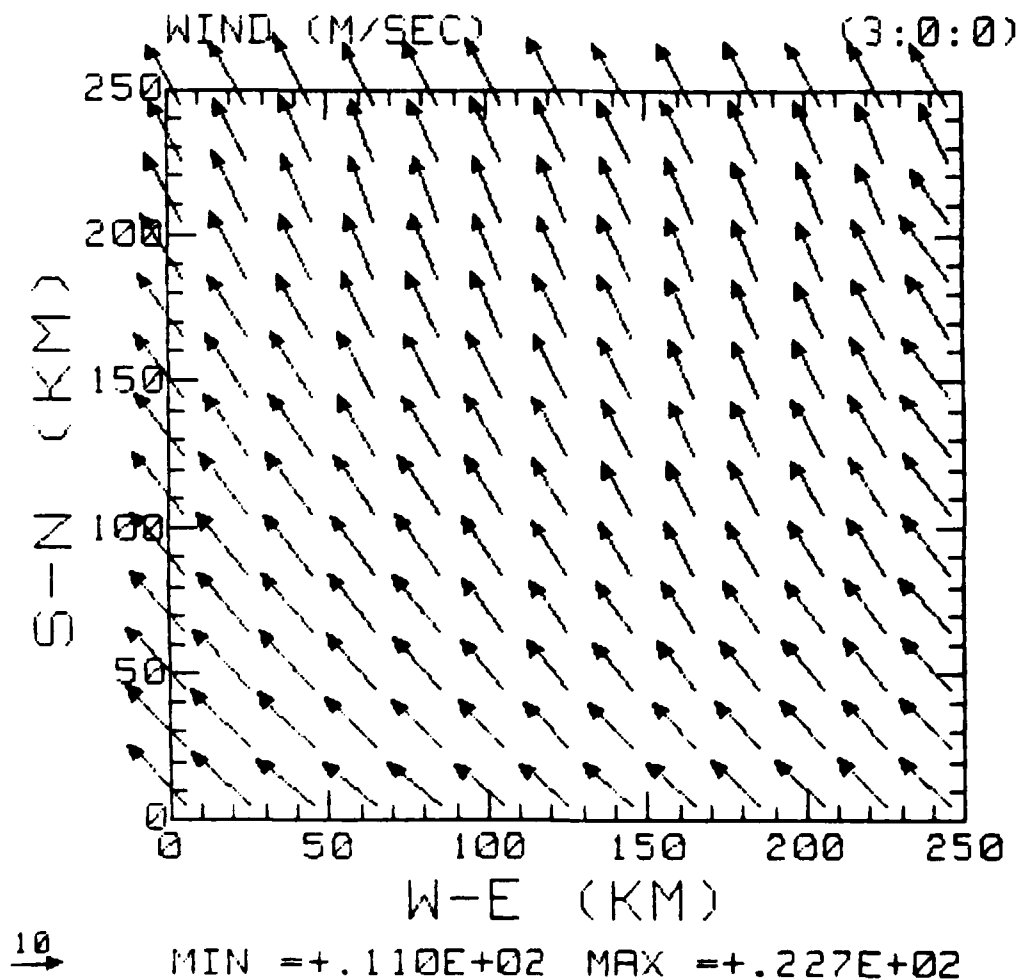
PLOTTING ON A SIGMA SURFACE= 13



MAX=	22.7133428627	XMAX=	260	YMAX=	190
MIN=	10.9635811686	XMIN=	260	YMIN=	210
AVERAGE VALUE=	10.9150691854				

Figure 3.3  
Same as Figure 3.1 but after 2 hours.

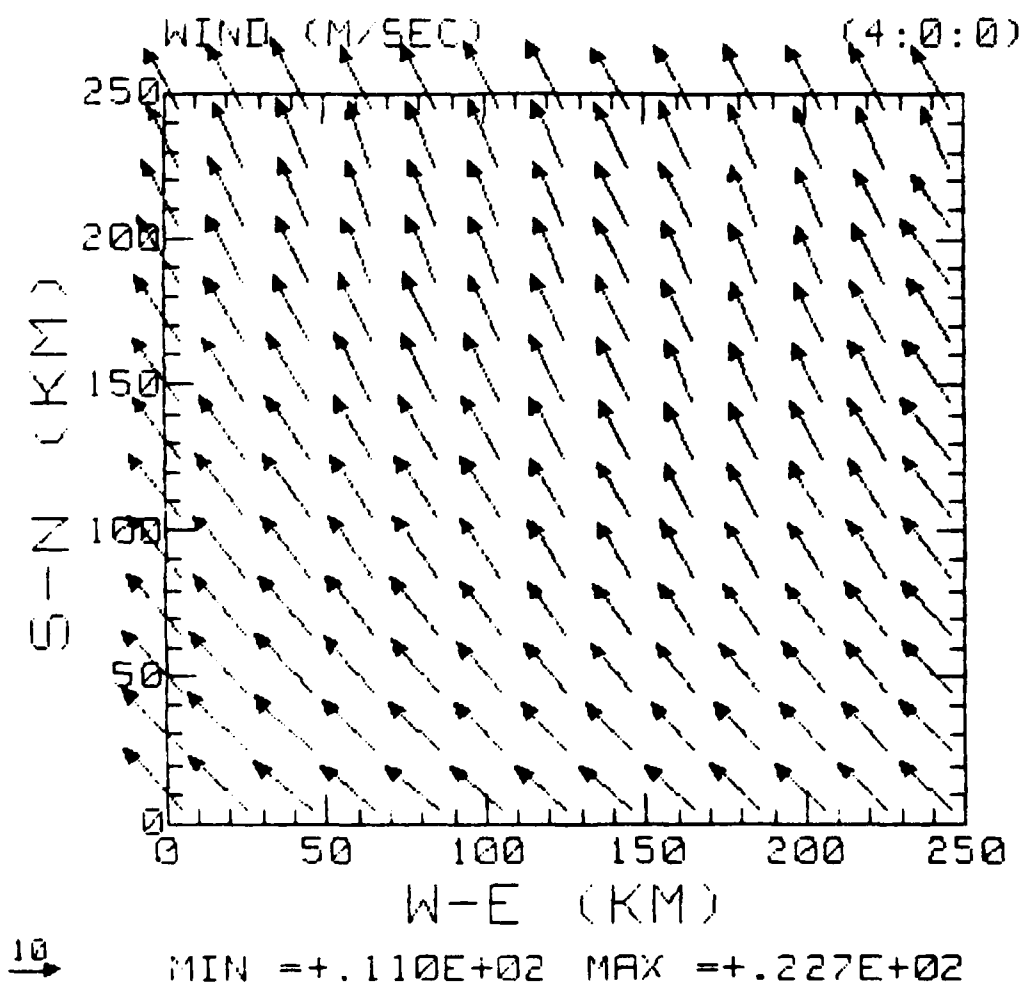
PLOTTING ON A SIGMA SURFACE= 13



MAX=	22.7133428627	XMAX=	260	YMAX=	190
MIN=	10.9635811686	XMIN=	260	YMIN=	210
AVERAGE VALUE=	17.1123498545				

Figure 3.4  
Same as Figure 3.1 but after 3 hours.

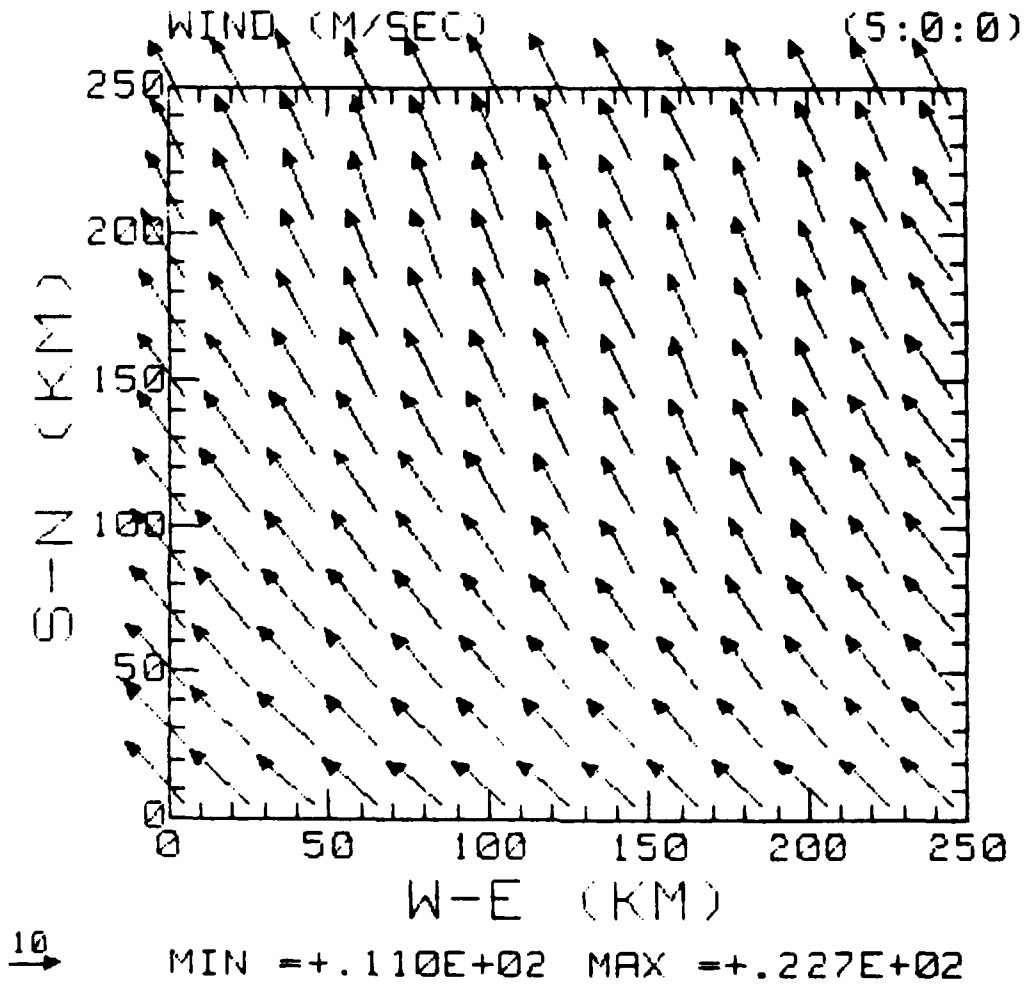
PLOTTING ON A SIGMA SURFACE= 13



MAX=	22.7133428627	XMAX=	260	YMAX=	190
MIN=	10.9635811686	XMIN=	260	YMIN=	210
AVERAGE VALUE=	17.401018989				

Figure 3.5  
Same as Figure 3.1 but after 4 hours.

PLOTTING ON A SIGMA SURFACE= 13

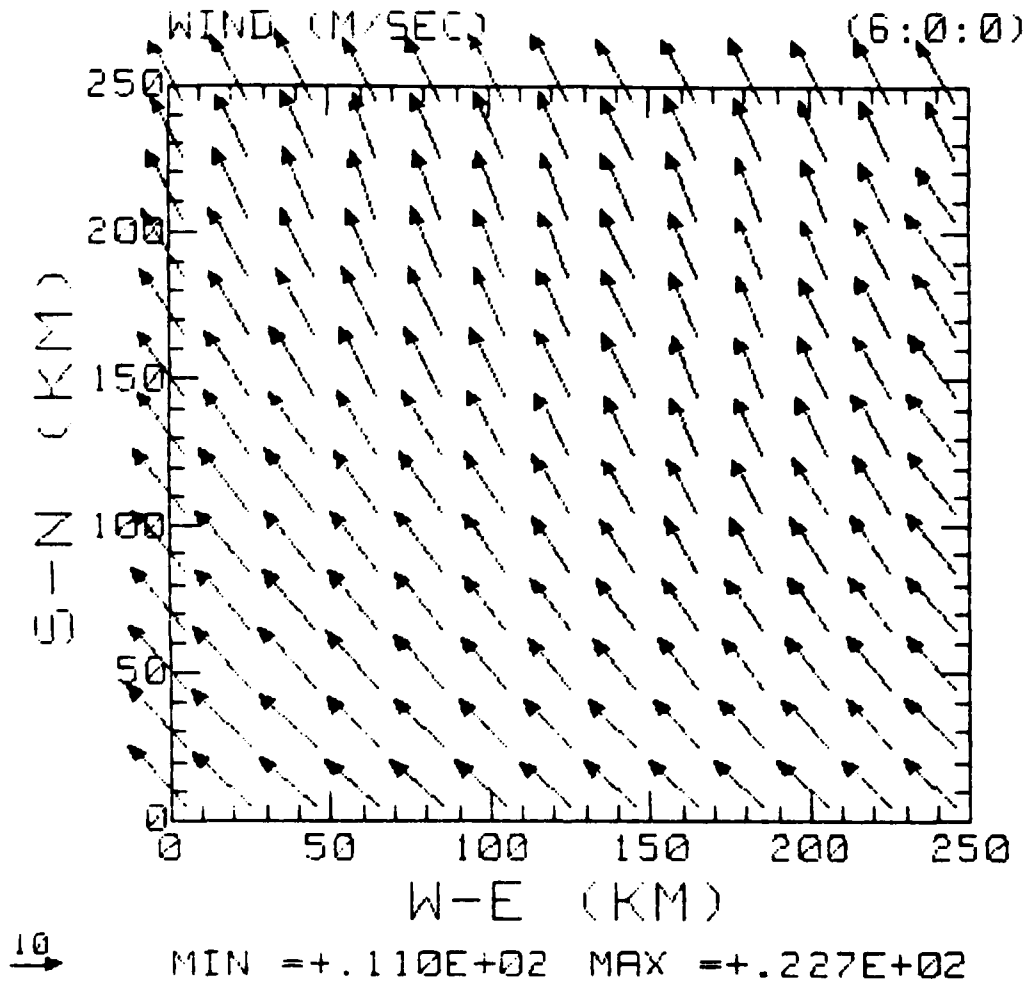


MAX=	22.7133428627	XMAX=	260	YMAX=	190
MIN=	10.9635811686	XMIN=	260	YMIN=	210
AVERAGE VALUE=	17.5464660933				

Figure 3.6  
Same as Figure 3.1 but after 5 hours.

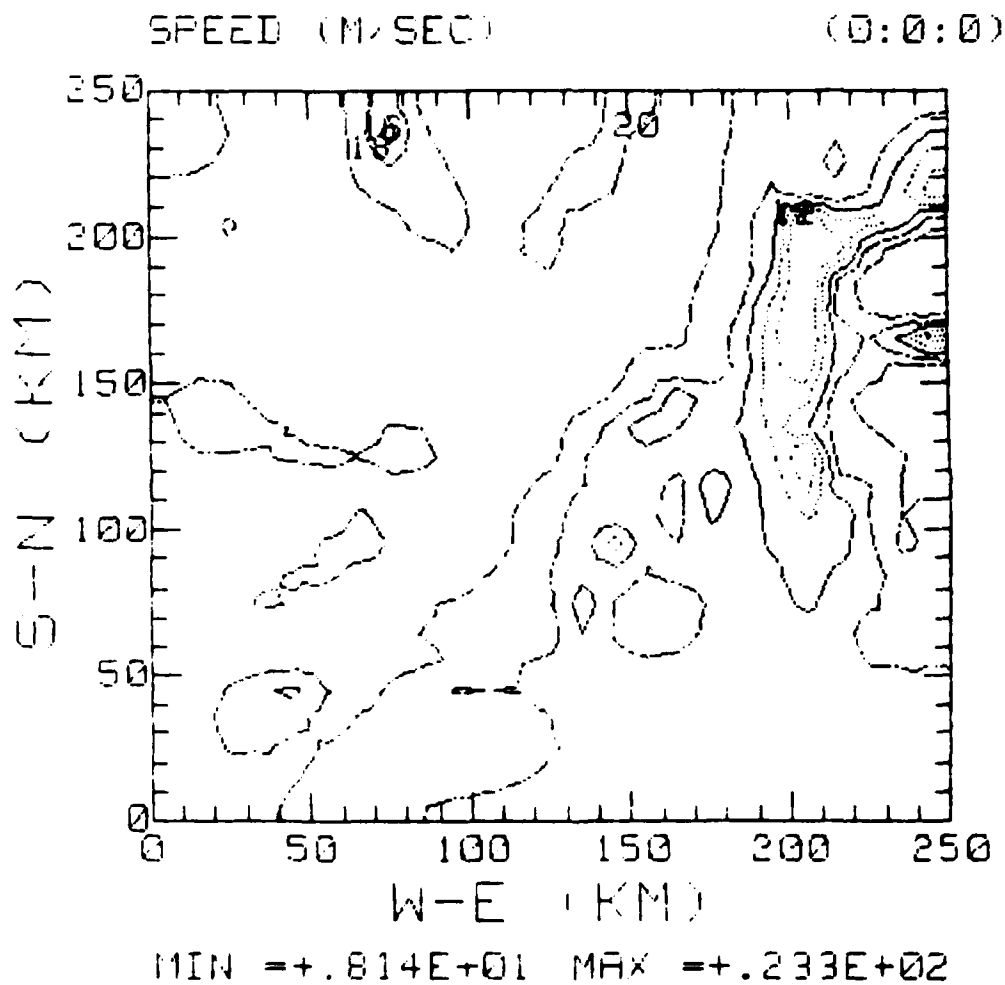


PLOTTING ON A SIGMA SURFACE= 13



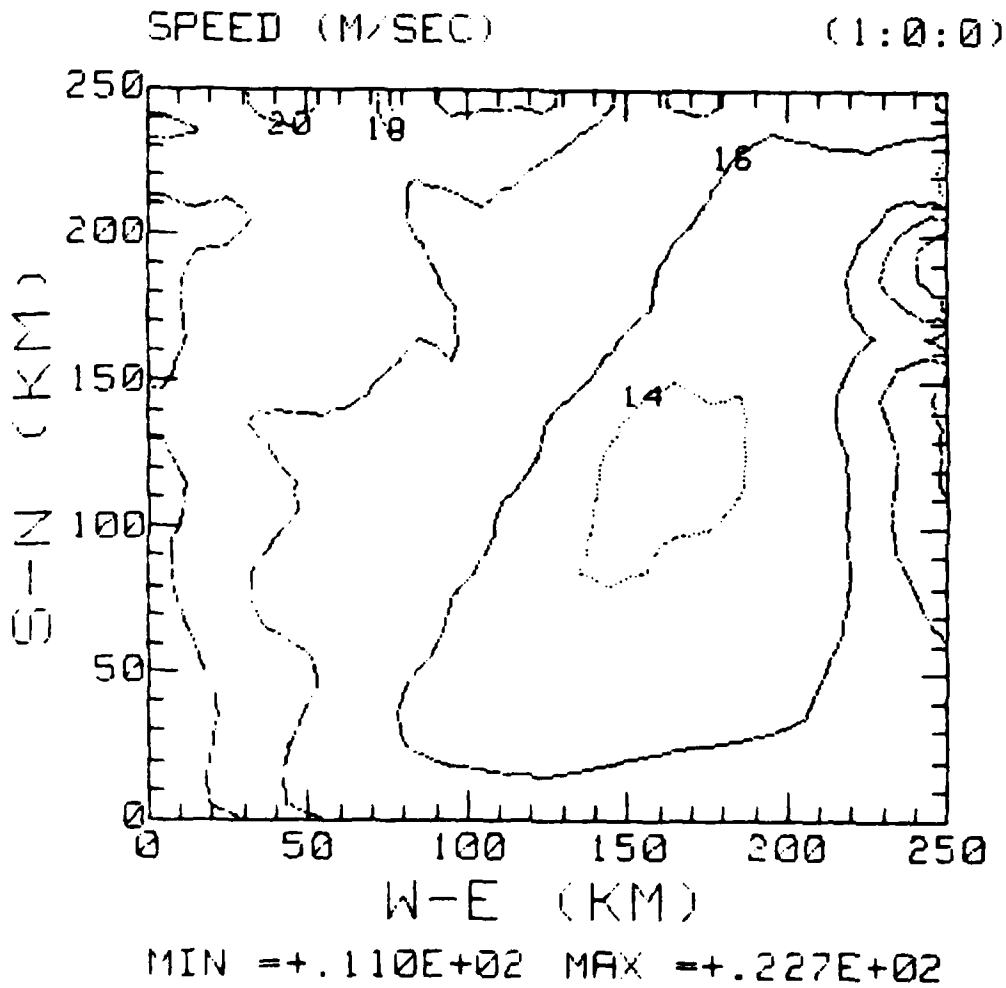
MAX=	22 7133420627	XMAX=	260	YMAX=	190
MIN=	10 9635811686	XMIN=	260	YMIN=	210
AVERAGE VALUE=	17 5698002727				

Figure 3.7  
Same as Figure 3.1 but after 6 hours.



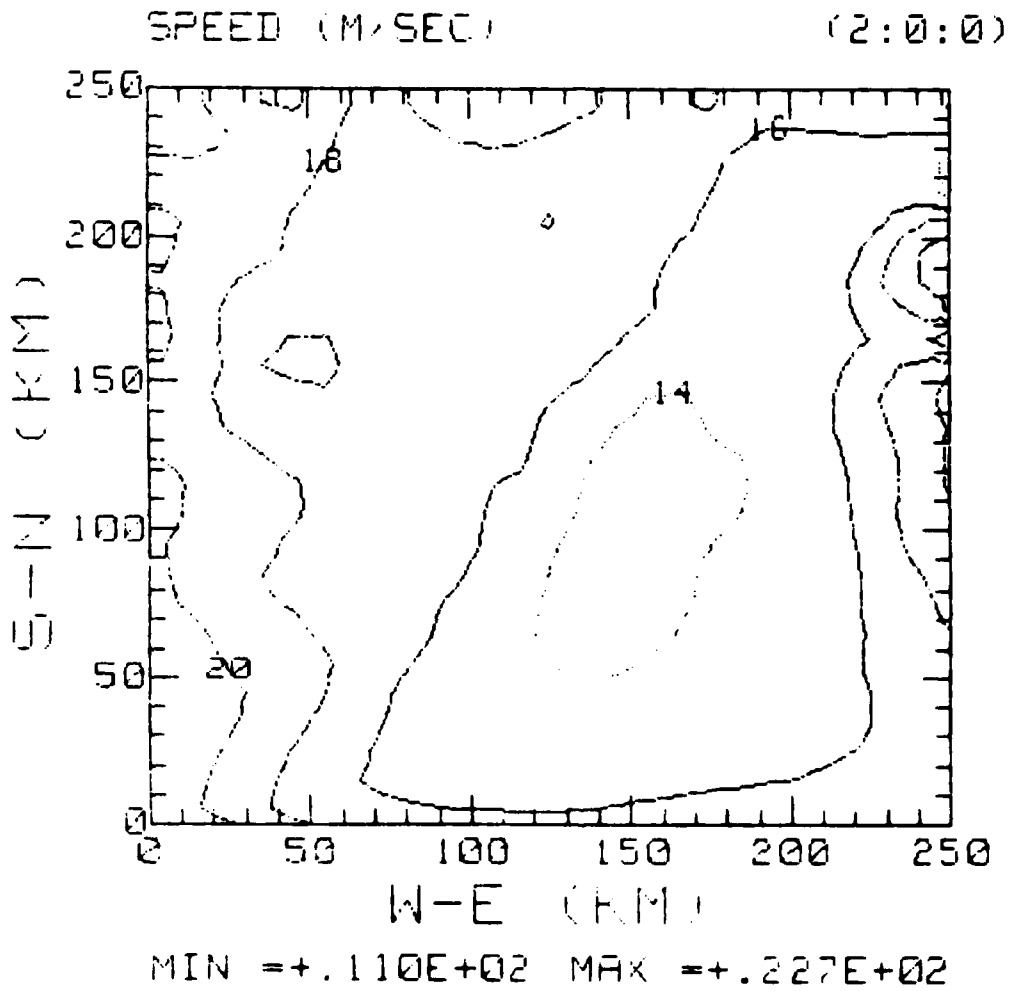
MAX=	23.3237896655	XMAX=	50	YMAX=	250
MIN=	8.1522102452	XMIN=	210	YMIN=	190
AVERAGE VALUE=	17.2308652395				

Figure 4.1  
Initial horizontal wind speed corresponding to  
Figure 3.1.



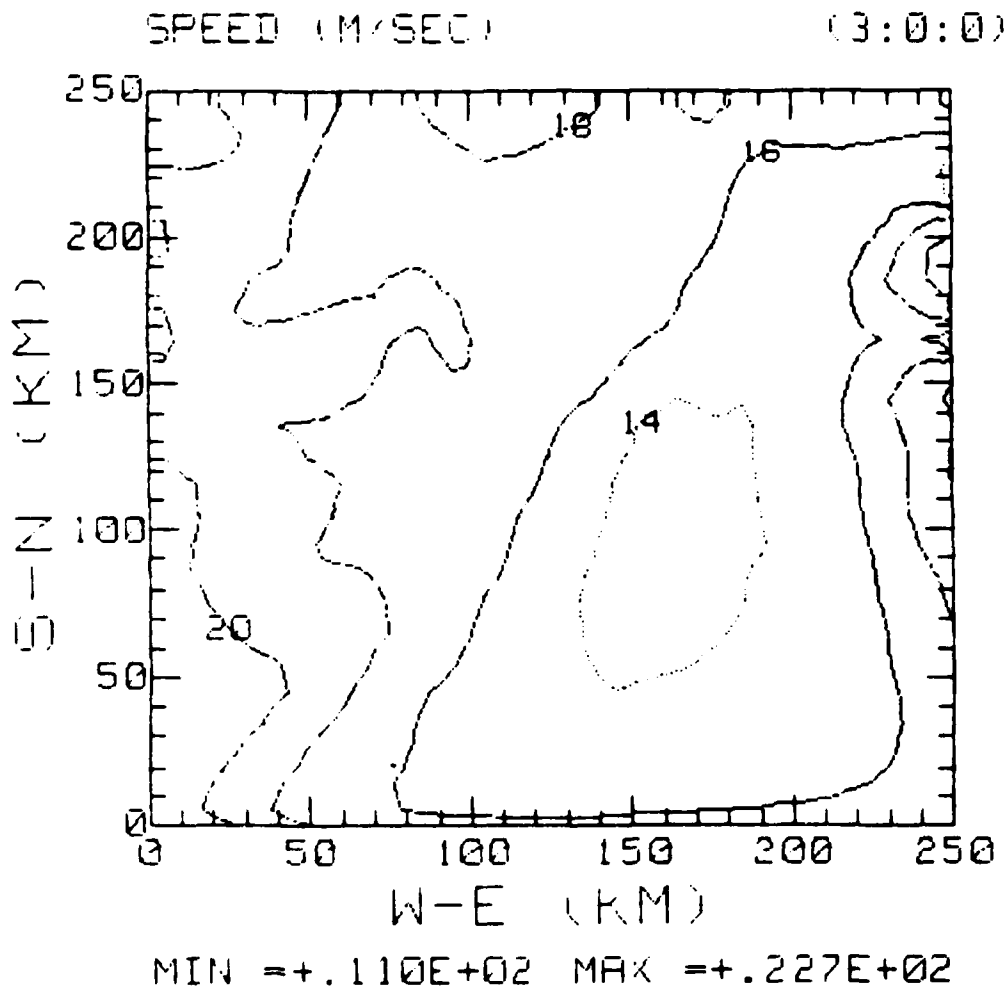
MAX=	22 7133428627	XMAX=	260	YMAX=	190
MIN=	10 9635811686	XMIN=	260	YMIN=	210
AVERAGE VALUE=	17 241867686				

Figure 4.2  
Same as Figure 4.1 but after 1 hour.



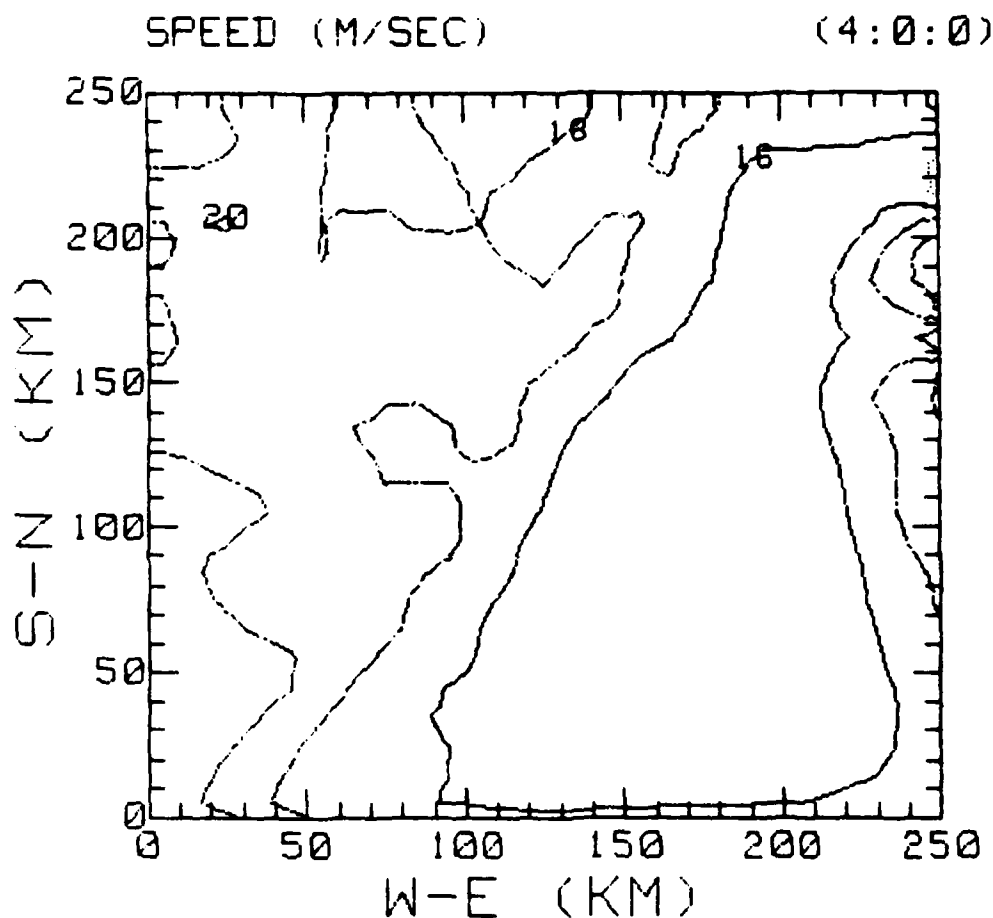
MAX=	02 1137421607	XMAX=	260	YMAX=	190
MIN=	10 9637811686	XMIN=	260	YMIN=	210
AVERAGE VALUE=	16 9150671354				

Figure 4.3  
Same as Figure 4.1 but after 2 hours.



MAX=	22.7133428627	XMAX=	260	YMAX=	190
MIN=	10.9635811686	XMIN=	260	YMIN=	210
AVERAGE VALUE=	17.1123498545				

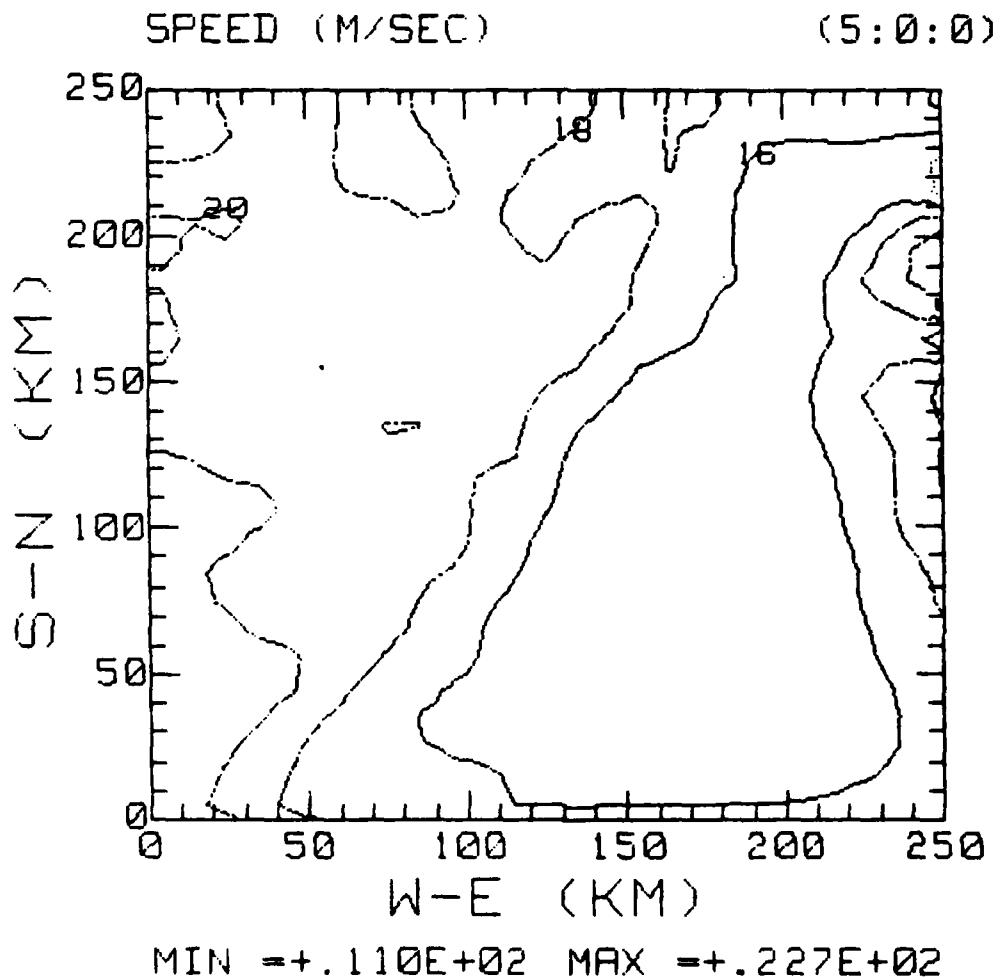
Figure 4.4  
Same as Figure 4.1 but after 3 hours.



MIN =+.110E+02 MAX =+.227E+02

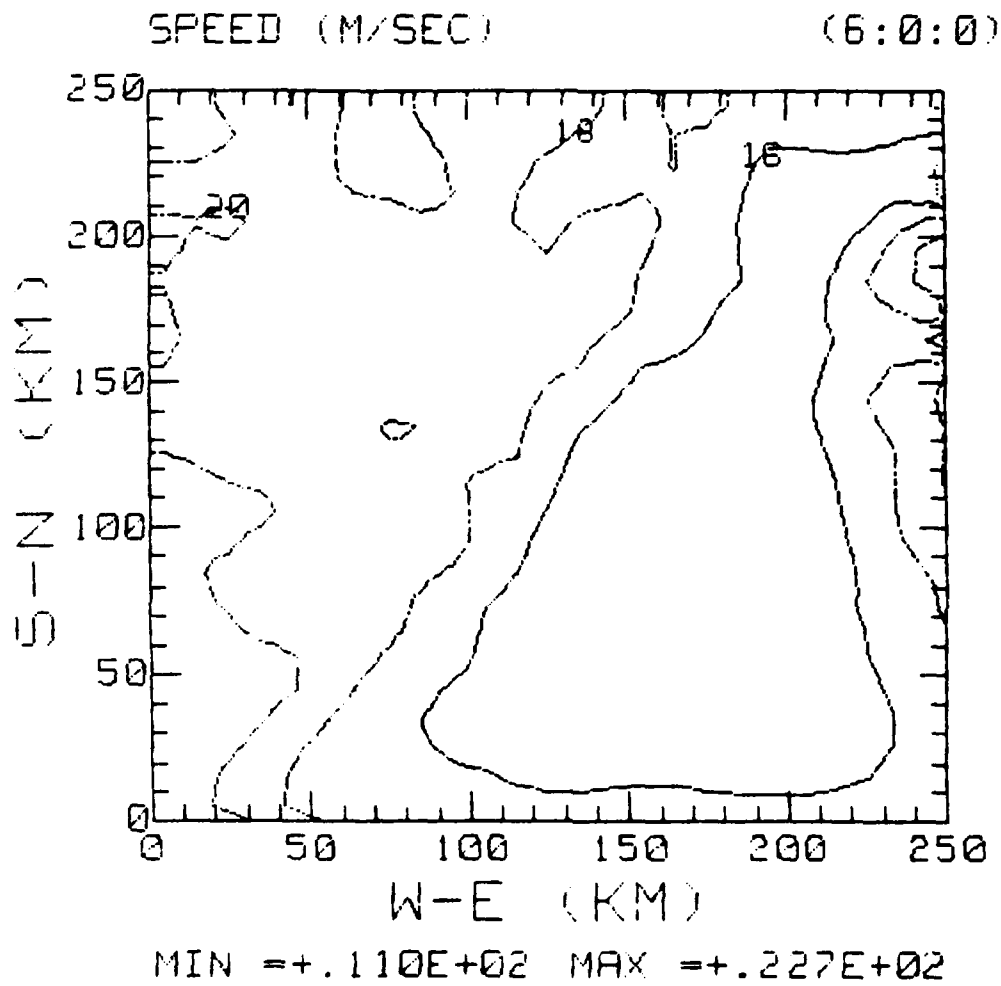
MAX=	22.7133428627	XMAX=	260	YMAX=	190
MIN=	10.9635811686	XMIN=	260	YMIN=	210
AVERAGE VALUE=	17.401018987				

Figure 4.5  
Same as Figure 4.1 but after 4 hours.



MAX=	22.7133428627	XMAX=	260	YMAX=	190
MIN=	10.9635811686	XMIN=	260	YMIN=	210
AVERAGE VALUE=	17.5464660933				

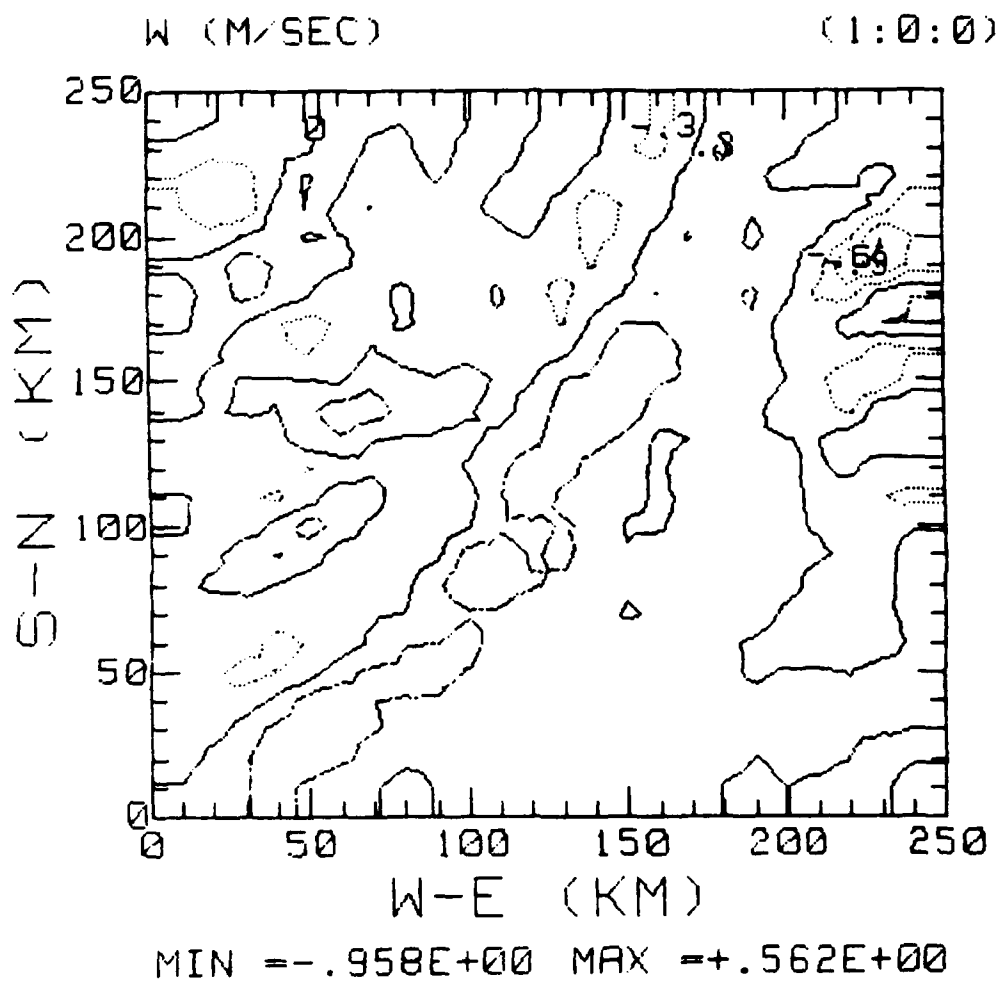
Figure 4.6  
Same as Figure 4.1 but after 5 hours.



MAX=	22.7133428627	XMAX=	260	YMAX=	170
MTN=	10.9635011686	XMIN=	260	YMIN=	210
AVERAGE VALUE=	17.5698002727				

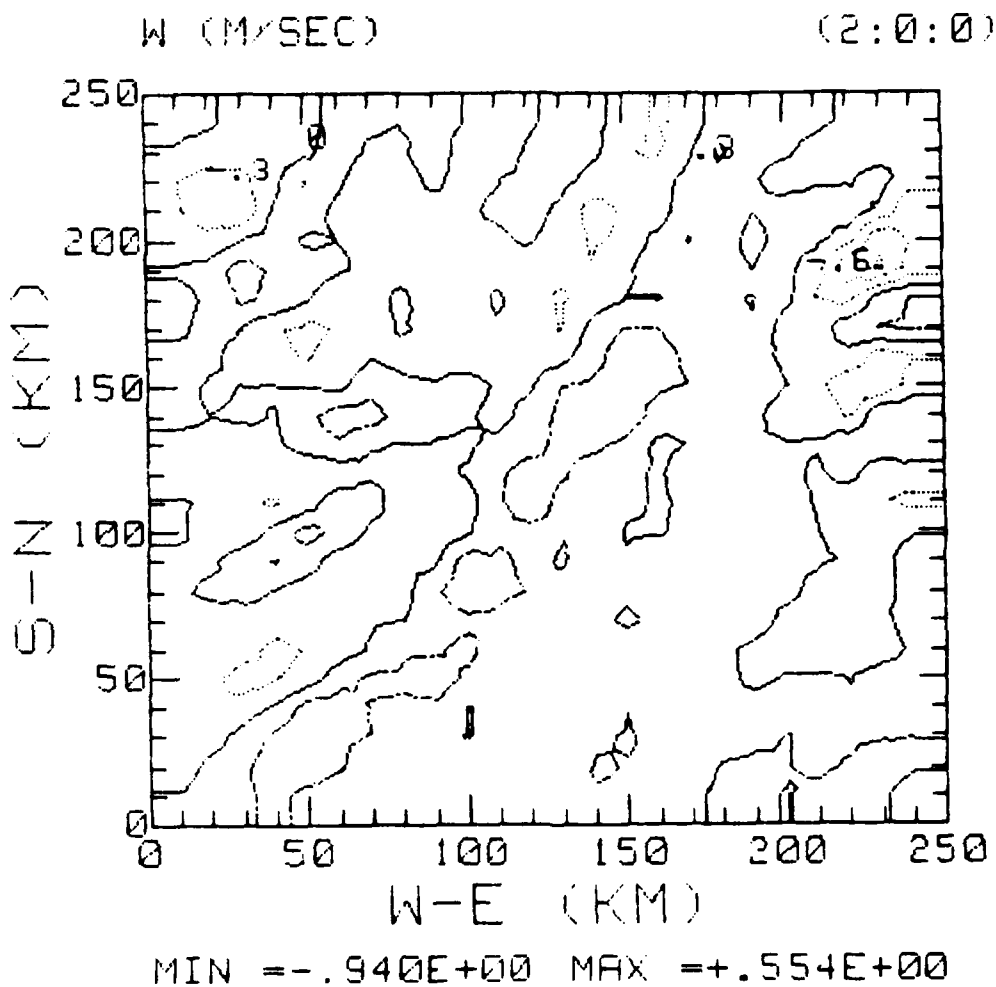
Figure 4.7  
Same as Figure 4.1 but after 6 hours.





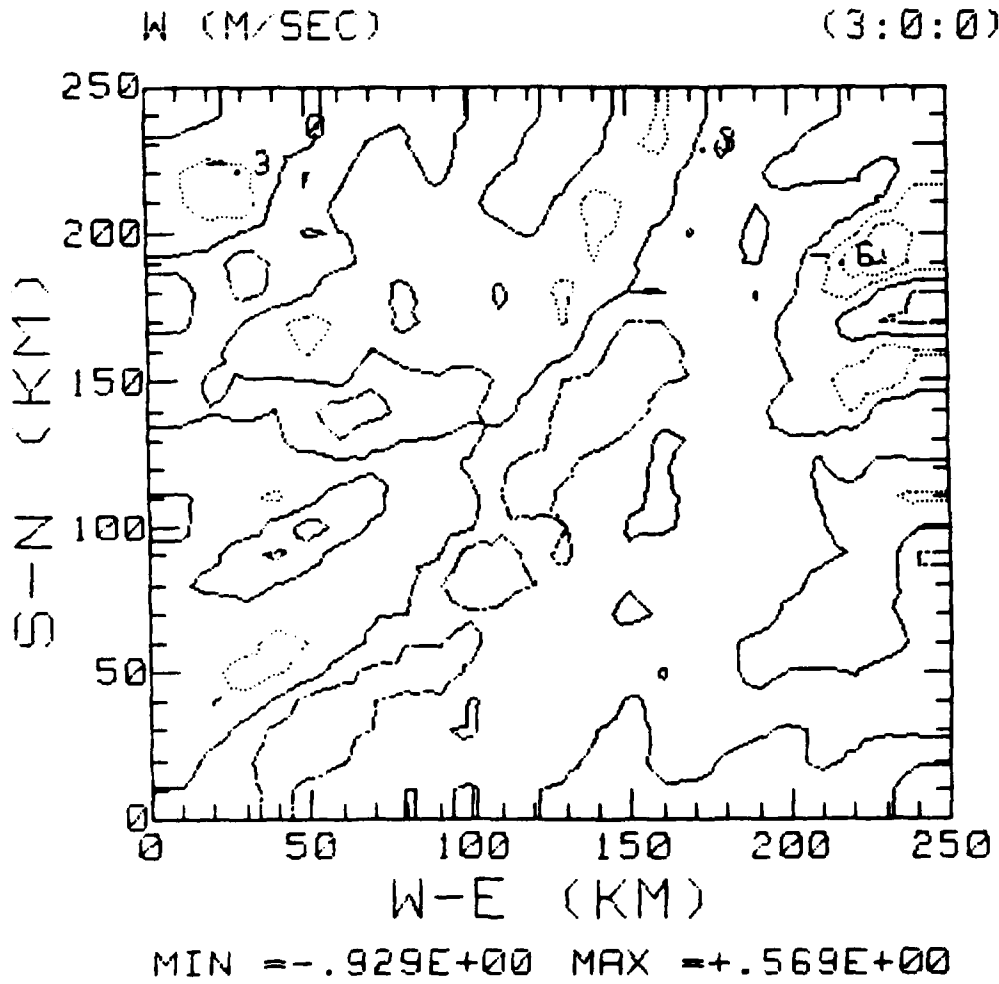
MAX=	.561632	XMAX=	140	YMAX=	140
MIN=	-.958355	XMIN=	230	YMIN=	190
AVERAGE VALUE=	.00865395266272				

Figure 5.1  
Vertical velocity for level 13 after 1 hour.



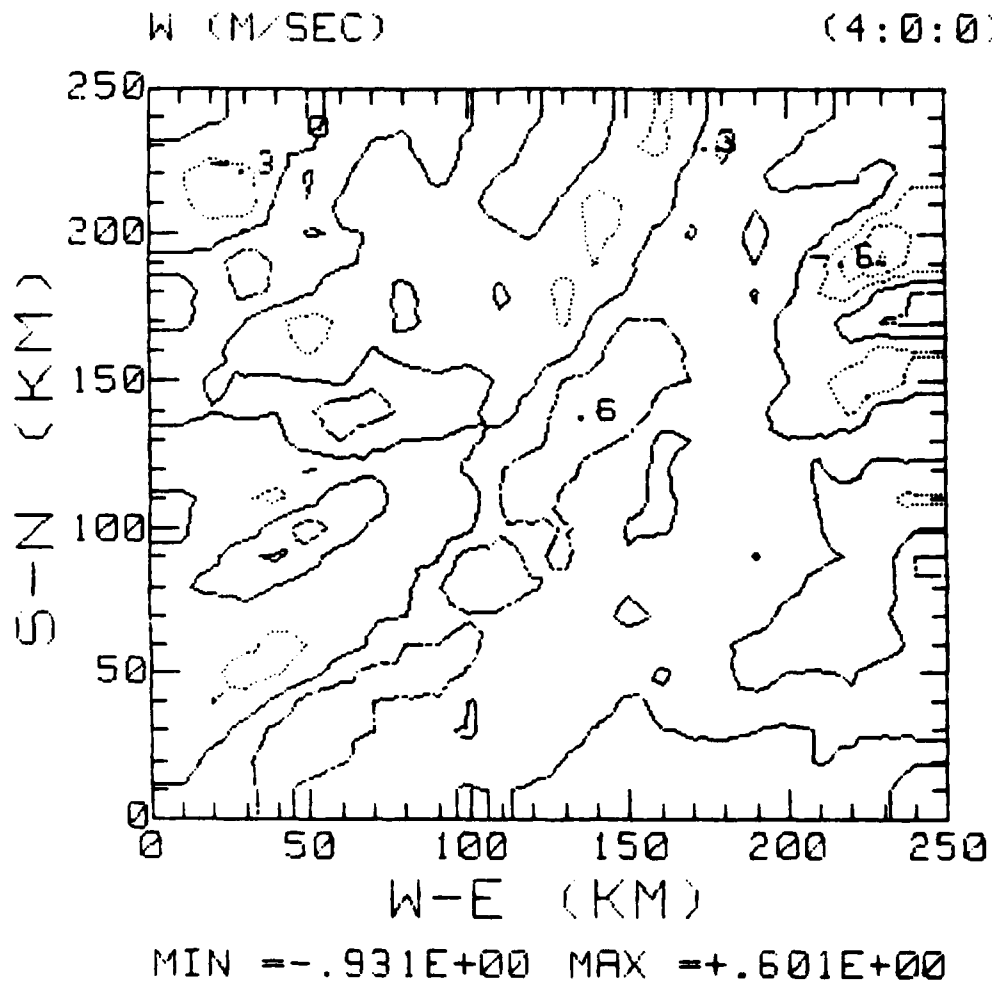
MAX=	55435	XMAX=	140	YMAX=	140
MIN=	-940138	XMIN=	230	YMIN=	190
AVERAGE VALUE=	.00800073668639				

Figure 5.2  
Vertical velocity for level 13 after 2 hours.



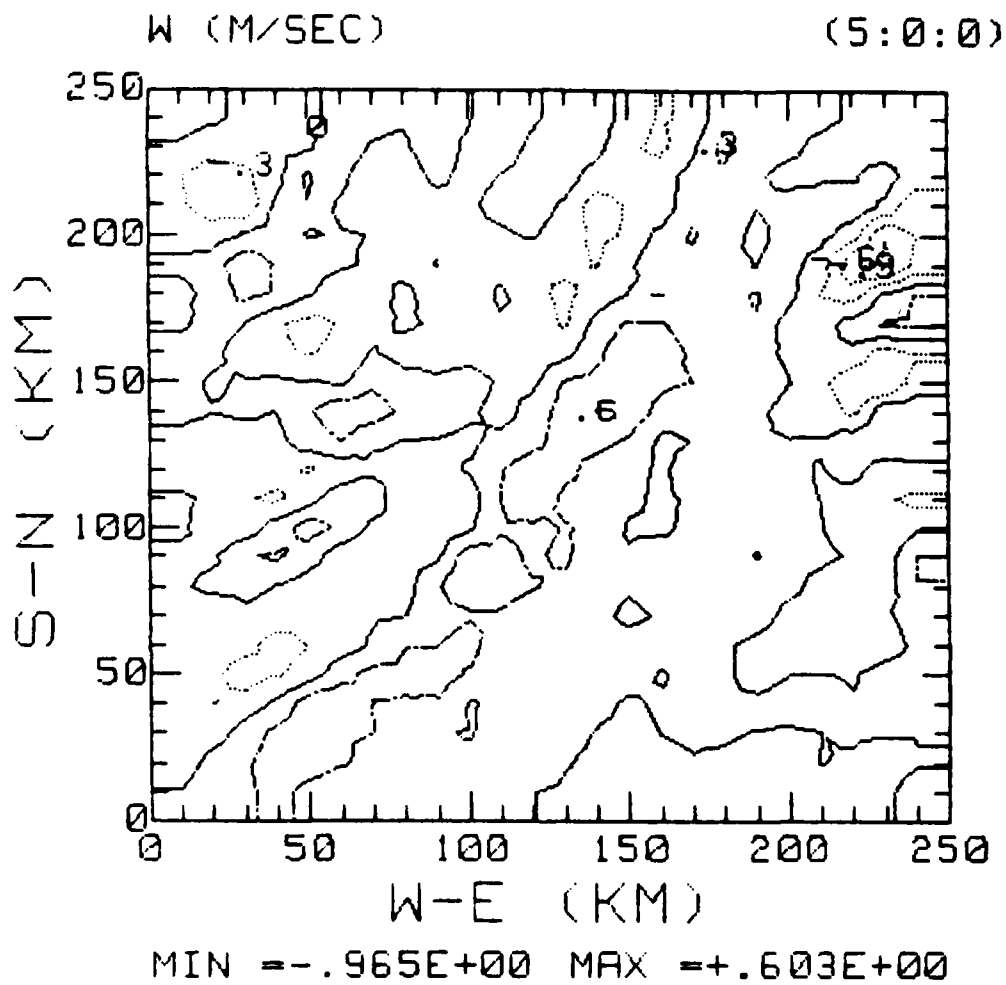
MAX=	568847	XMAX=	140	YMAX=	140
MIN=	929497	XMIN=	230	YMIN=	190
AVERAGE VALUE=	.0106868150888				

Figure 5.3  
Vertical velocity for level 13 after 3 hours.



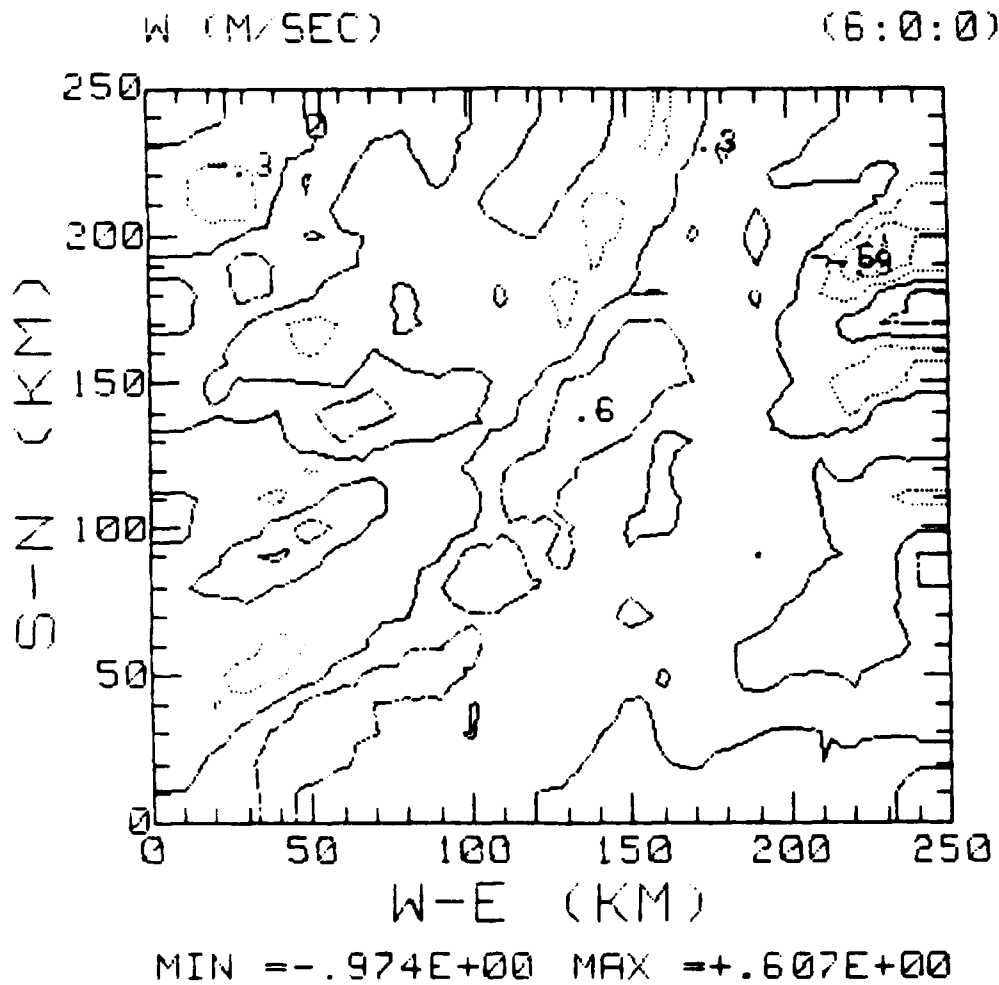
MAX=	.60118	XMAX=	140	YMAX=	140
MIN=	-.931102	XMIN=	230	YMIN=	190
AVERAGE VALUE=	.0126404866864				

Figure 5.4  
Vertical velocity for level 13 after 4 hours.



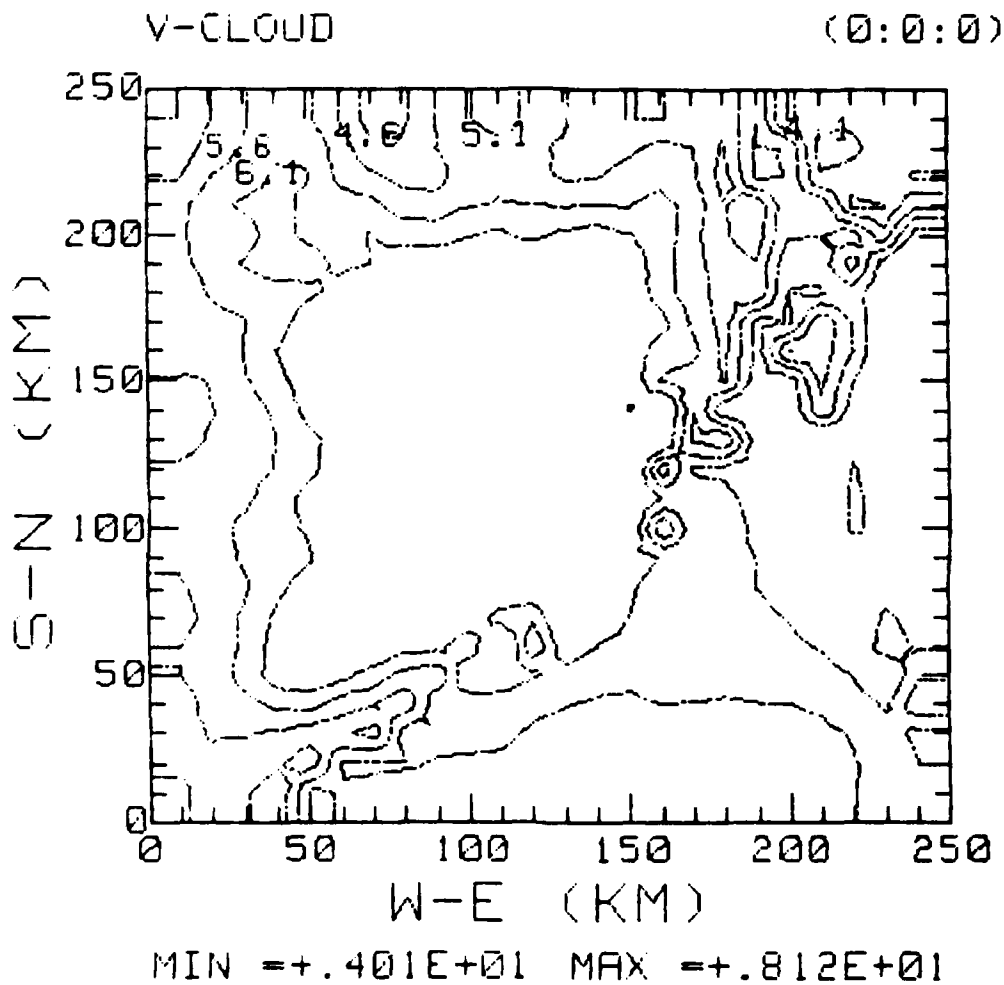
MAX=	602921	XMAX=	140	YMAX=	140
MIN=	-.965447	XMIN=	230	YMIN=	190
AVERAGE VALUE=	.0125425384615				

Figure 5.5  
Vertical velocity for level 13 after 5 hours.



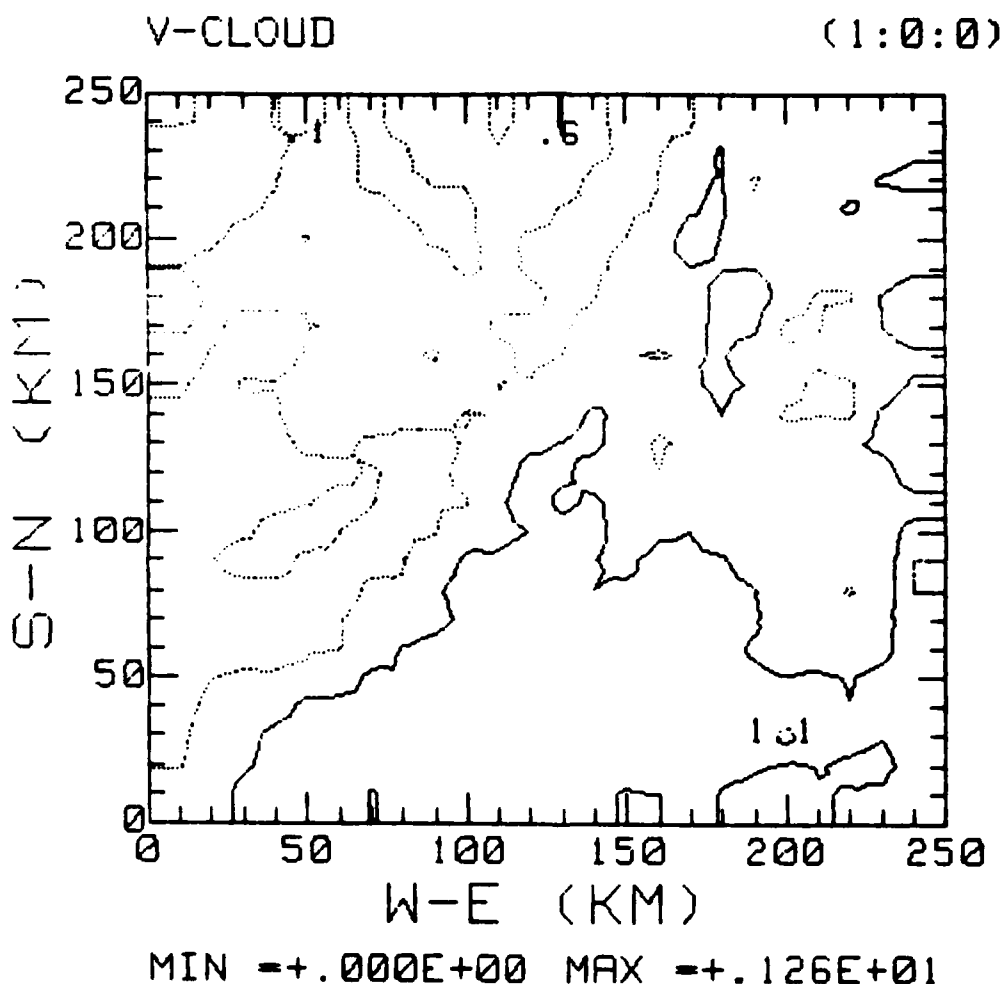
MAX=	.607115	XMAX=	140	YMAX=	140
MIN=	-.974163	XMIN=	230	YMIN=	190
AVERAGE VALUE=	.0124007485207				

Figure 5.6  
Vertical velocity for level 13 after 6 hours.



MAX=	8.1186	XMAX=	110	YMAX=	120
MIN=	4.0074	XMIN=	210	YMIN=	230
AVERAGE VALUE=	5.89820887574				

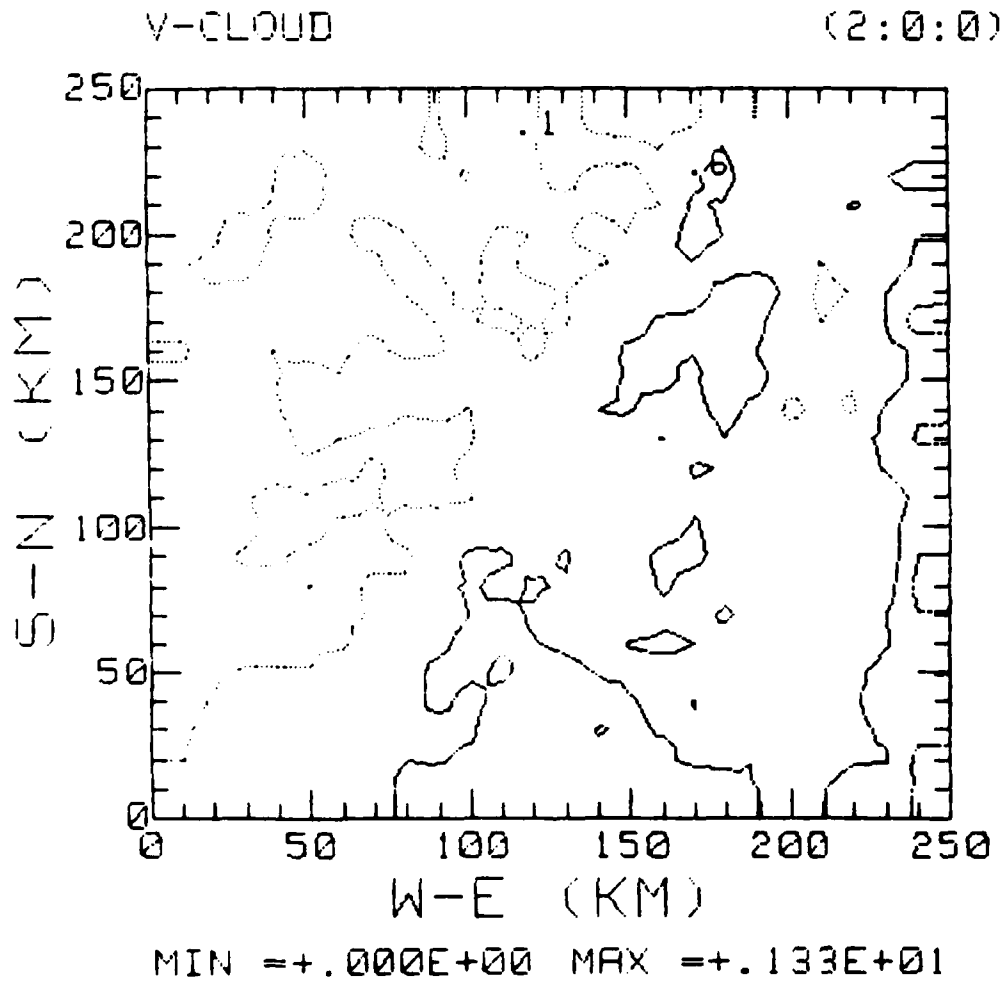
Figure 6.1  
Initial vertically integrated cloud water



MAX=	1.2631	XMAX=	200	YMAX=	30
MIN=	0	XMIN=	90	YMIN=	210
AVERAGE VALUE=	.38094556213				

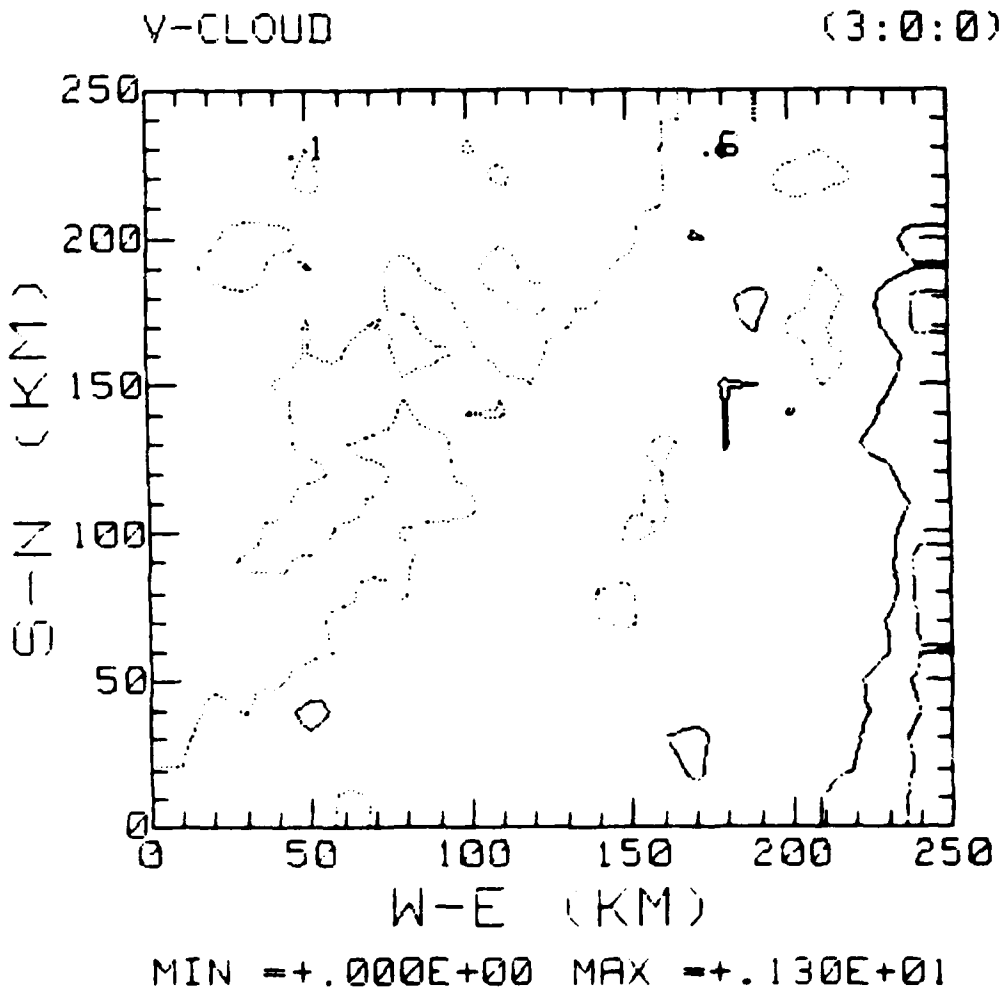
Figure 6.2  
Vertically integrated cloud water after 1 hour.





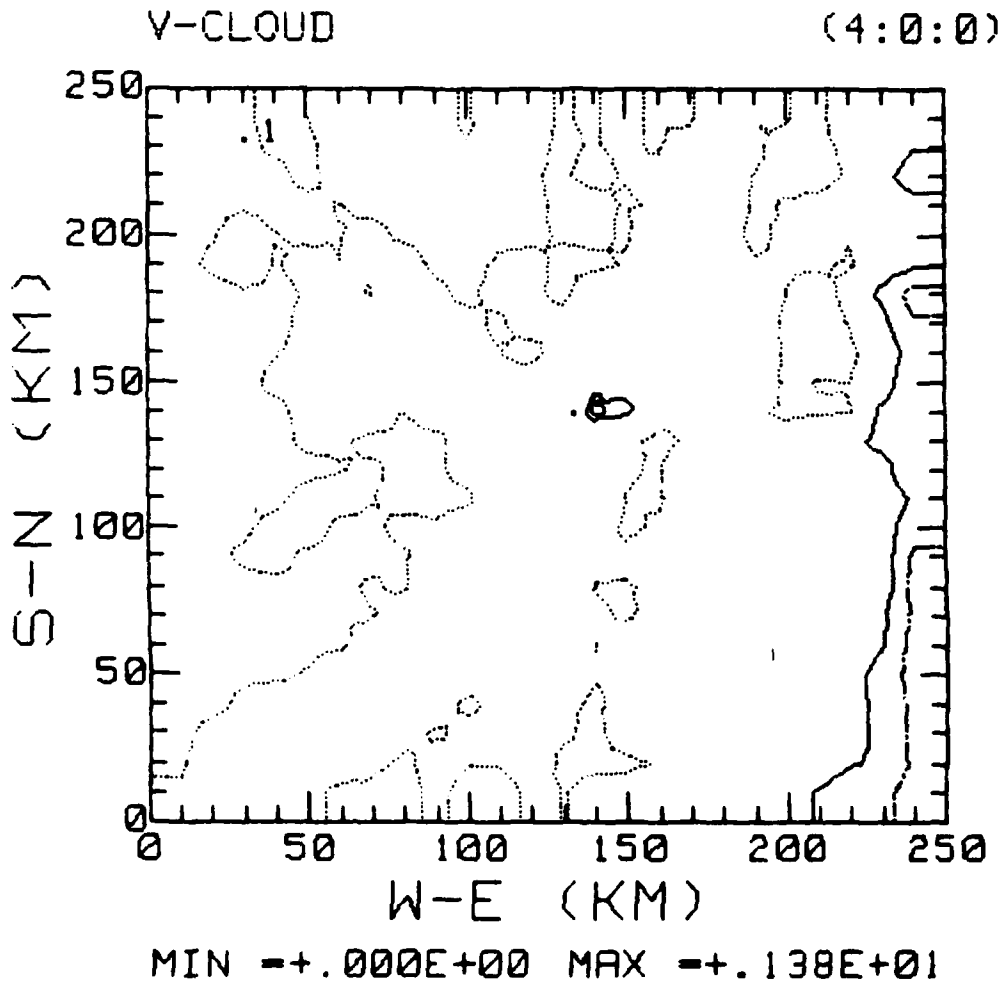
MAX=	1 3323	XMAX=	250	YMAX=	170
MIN=	0	XMIN=	110	YMIN=	240
AVERAGE VALUE=			346173816568		

Figure 6.3  
Vertically integrated cloud water after 2 hours.



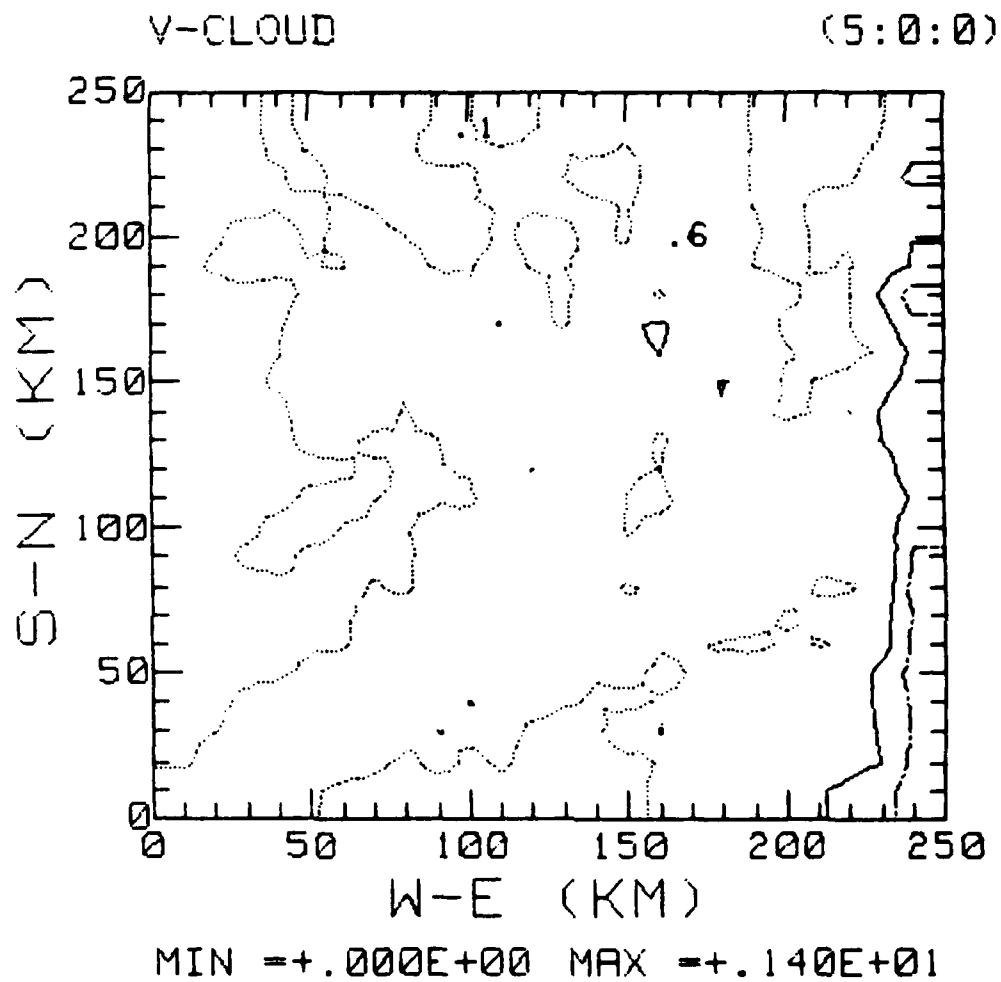
MAX=	1 3049	XMAX=	250	YMAX=	90
MIN=	0	XMIN=	160	YMIN=	130
AVERAGE VALUE=	.285112130178				

Figure 6.4  
Vertically integrated cloud water after 3 hours.



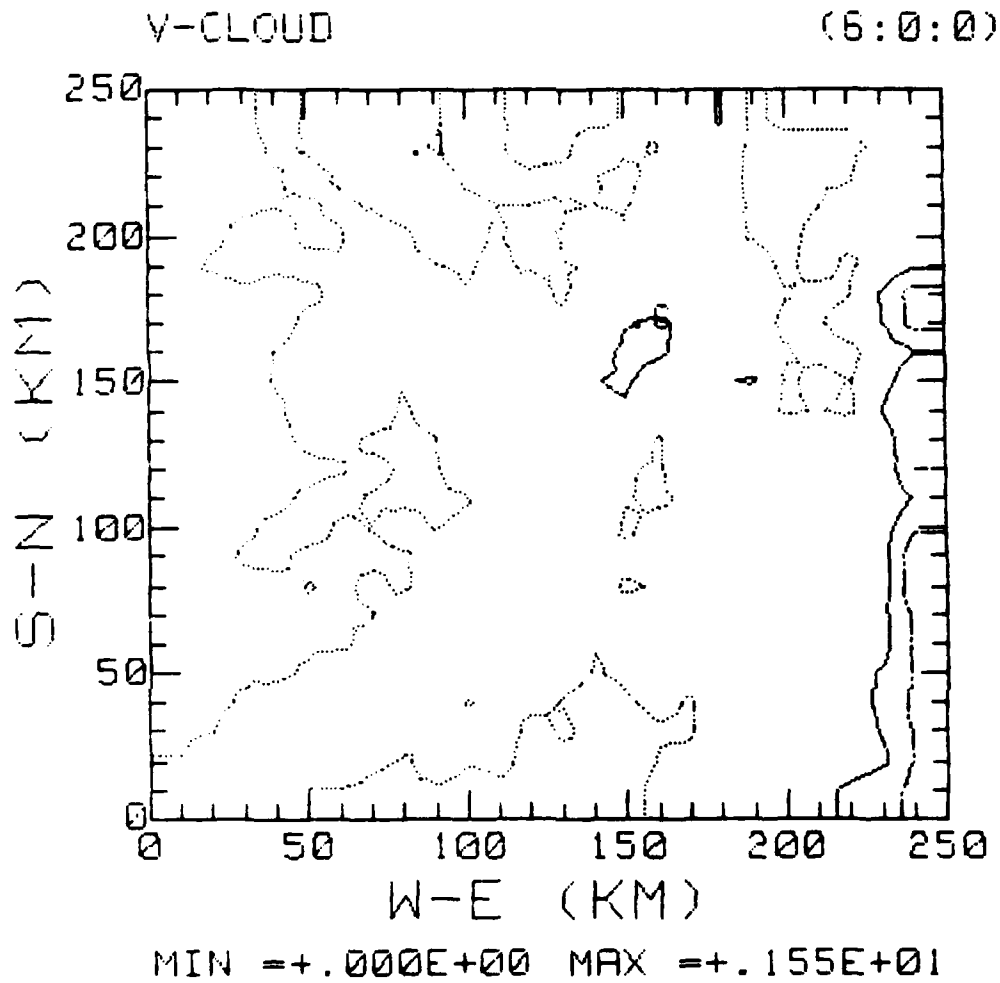
MAX=	1.3769	XMAX=	250	YMAX=	0
MIN=	0	XMIN=	210	YMIN=	170
AVERAGE VALUE=	.251568639053				

Figure 6.5  
Vertically integrated cloud water after 4 hours.



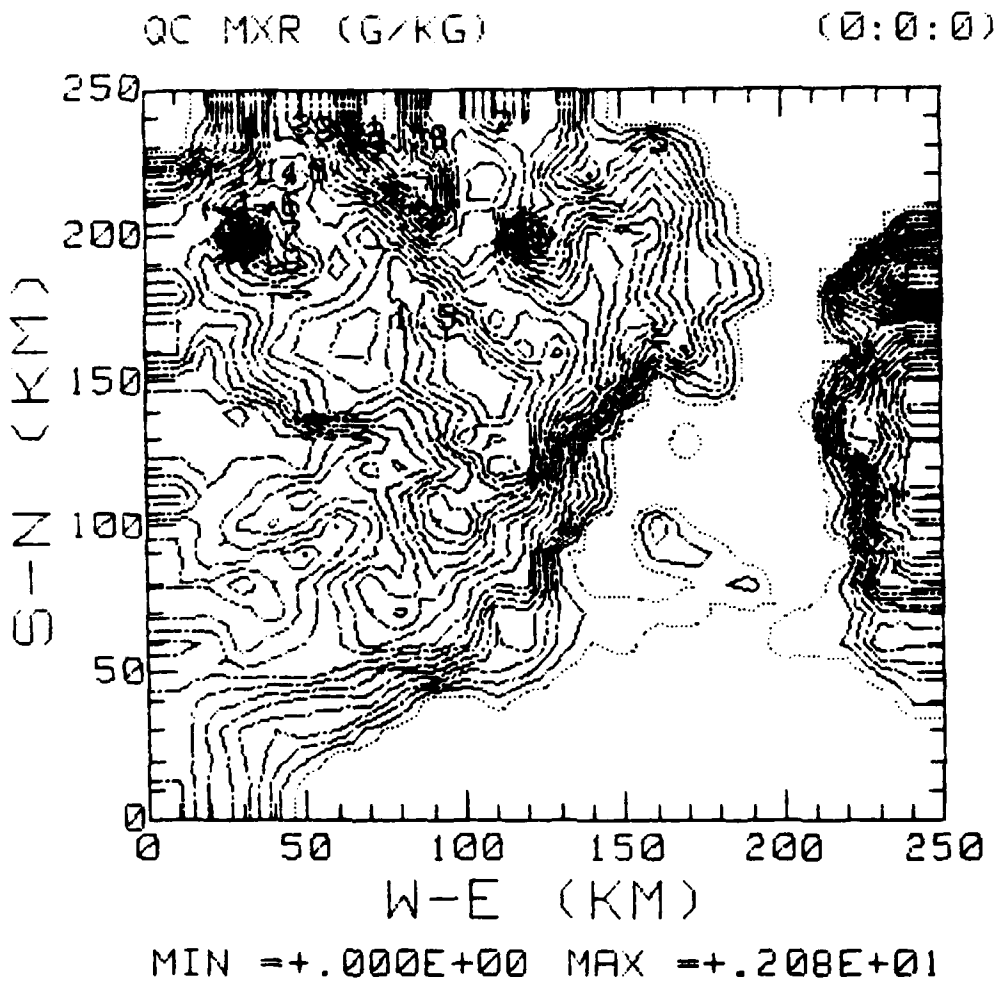
MAX=	1.3965	XMAX=	250	YMAX=	0
MIN=	0	XMIN=	220	YMIN=	230
AVERAGE VALUE=	.244089349112				

Figure 6.6  
Vertically integrated cloud water after 5 hours.



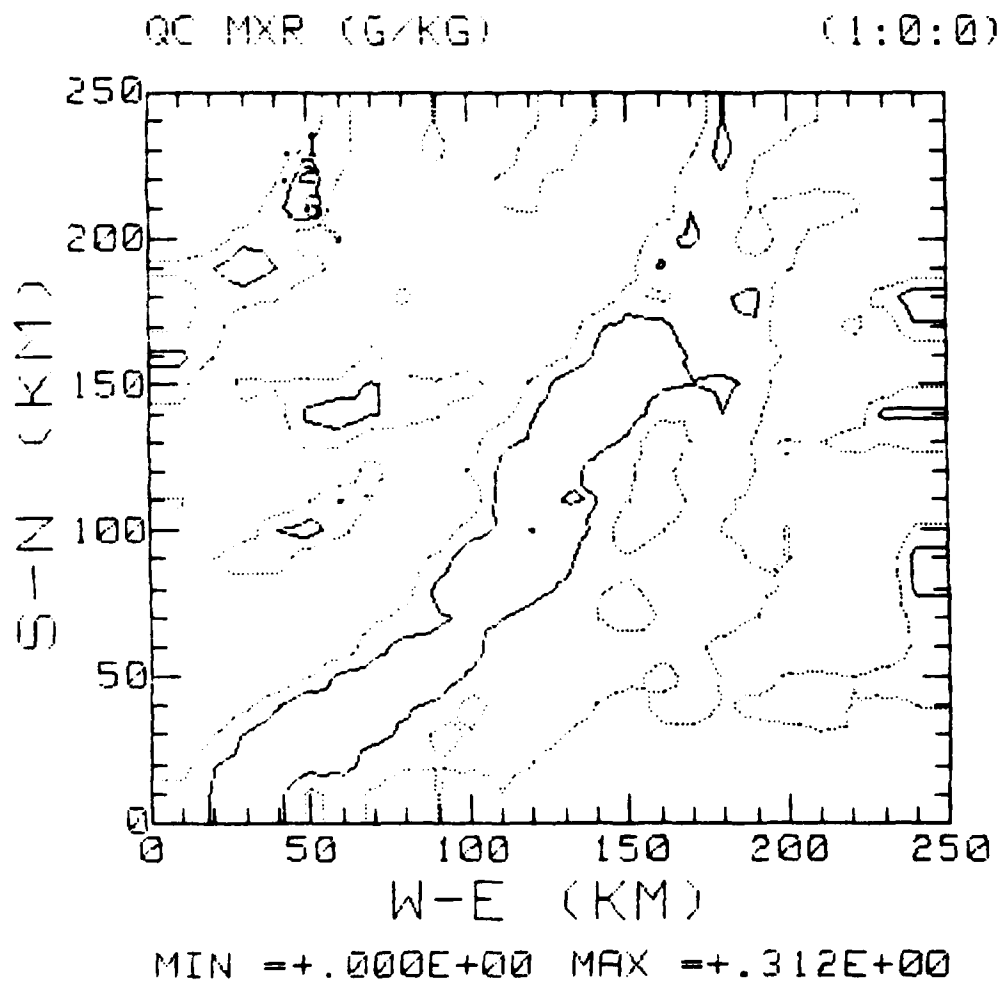
MAX=	1.5512	XMAX=	250	YMAX=	80
MIN=	0	XMIN=	220	YMIN=	230
AVERAGE VALUE=	.249939497041				

Figure 6.7  
Vertically integrated cloud water after 6 hours.



MAX=	2.084	XMAX=	100	YMAX=	160
MIN=	0	XMIN=	250	YMIN=	0
AVERAGE VALUE=	.632520106509				

Figure 7.1  
Initial cloud water mixing ratio for level 13.



MAX=	.312	XMAX=	50	YMAX=	210
MIN=	0	XMIN=	250	YMIN=	0
AVERAGE VALUE=	0872707100592				

Figure 7.2  
Cloud water mixing ratio for level 13  
after 1 hour.

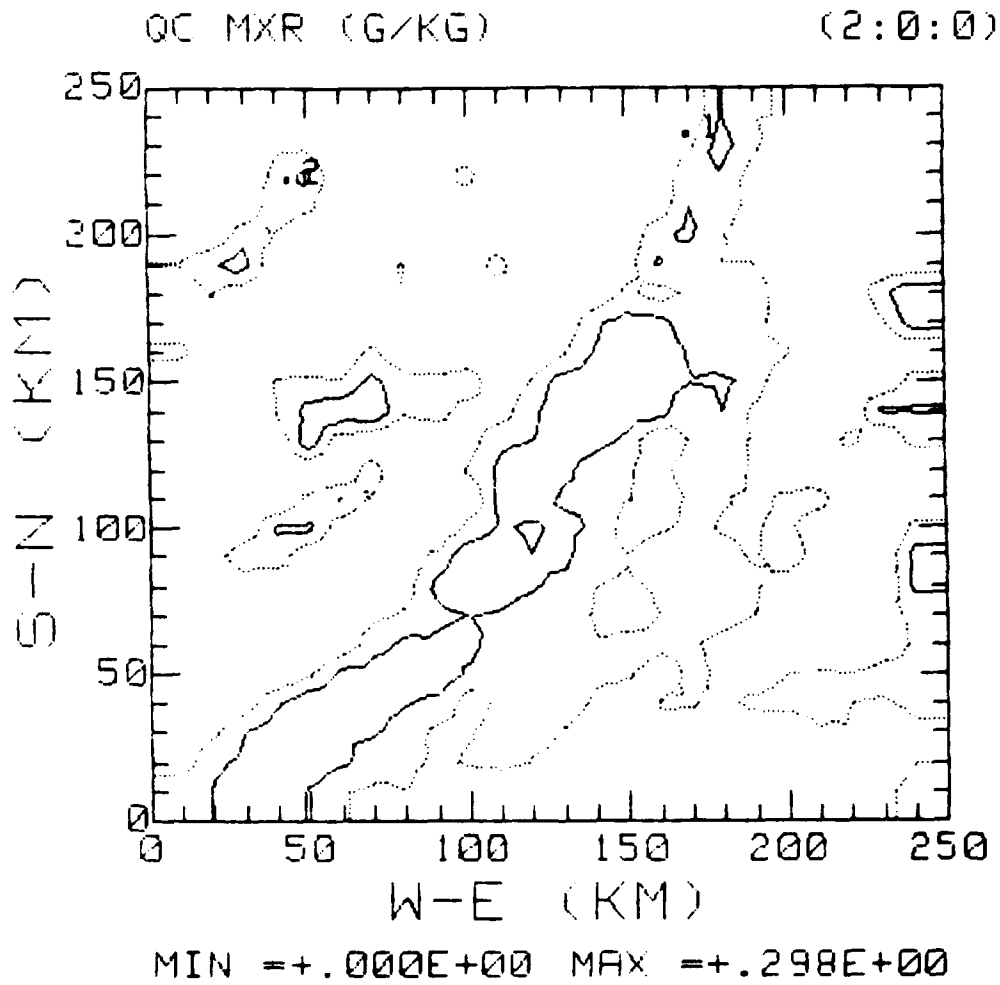
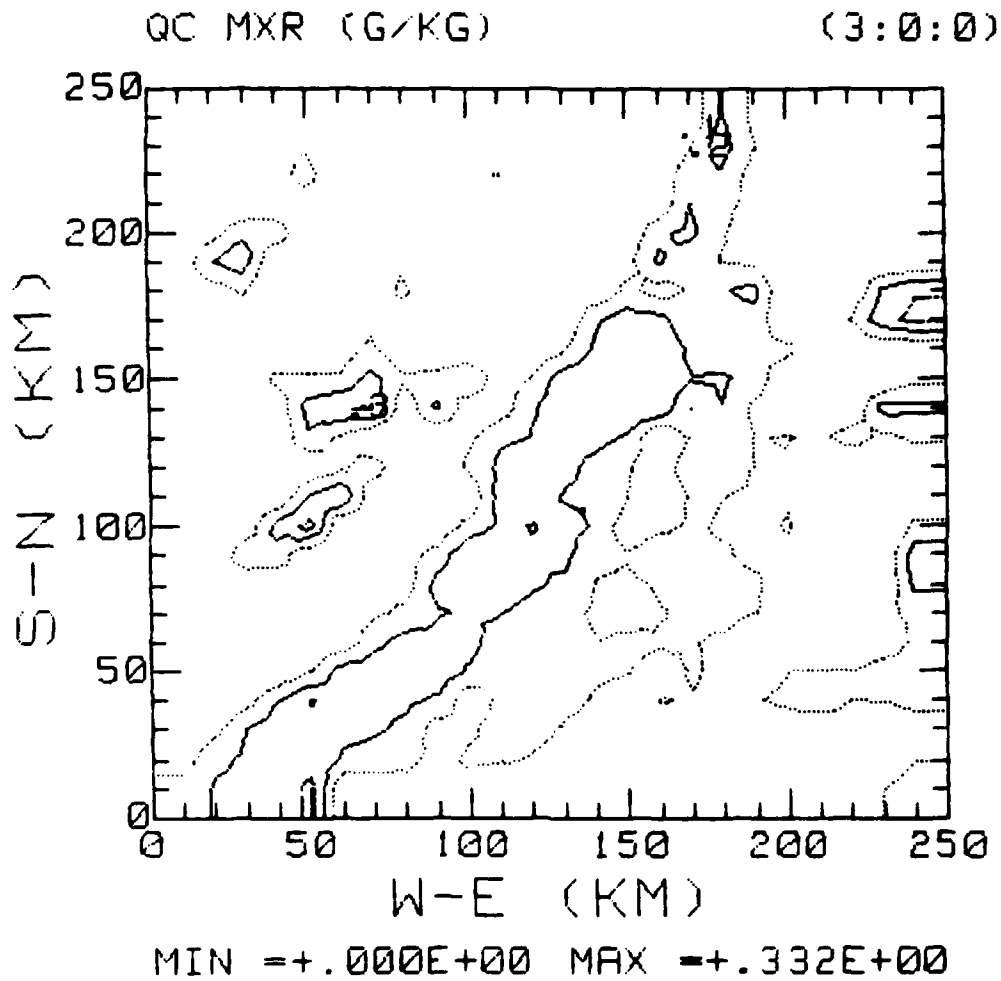


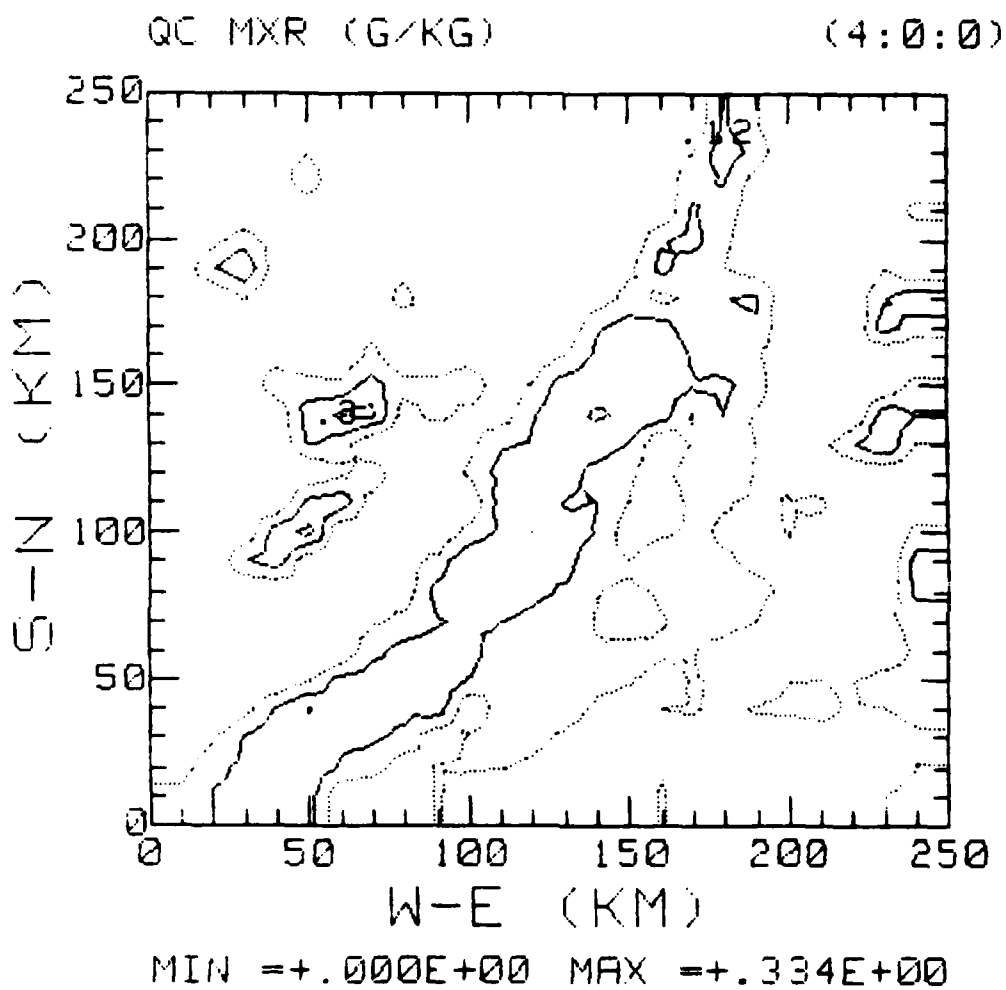
Figure 7.3  
Cloud water mixing ratio for level 13  
after 2 hours.





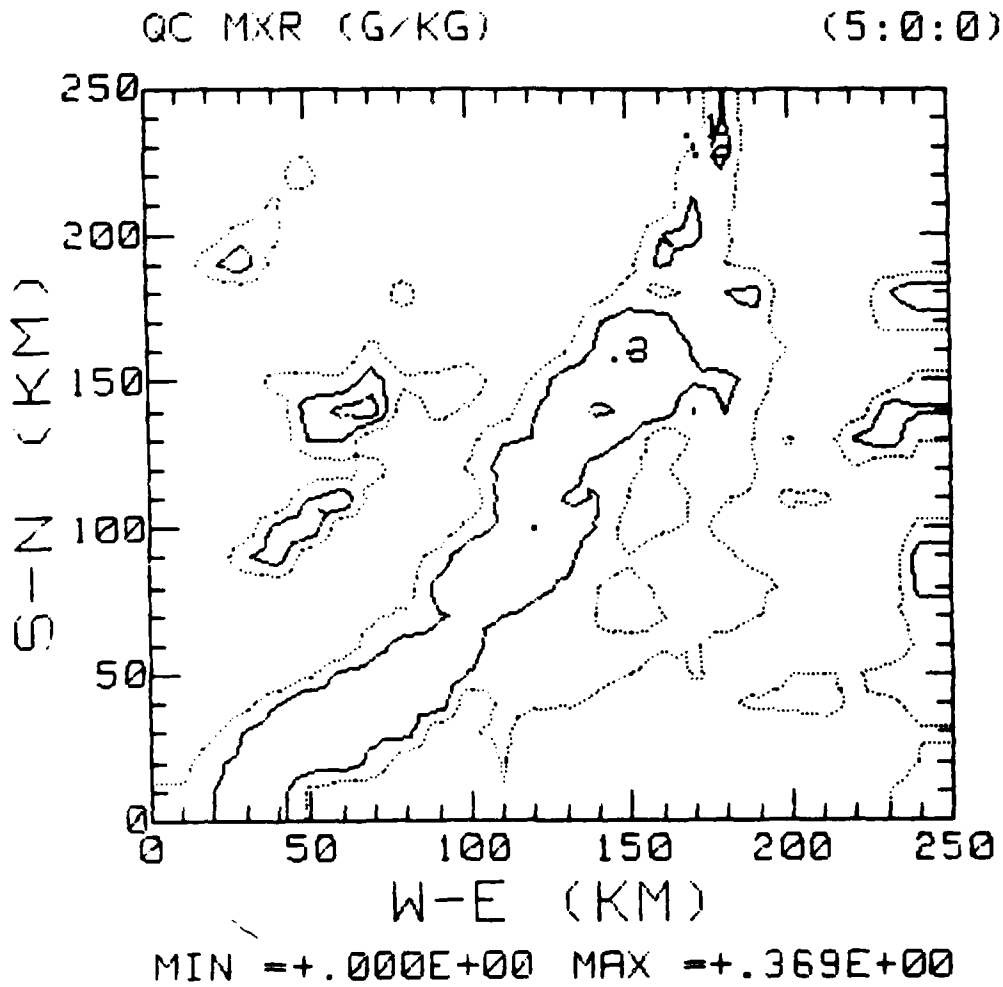
MAX=	.332	XMAX=	50	YMAX=	100
MIN=	0	XMIN=	250	YMIN=	110
AVERAGE VALUE=	.0765769270769				

Figure 7.4  
Cloud water mixing ratio for level 13  
after 3 hours.



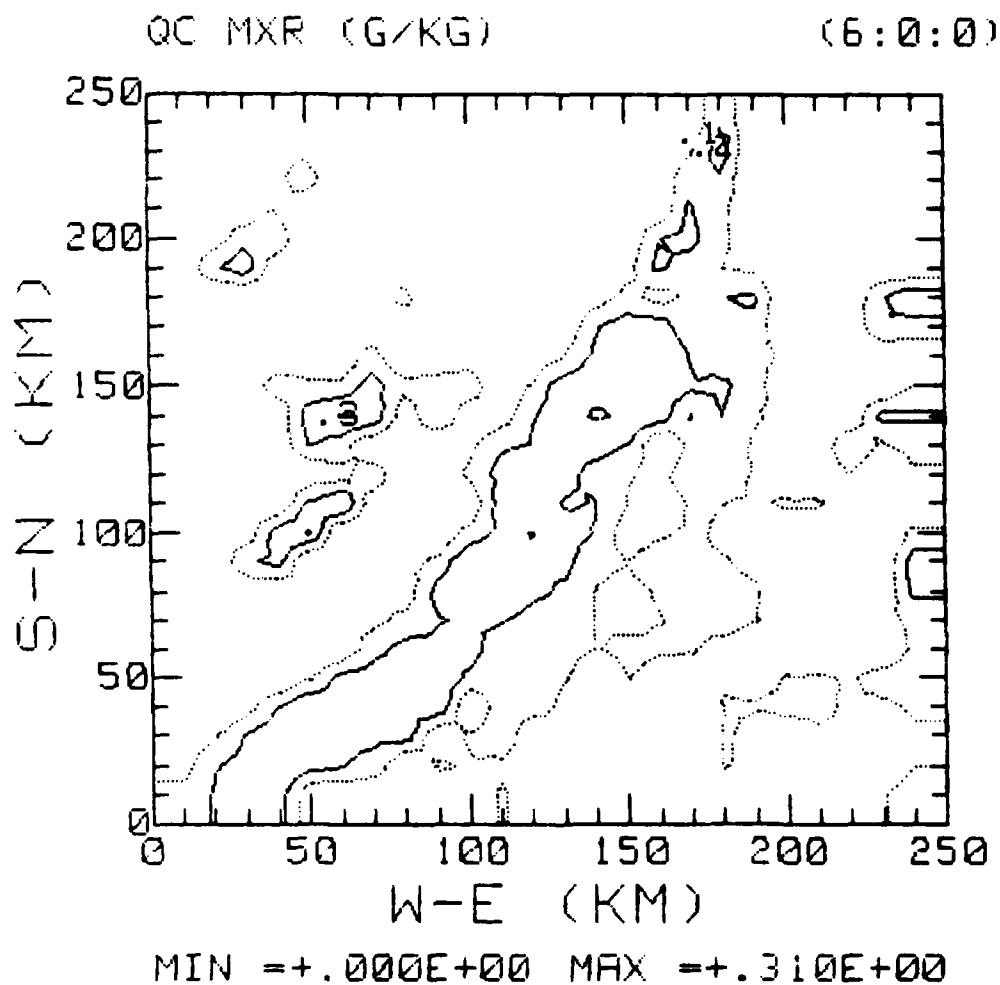
MAX=	334	XMAX=	50	YMAX=	100
MIN=	0	XMIN=	250	YMIN=	110
AVERAGE VALUE=	0777100591710				

Figure 7.5  
Cloud water mixing ratio for level 13  
after 4 hours.



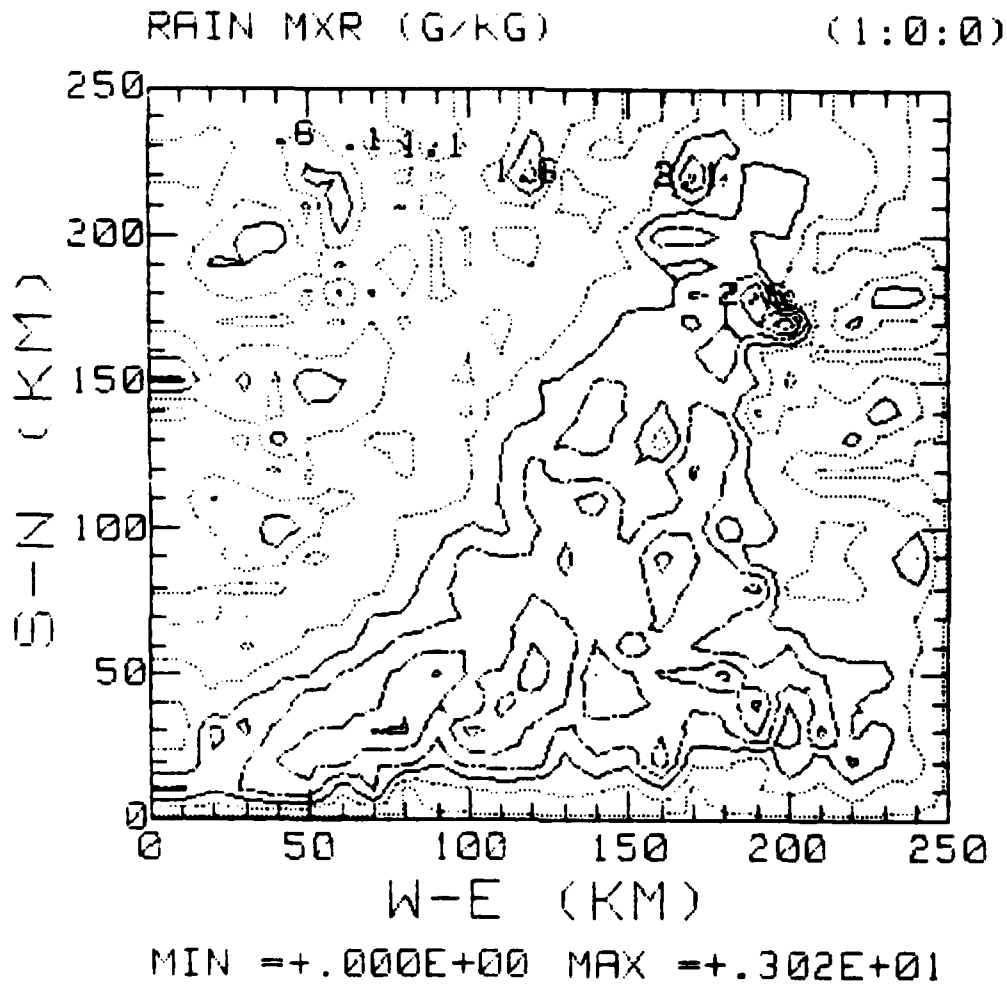
MAX=	.369	XMAX=	70	YMAX=	140
MIN=	0	XMIN=	250	YMIN=	110
AVERAGE VALUE=	.0749704142012				

Figure 7.6  
Cloud water mixing ratio for level 13  
after 5 hours.



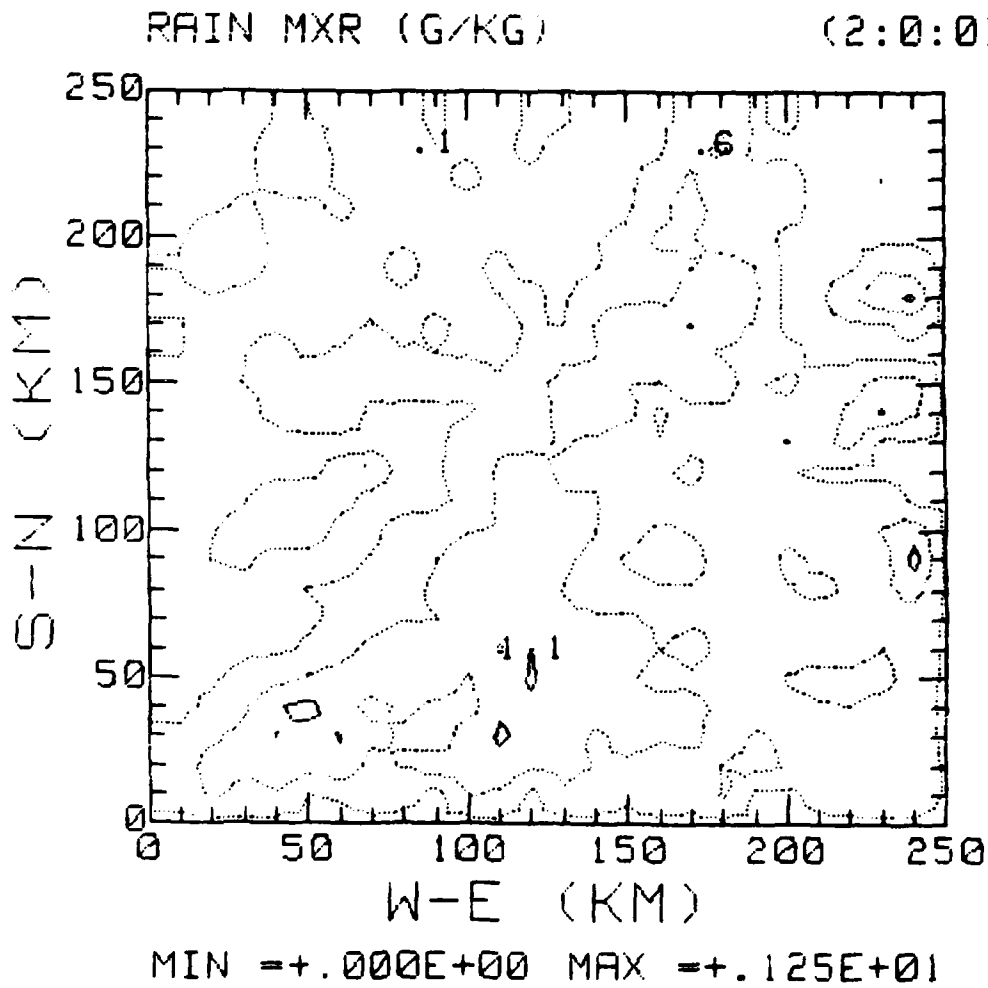
MAX=	.31	XMAX=	60	YMAX=	140
MIN=	0	XMIN=	250	YMIN=	110
AVERAGE VALUE=	.0729807692303				

Figure 7.7  
Cloud water mixing ratio for level 13  
after 6 hours.



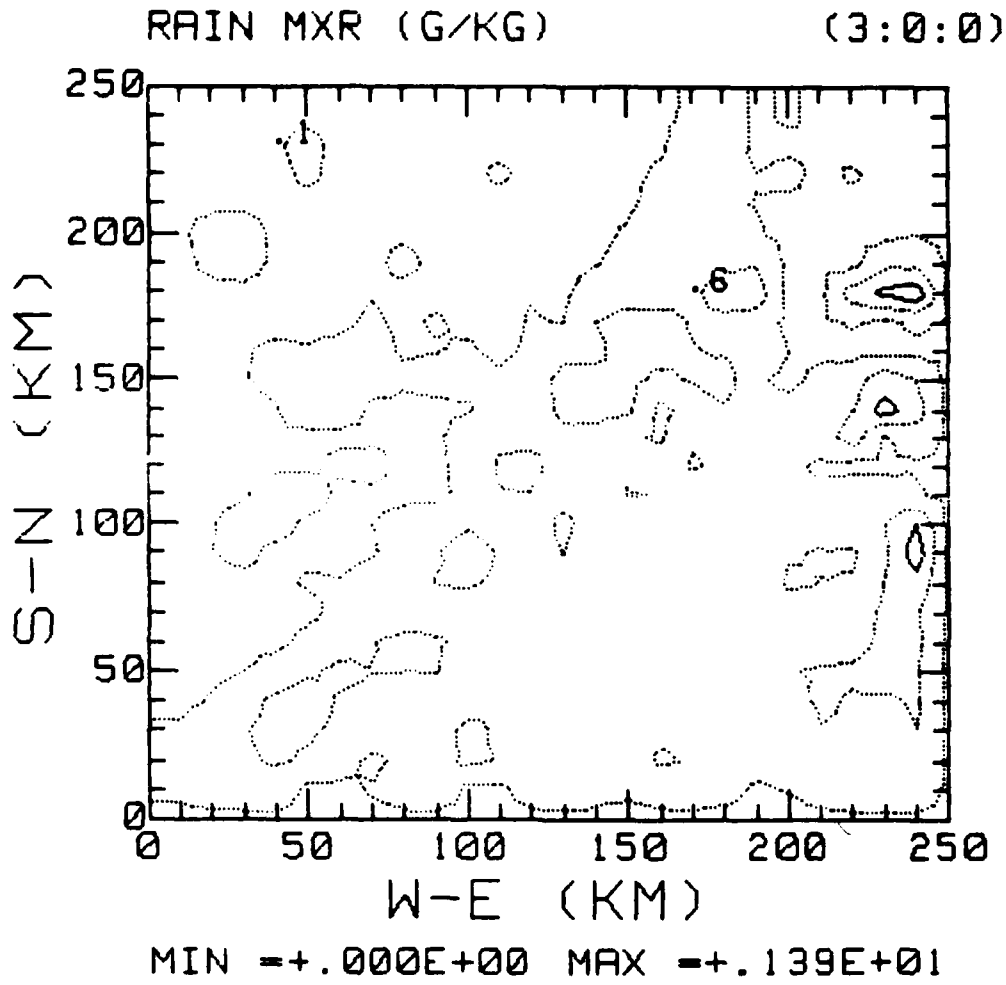
MAX=	3.019	XMAX=	200	YMAX=	170
MIN=	0	XMIN=	250	YMIN=	0
AVERAGE VALUE=	.644304733728				

Figure 8.1  
Rain water mixing ratio for level 13 after 1 hour.



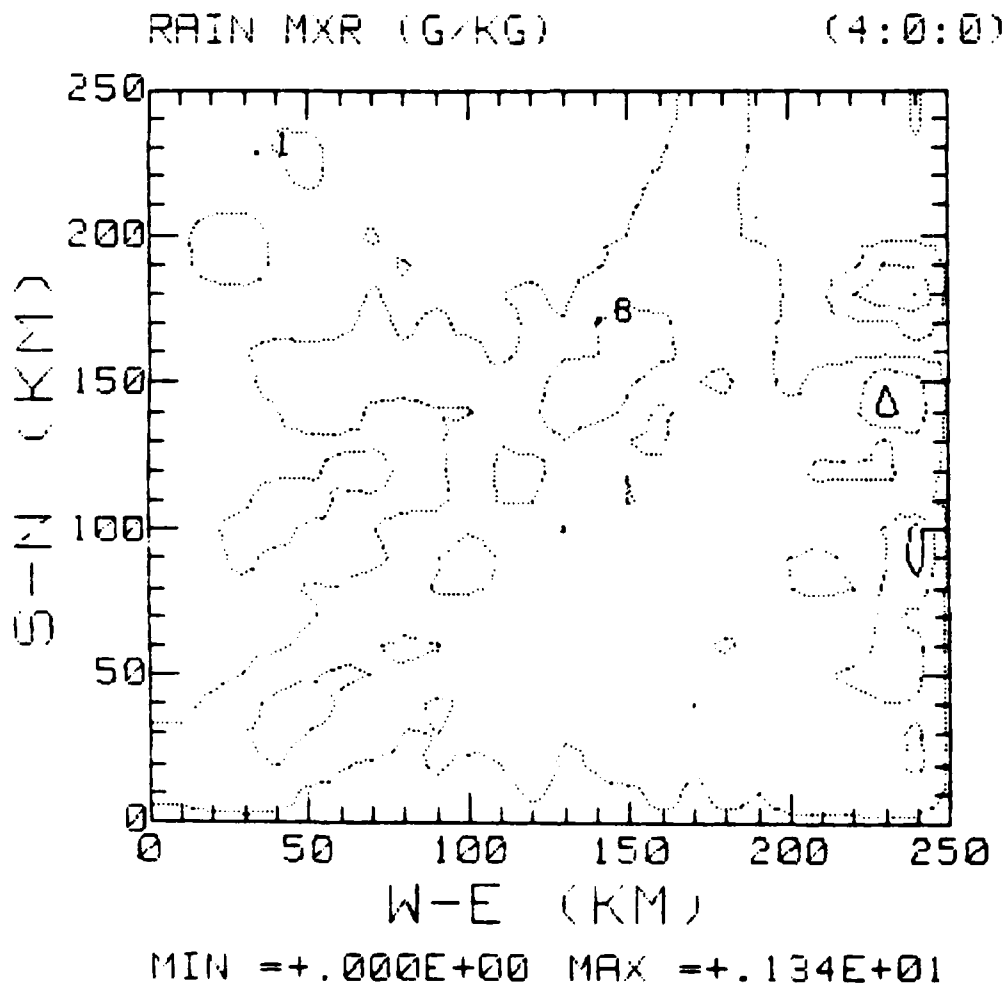
MAX=	1.254	XMAX=	240	YMAX=	90
MIN=	0	XMIN=	250	YMIN=	0
AVERAGE VALUE=	.292029585799				

Figure 8.2  
Rain water mixing ratio for level 13 after 2 hours.



MAX=	1.392	XMAX=	240	YMAX=	180
MIN=	0	XMIN=	250	YMIN=	0
AVERAGE VALUE=	.221121301775				

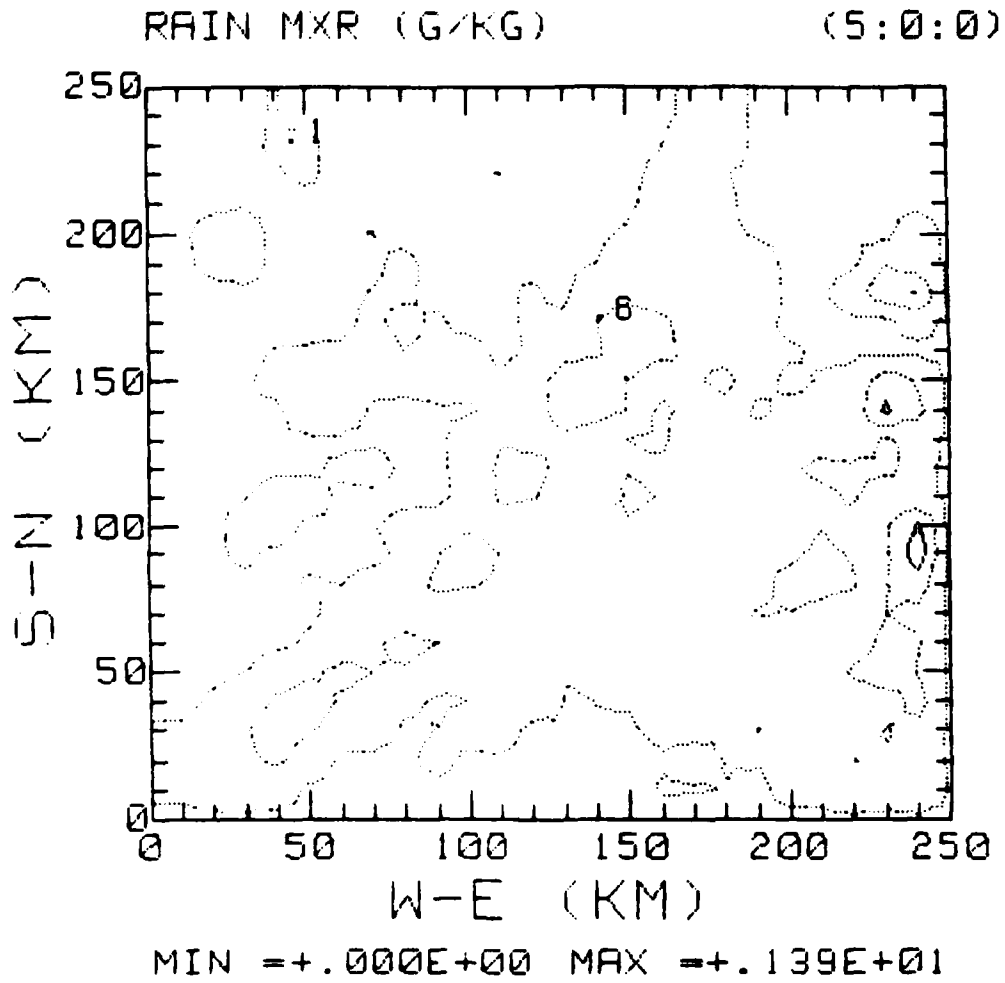
Figure 8.3  
Rain water mixing ratio for level 13 after 3 hours.



MAX=	1.34	XMAX=	240	YMAX=	90
MIN=	0	XMIN=	250	YMIN=	0
AVERAGE VALUE=	190715976331				

Figure 8.4  
Rain water mixing ratio for level 13 after 4 hours.





MAX= 1.39 XMAX= 240 YMAX= 90  
MIN= 0 XMIN= 250 YMIN= 0  
AVERAGE VALUE= 177875739645

Figure 8.5  
Rain water mixing ratio for level 13 after 5 hours.

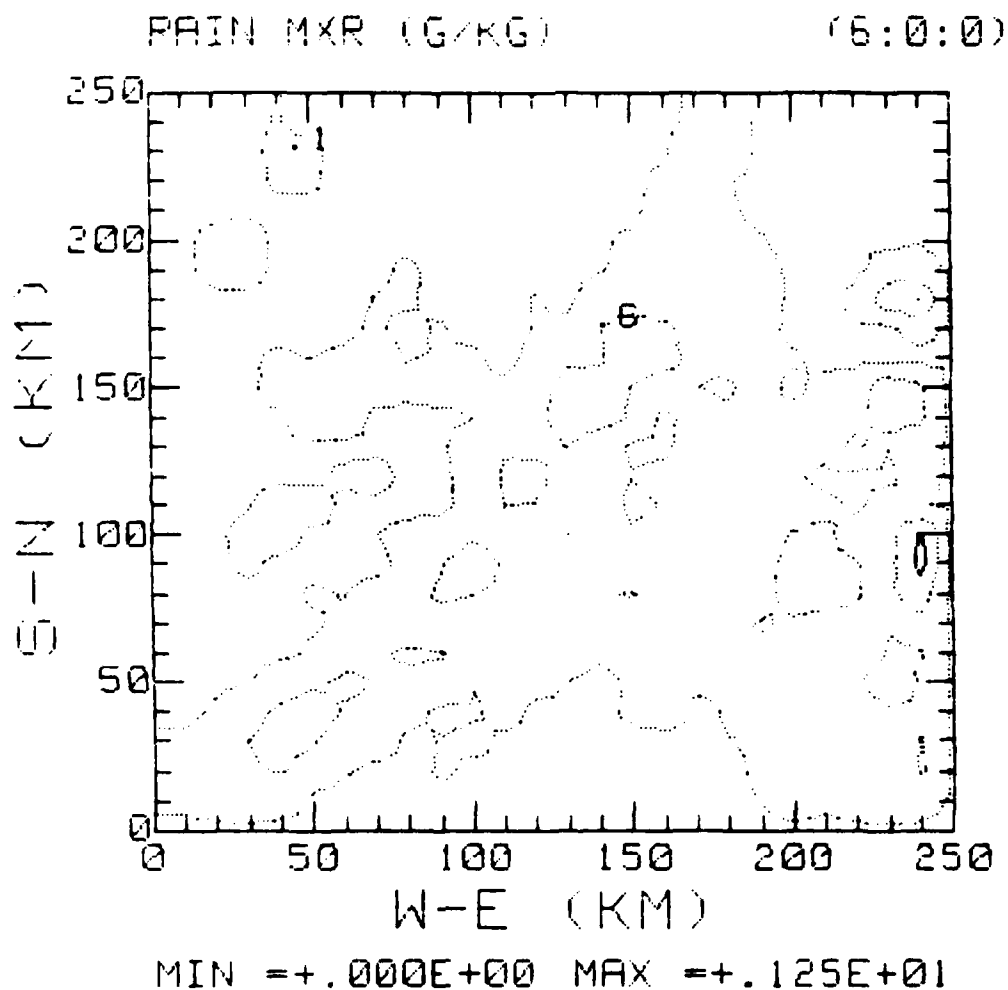
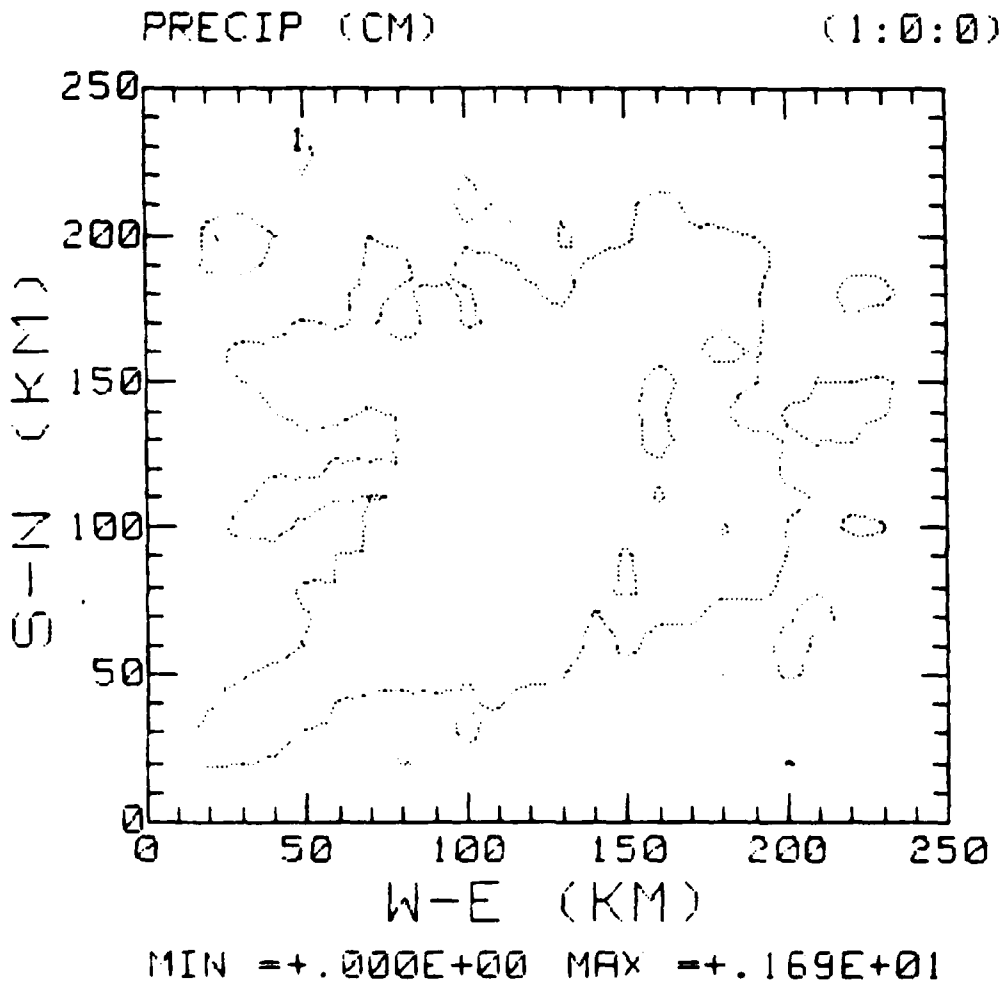
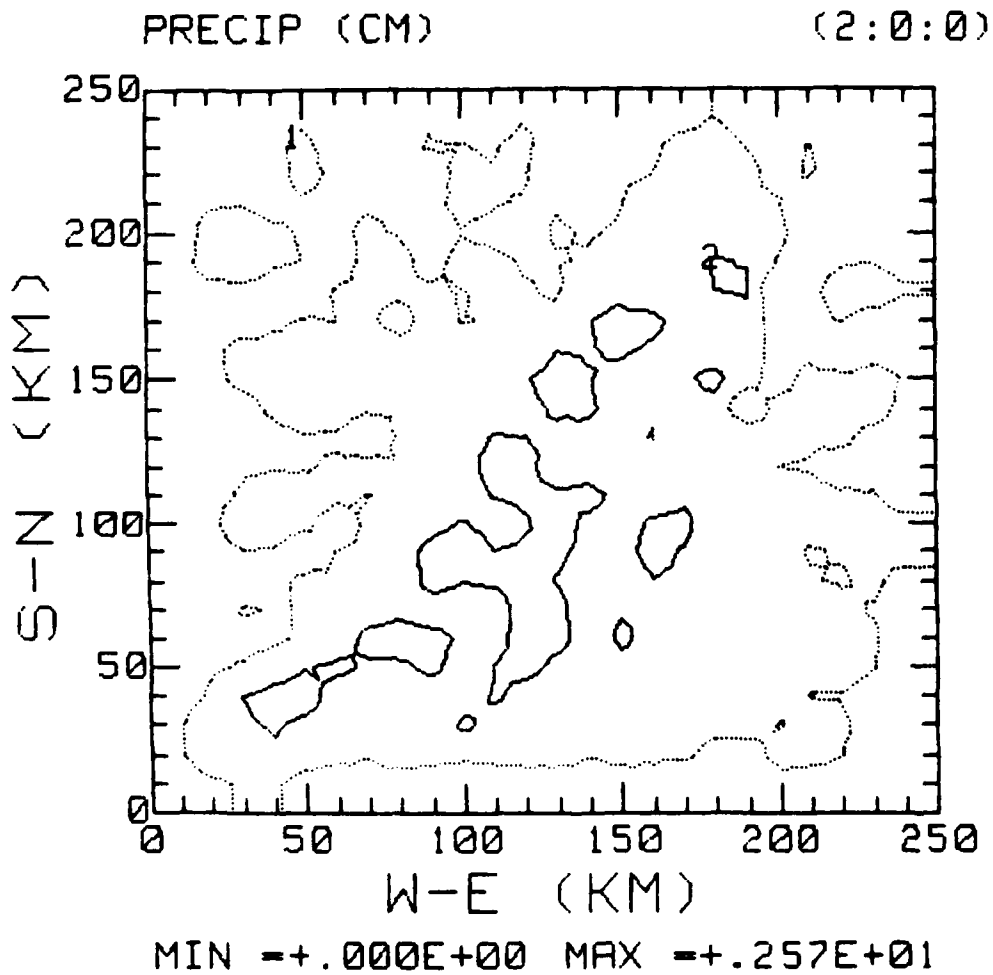


Figure 8.6  
Rain water mixing ratio for level 13 after 6 hours.



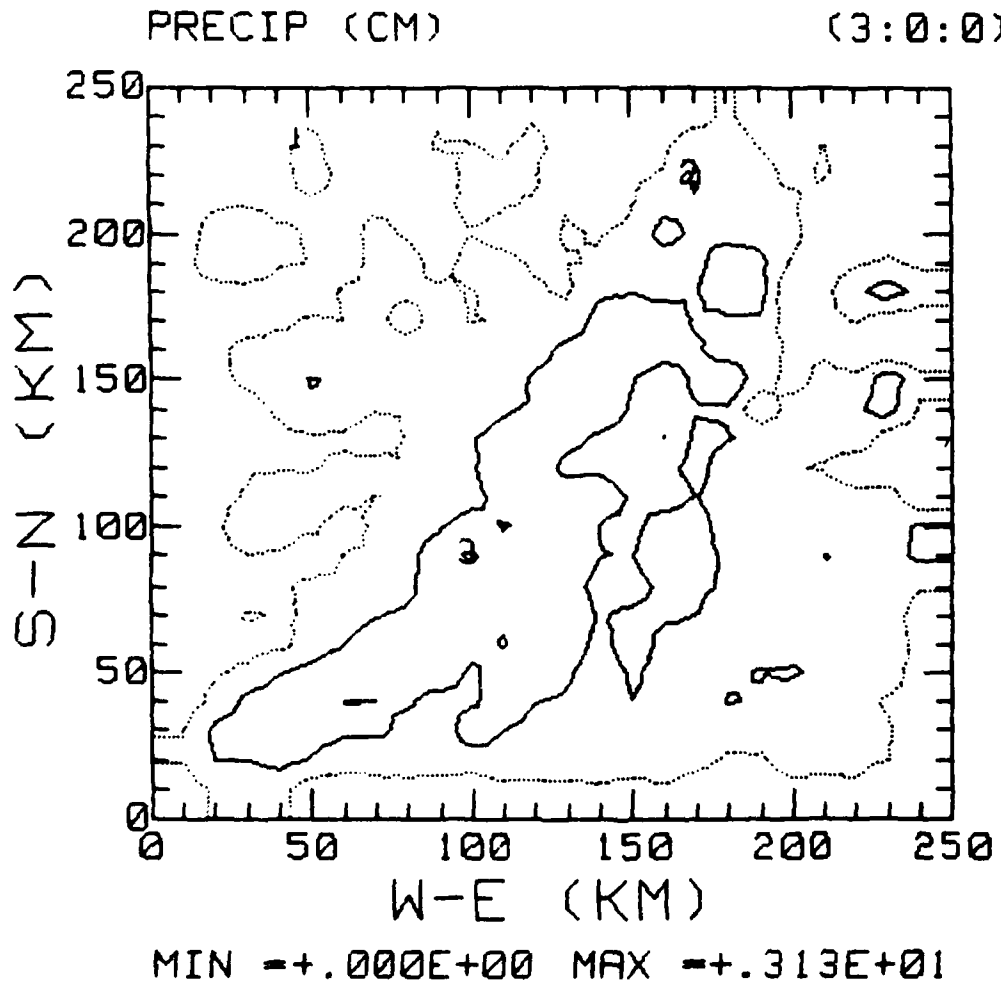
MAX=	1.63547	XMAX=	130	YMAX=	150
MIN=	0	XMIN=	250	YMIN=	0
AVERAGE VALUE=			77178964497		

Figure 9.1  
Forecast rainfall after 1 hour.



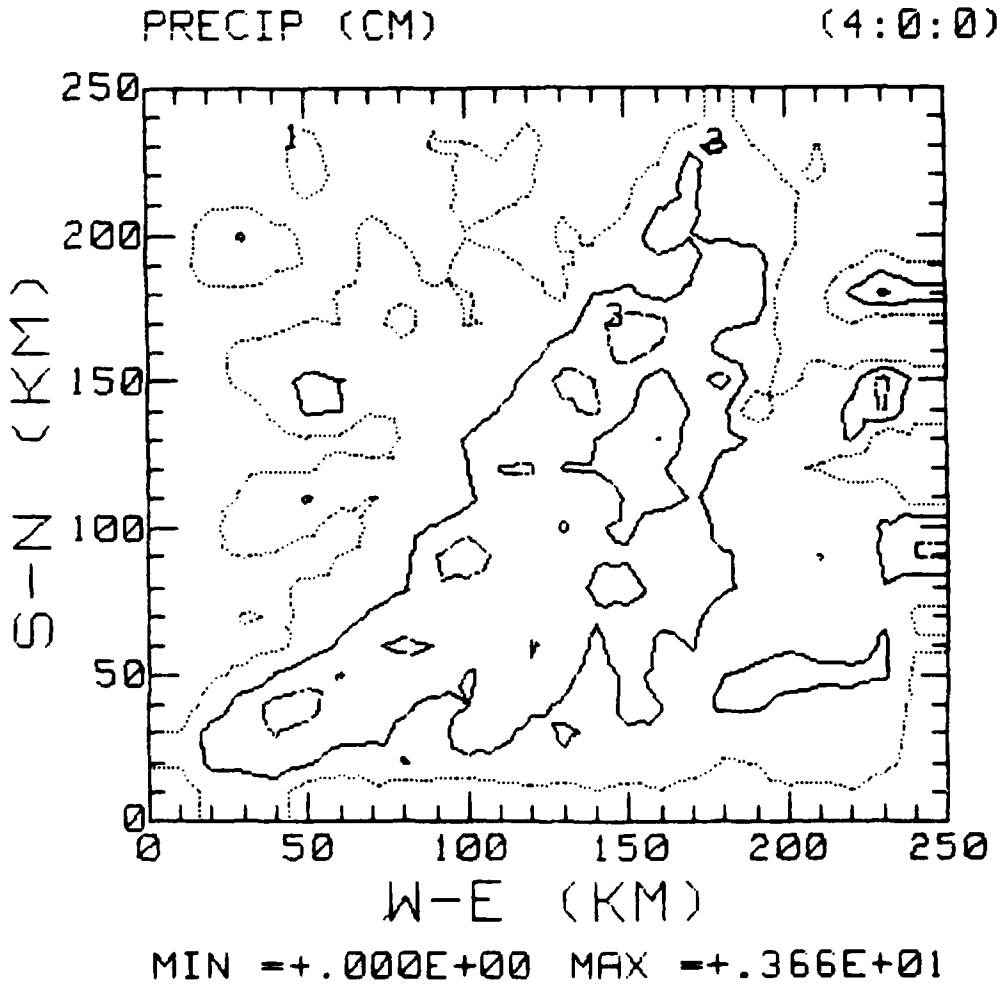
MAX=	2.569308	XMAX=	100	YMAX=	90
MIN=	0	XMIN=	250	YMIN=	220
AVERAGE VALUE=	1.07709638018				

Figure 9.2  
Forecast rainfall after 2 hours.



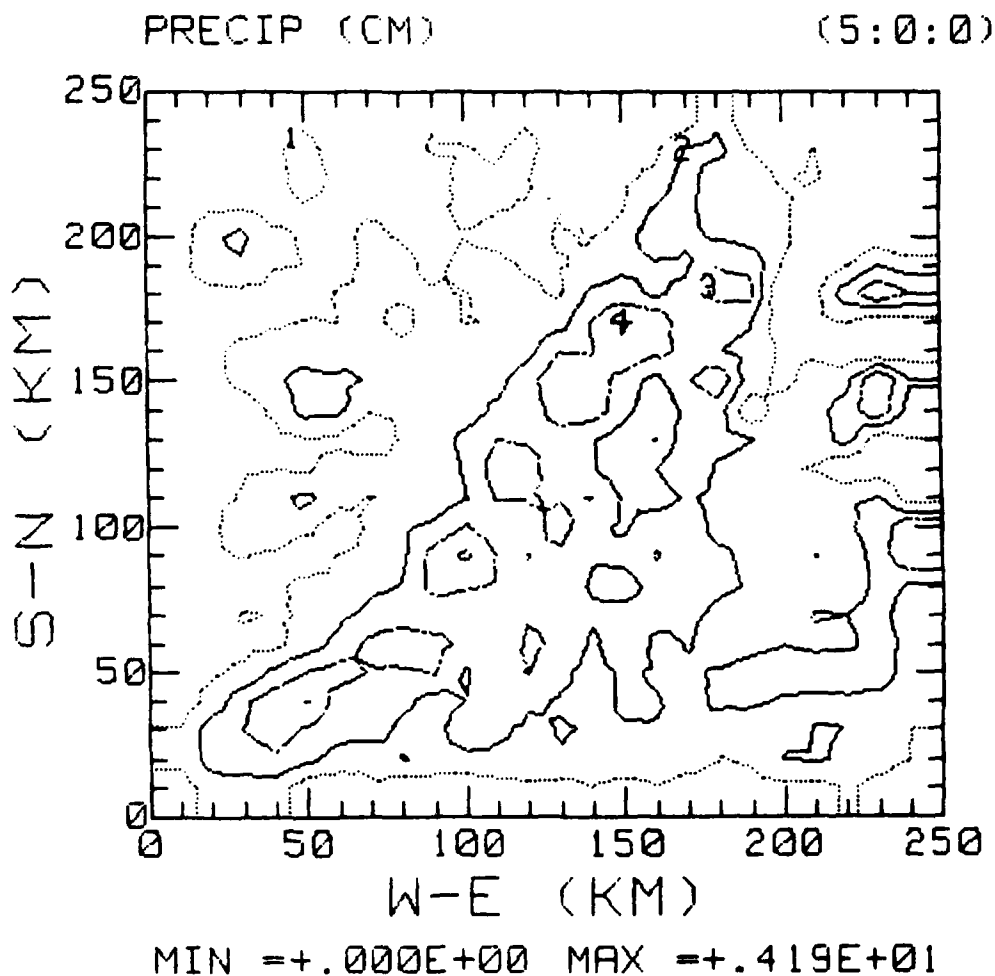
MAX=	3.13094	XMAX=	100	YMAX=	90
MIN=	0	XMIN=	250	YMIN=	220
AVERAGE VALUE=			1.22053258284		

Figure 9.3  
Forecast rainfall after 3 hours.



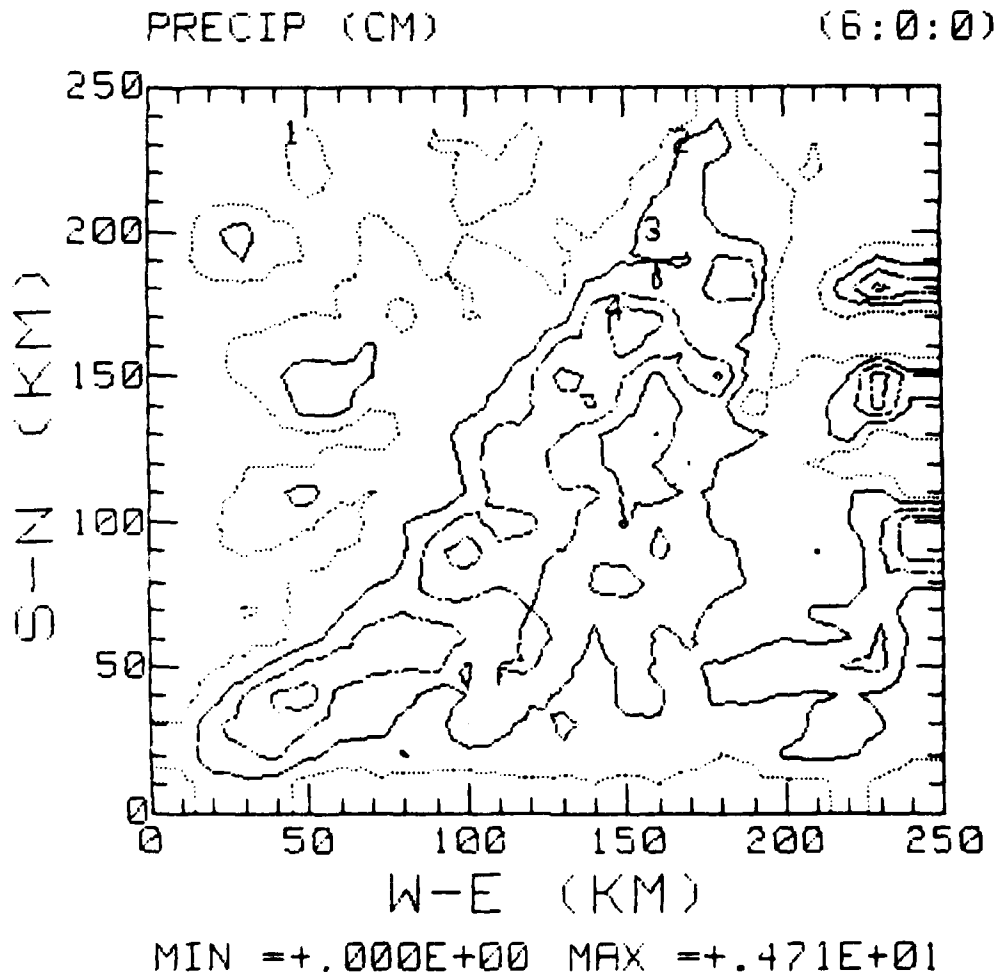
MAX=	3.65796	XMAX=	100	YMAX=	90
MIN=	0	XMIN=	250	YMIN=	220
AVERAGE VALUE=	1.33212508432				

Figure 9.4  
Forecast rainfall after 4 hours.



MAX=	4.186144	XMAX=	100	YMAX=	90
MIN=	0	XMIN=	250	YMIN=	220
AVERAGE VALUE=	1.42727654734				

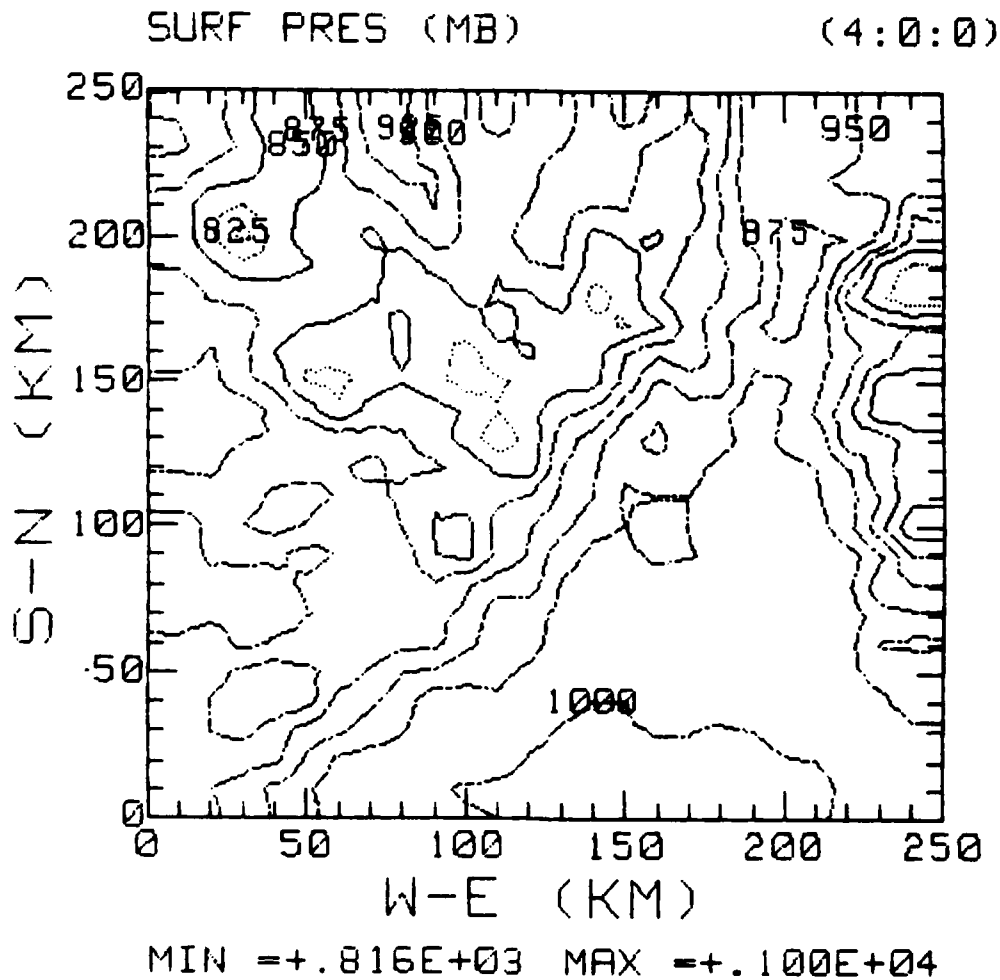
Figure 9.5  
Forecast rainfall after 5 hours.



MAX=	4.714965	XMAX=	100	YMAX=	90
MIN=	0	XMIN=	250	YMIN=	220
AVERAGE VALUE=	1.51357595858				

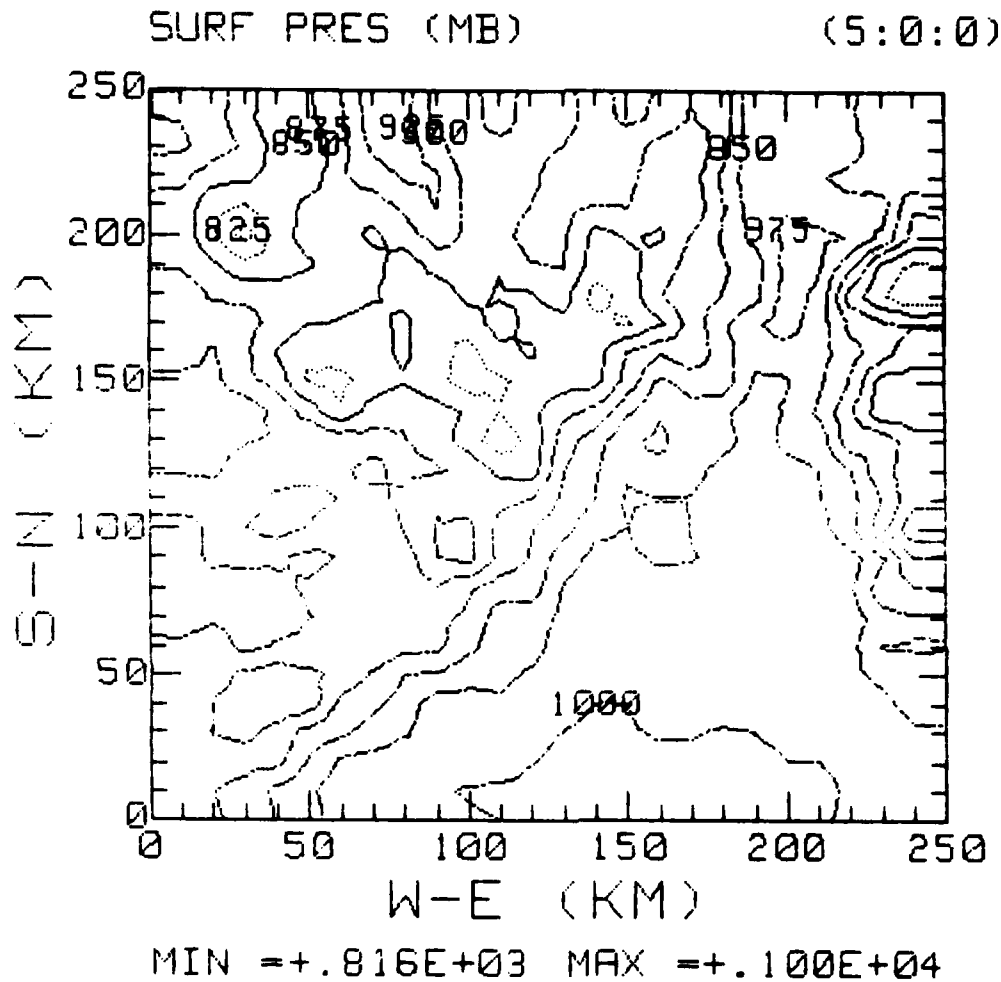
Figure 9.6  
Forecast rainfall after 6 hours.





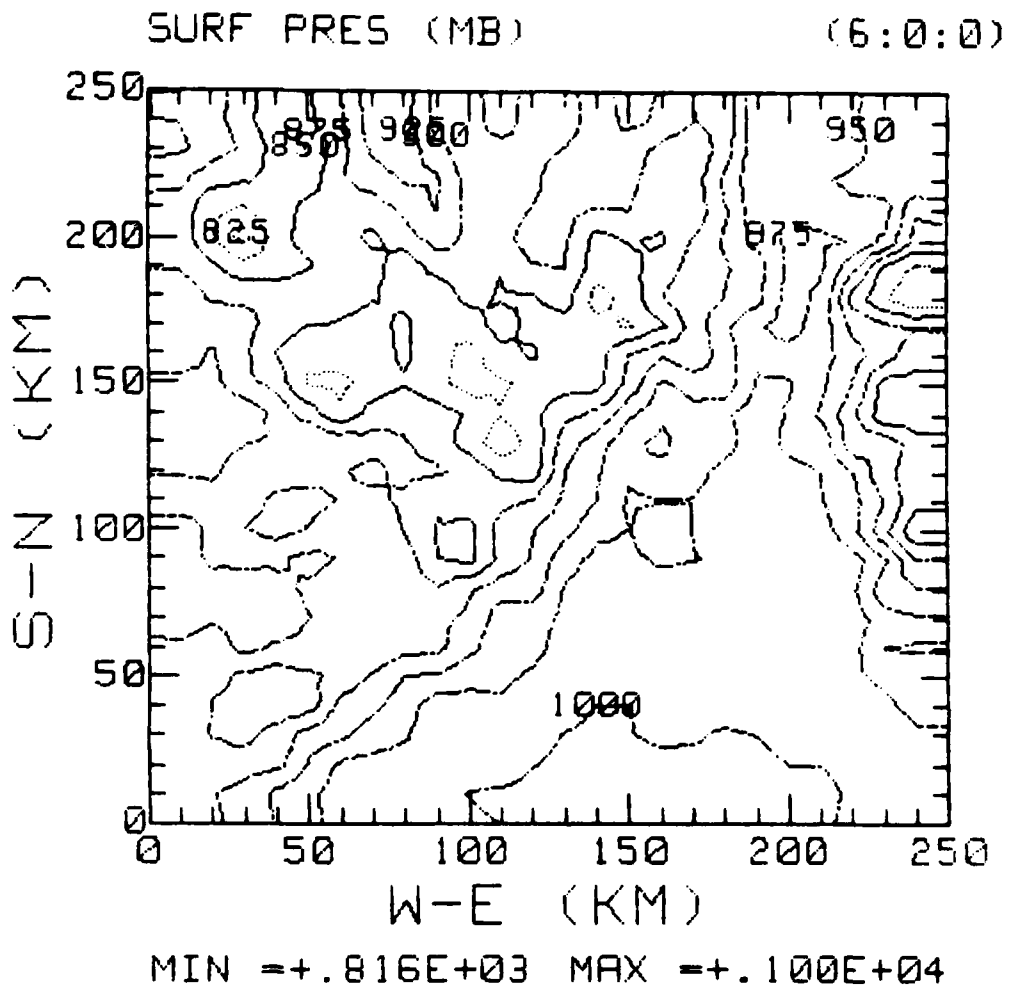
MAX=	1003.94382949	XMAX=	120	YMAX=	10
MIN=	816.26946705	XMIN=	30	YMIN=	200
AVERAGE VALUE=	930.764363926				

Figure 10.1  
Surface Pressure after 4 hours.



MAX=	1004.10106346	XMAX=	160	YMAX=	10
MIN=	816.04688238	XMIN=	30	YMIN=	200
AVERAGE VALUE=	930.717701694				

Figure 10.2  
Surface Pressure after 5 hours.



MAX=	1003.43513804	XMAX=	160	YMAX=	10
MIN=	816.15877444	XMIN=	30	YMIN=	200
AVERAGE VALUE=	930.710306615				

Figure 10.3  
Surface Pressure after 6 hours.

DATE= 15 Oct 1985 TIME= 13 59 50  
The distance from the southern boundary in kilometers = 170

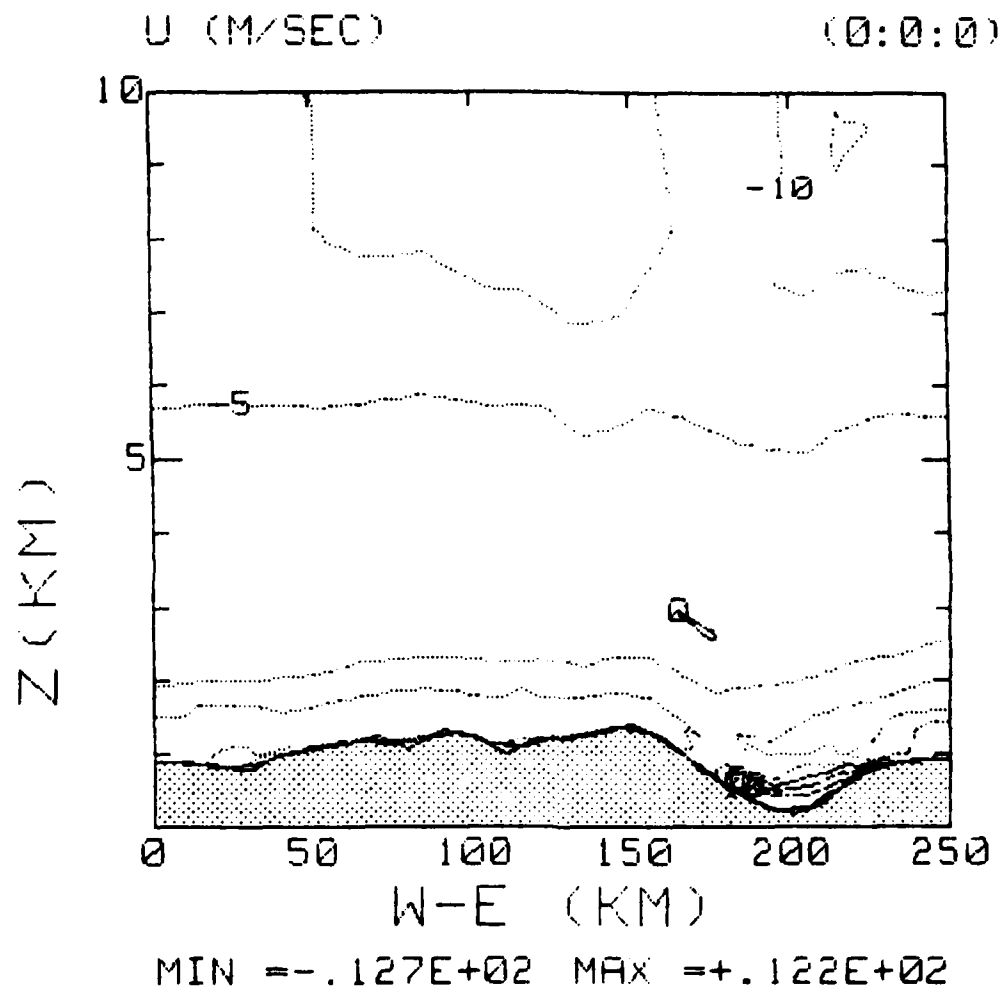


Figure 11.1  
West-East vertical cross section of u, 170 km from  
Southern boundary at time 0.

The distance from the southern boundary in kilometers = 170

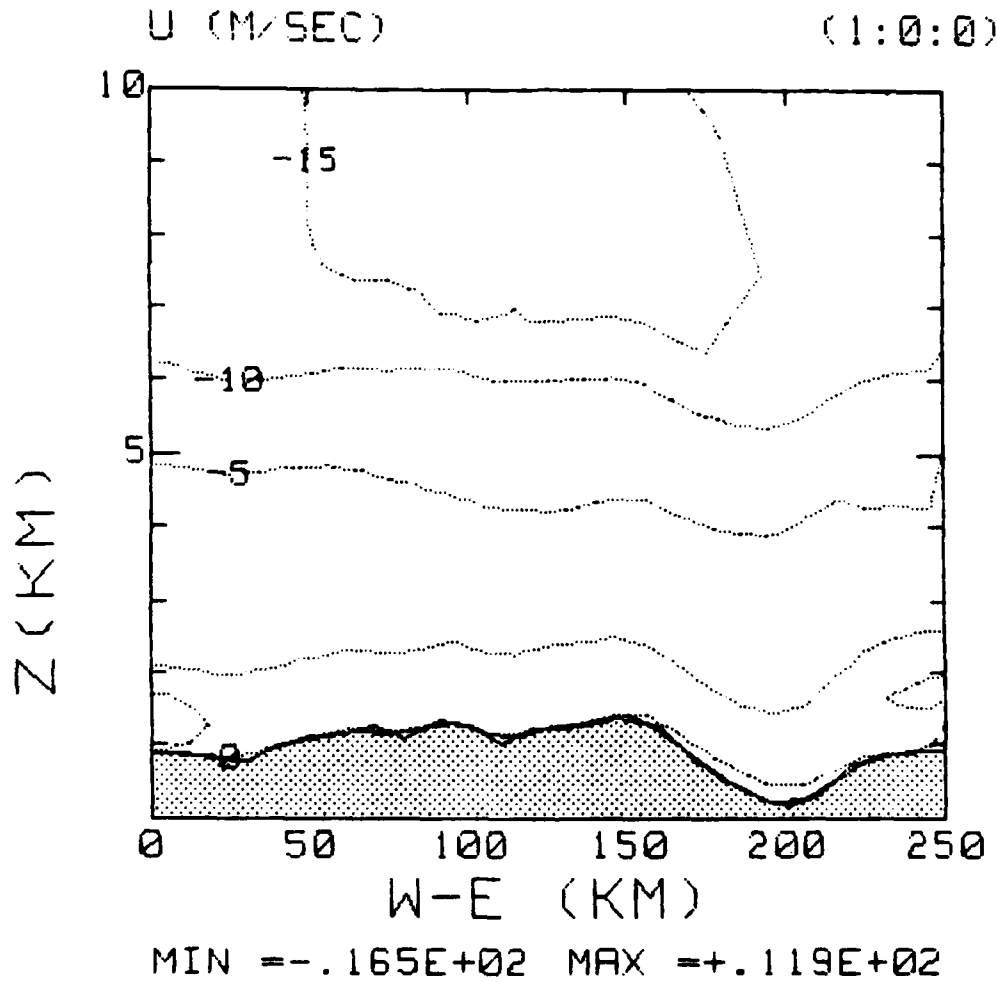


Figure 11.2  
Same as Figure 11.1 but after 1 hour.

The distance from the southern boundary in kilometers = 170

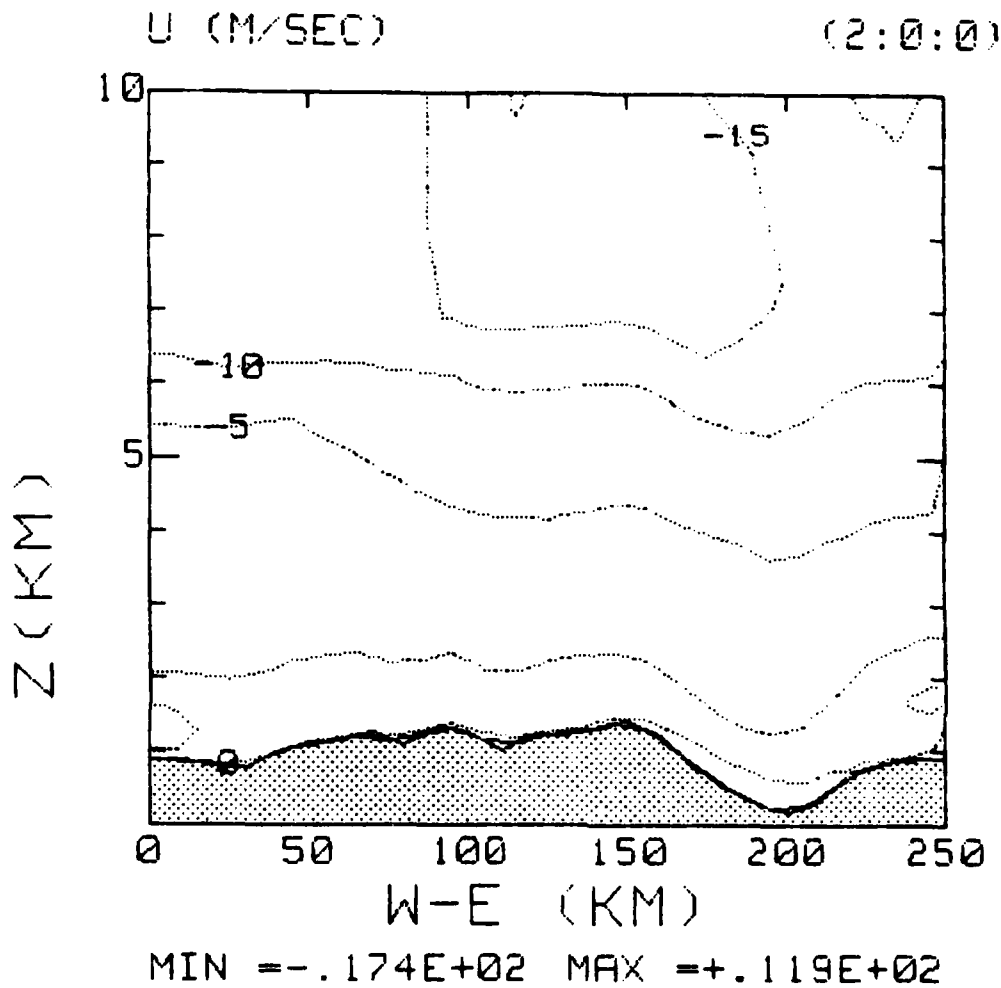


Figure 11.3  
Same as Figure 11.1 but after 2 hours.

The distance from the southern boundary in kilometers = 170

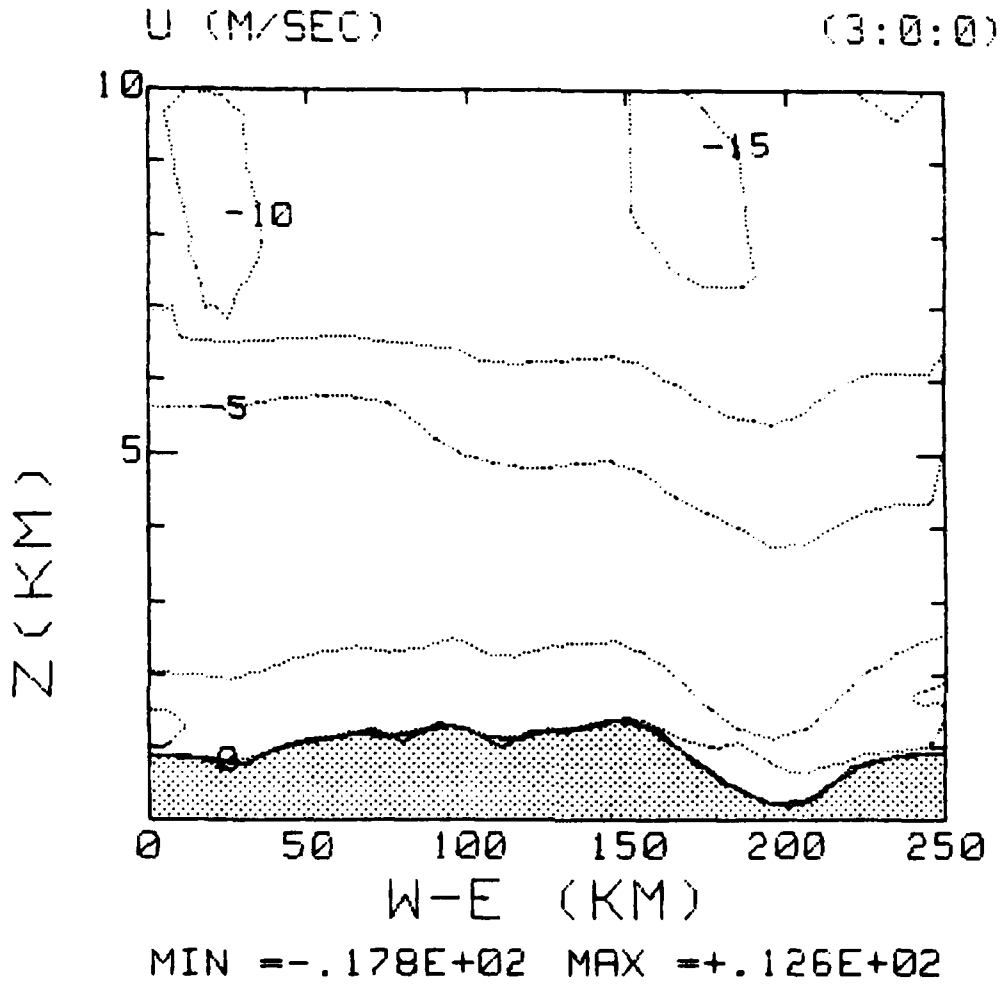


Figure 11.4  
Same as Figure 11.1 but after 3 hours.

The distance from the southern boundary in kilometers = 170

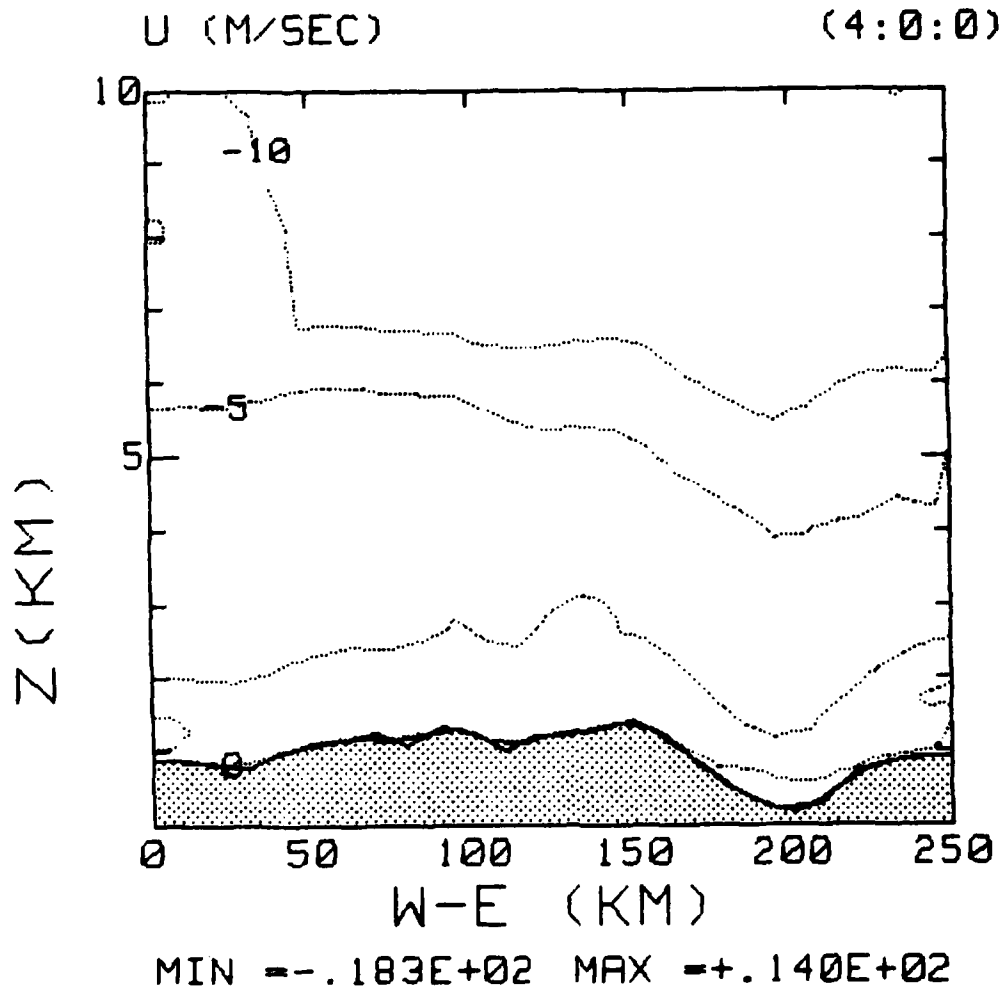


Figure 11.5  
Same as Figure 11.1 but after 4 hours.



The distance from the southern boundary in kilometers = 170

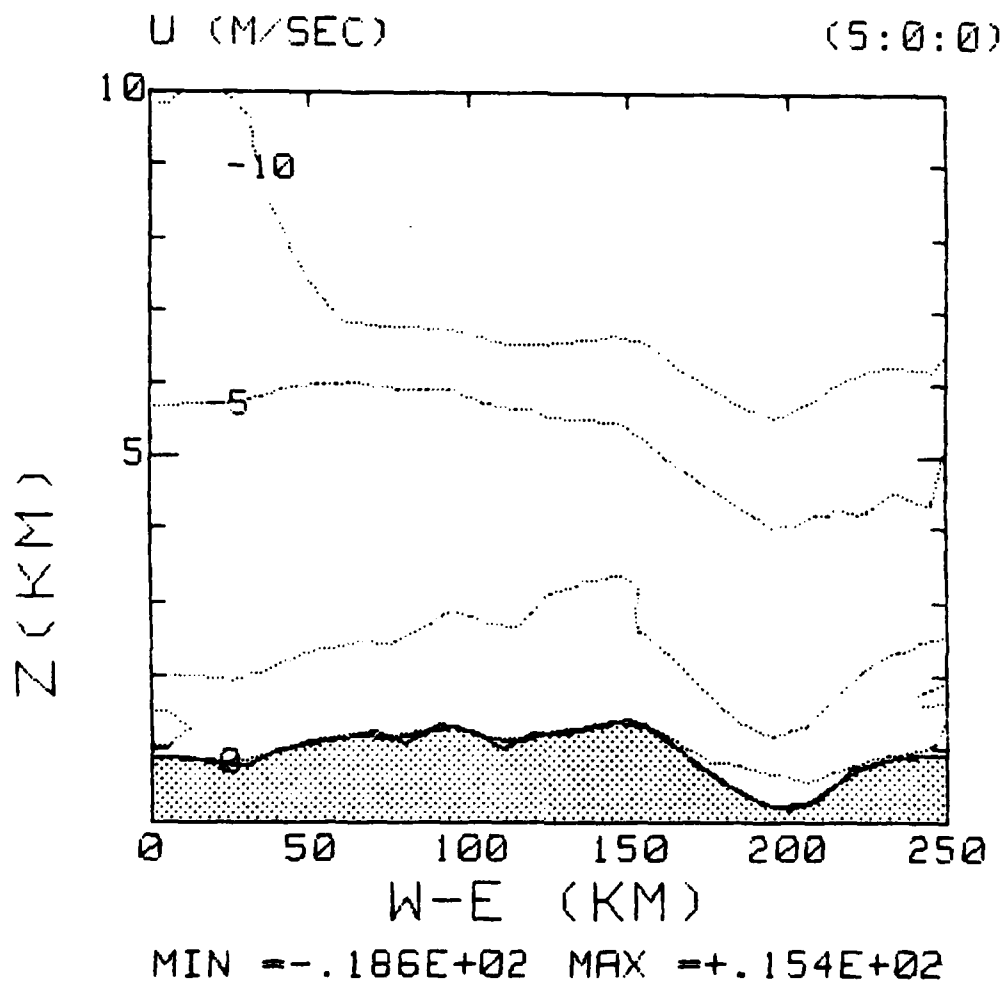


Figure 11.6  
Same as Figure 11.1 but after 5 hours.

The distance from the southern boundary in kilometers = 170

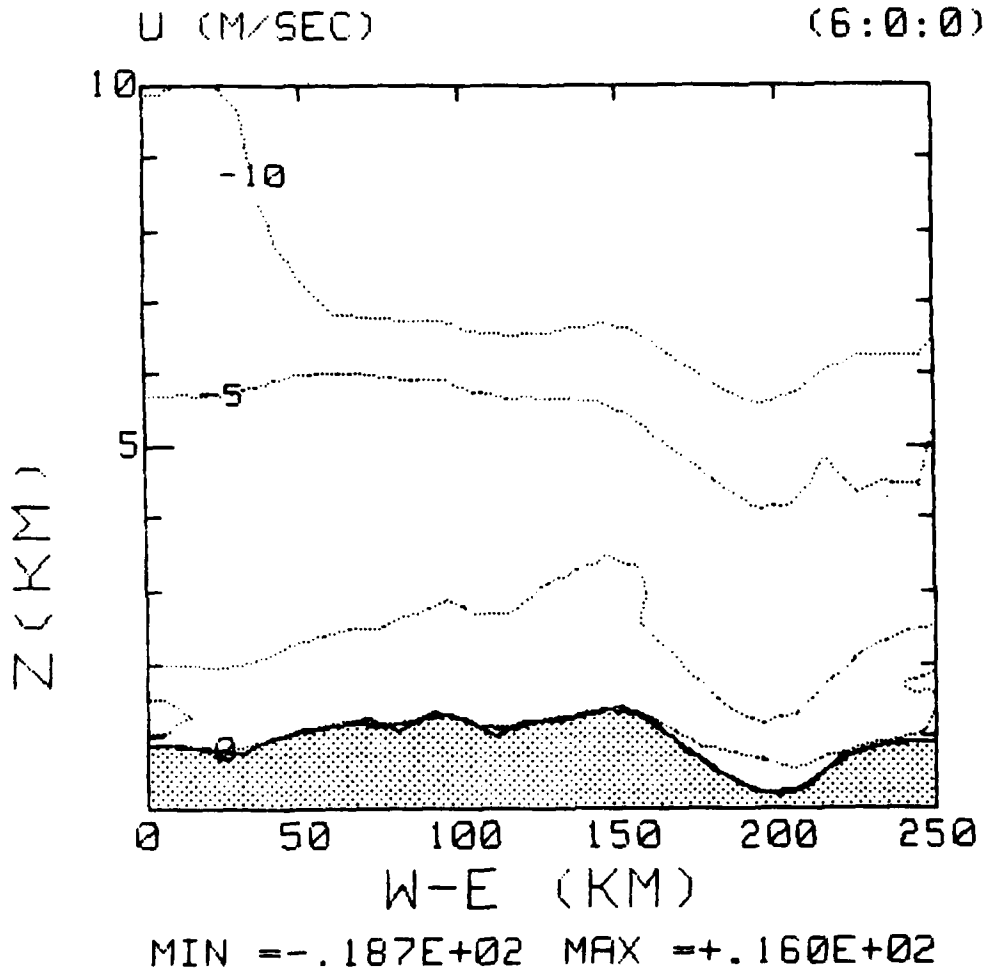


Figure 11.7  
Same as Figure 11.1 but after 6 hours.

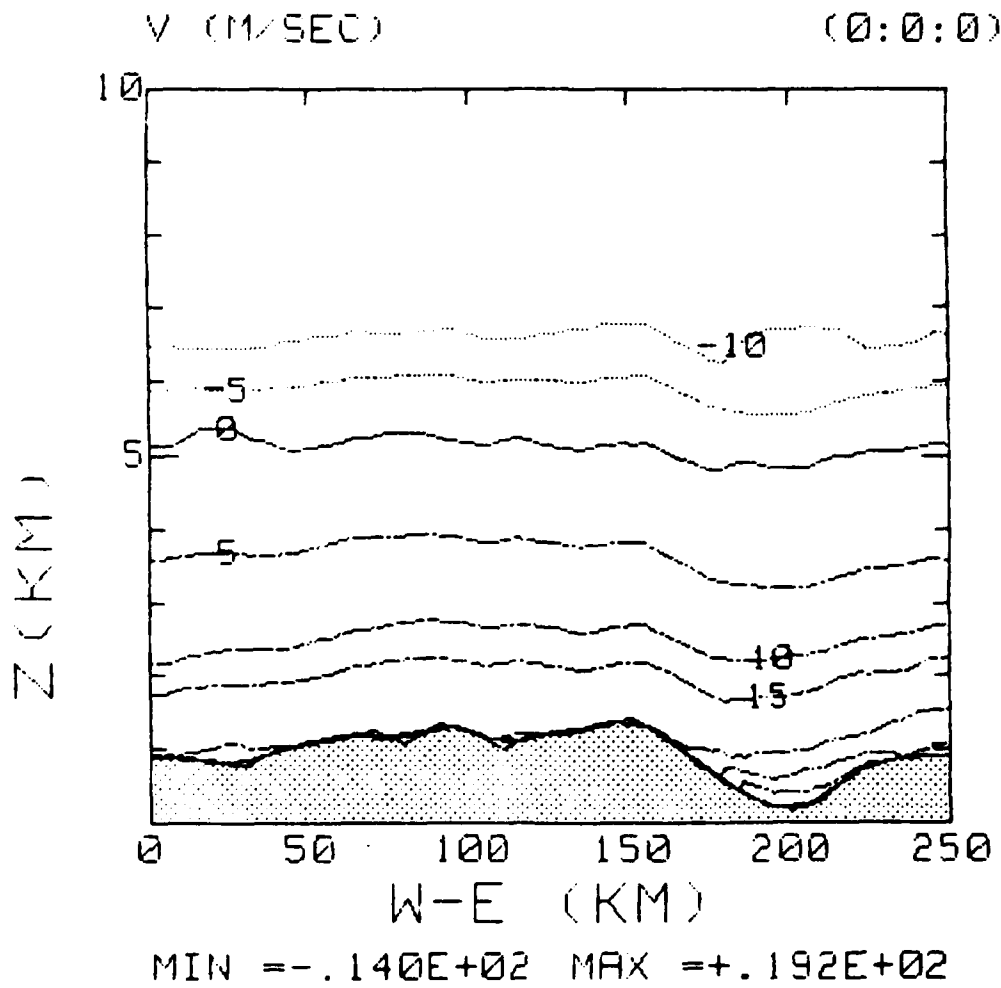


Figure 12.1  
West-East vertical cross section of V, 170 km from southern boundary at time 0.

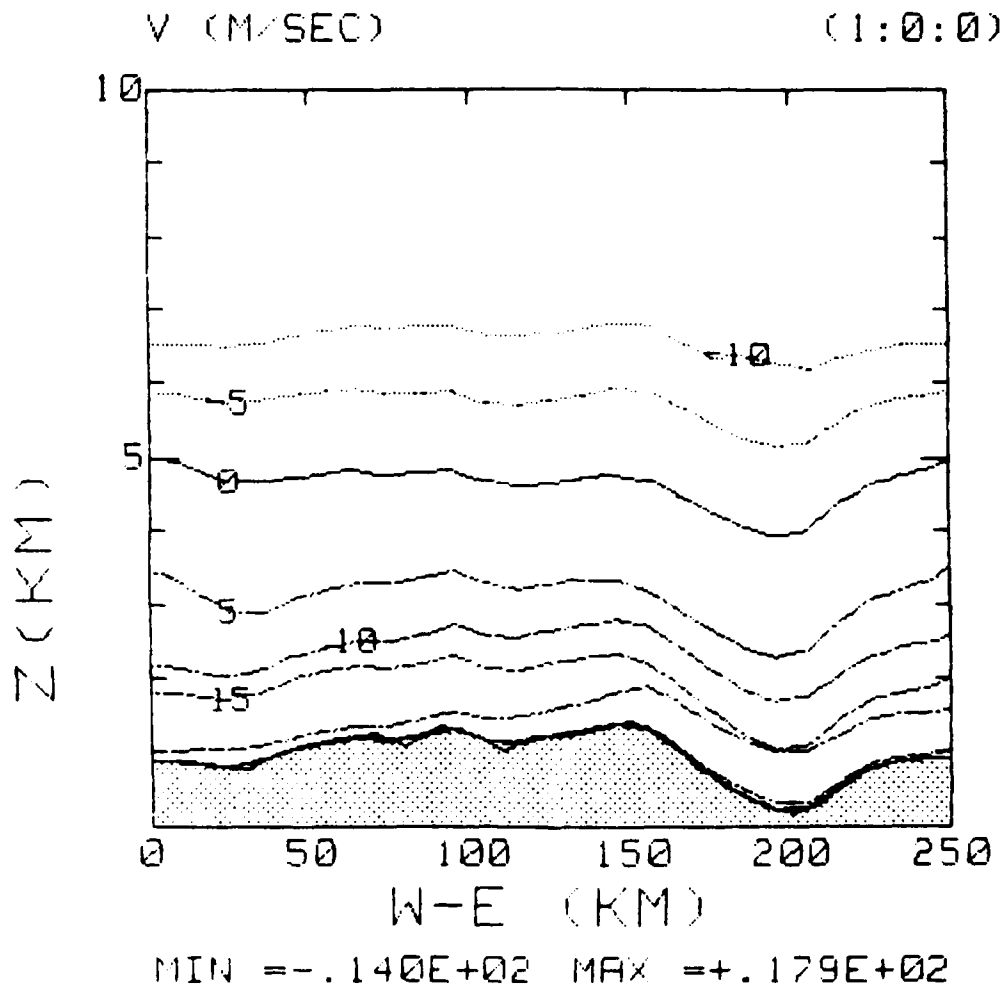


Figure 12.2  
Same as Figure 12.1 but after 1 hour.

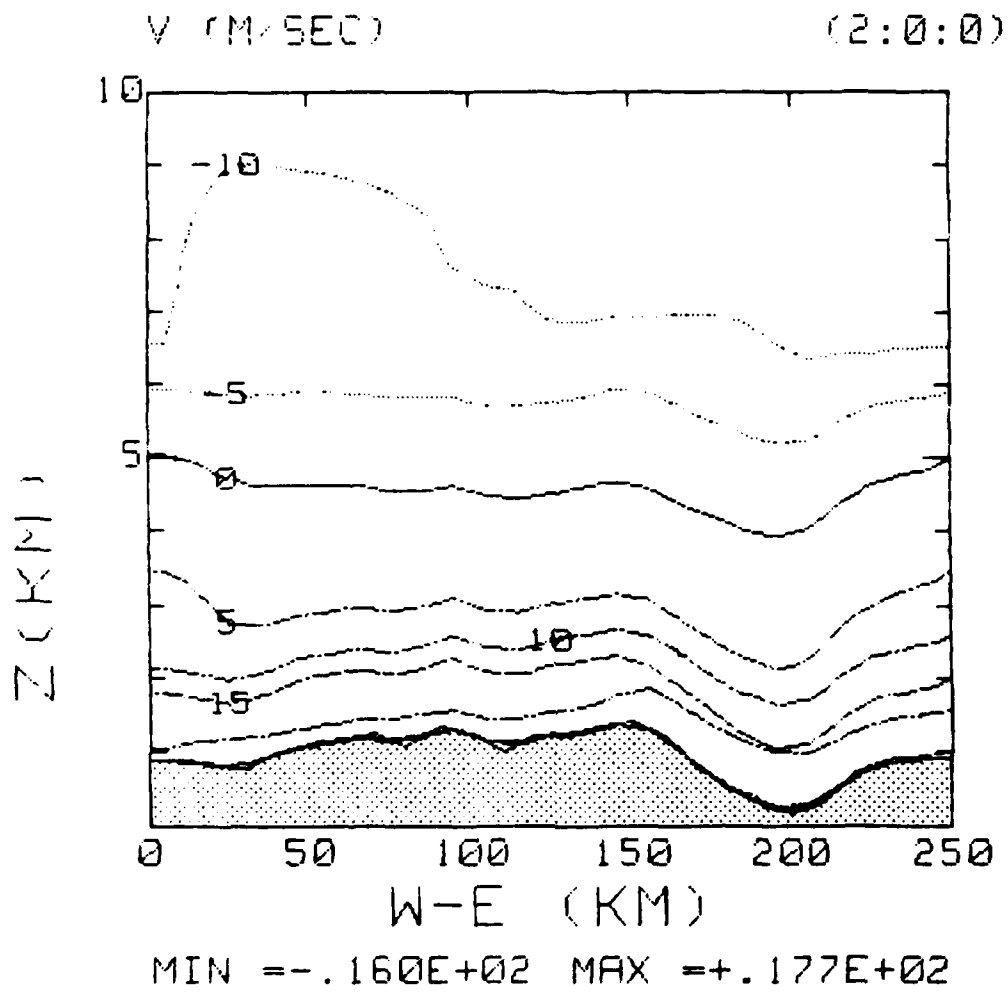


Figure 12.3  
Same as Figure 12.1 but after 2 hours.

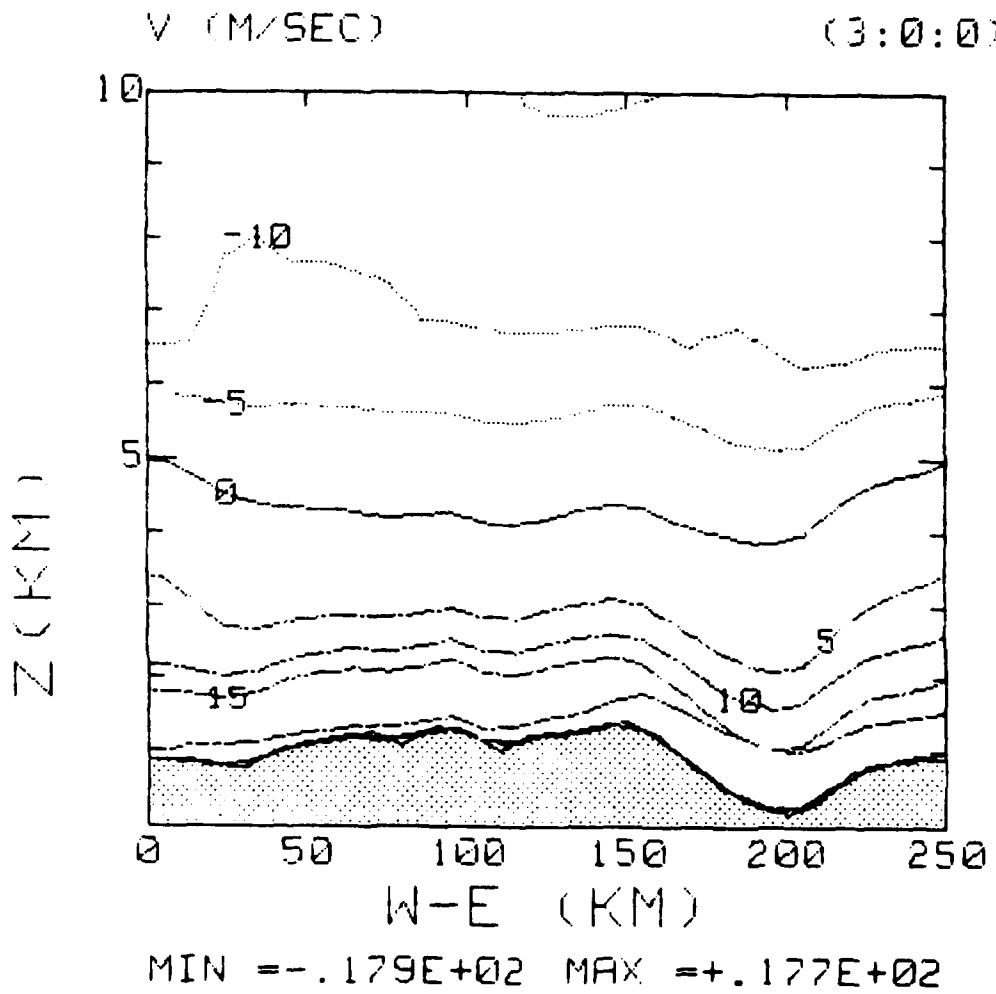


Figure 12.4  
Same as Figure 12.1 but after 3 hours.

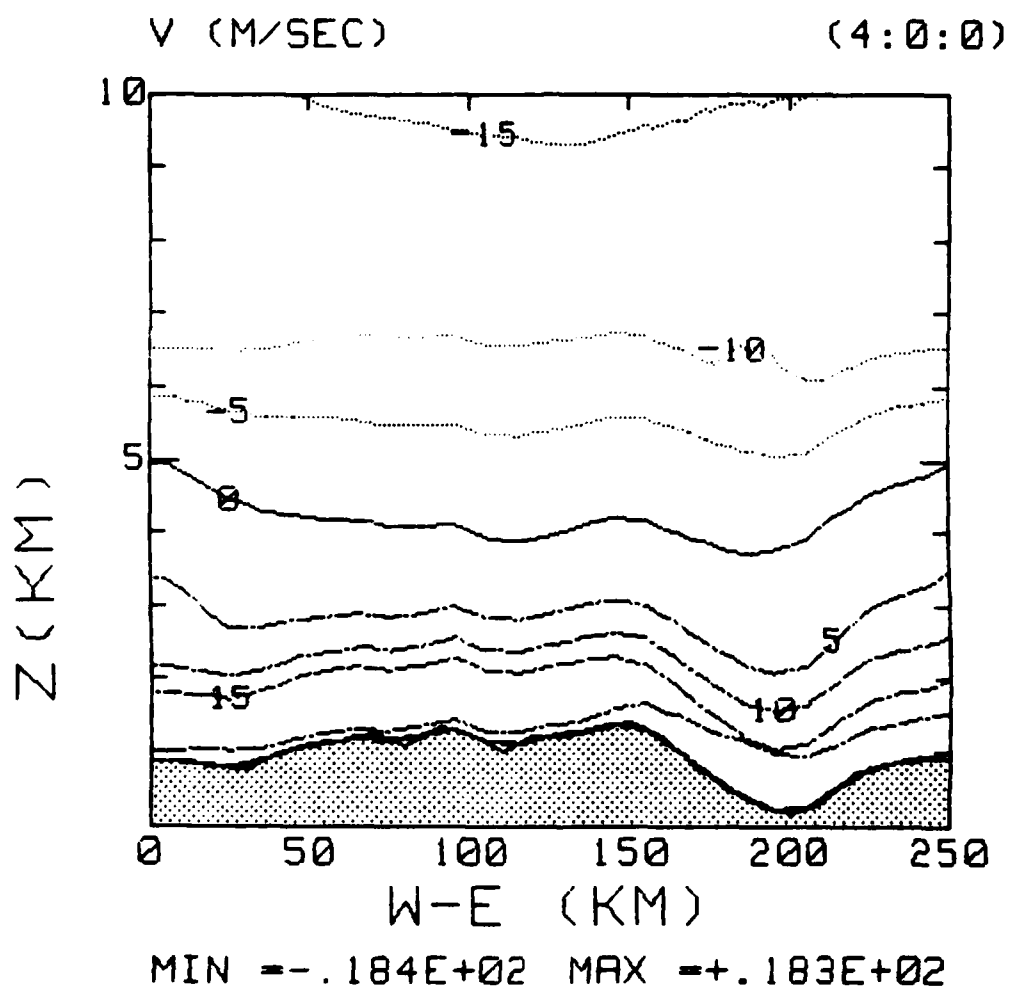


Figure 12.5  
Same as Figure 12.1 but after 4 hours.

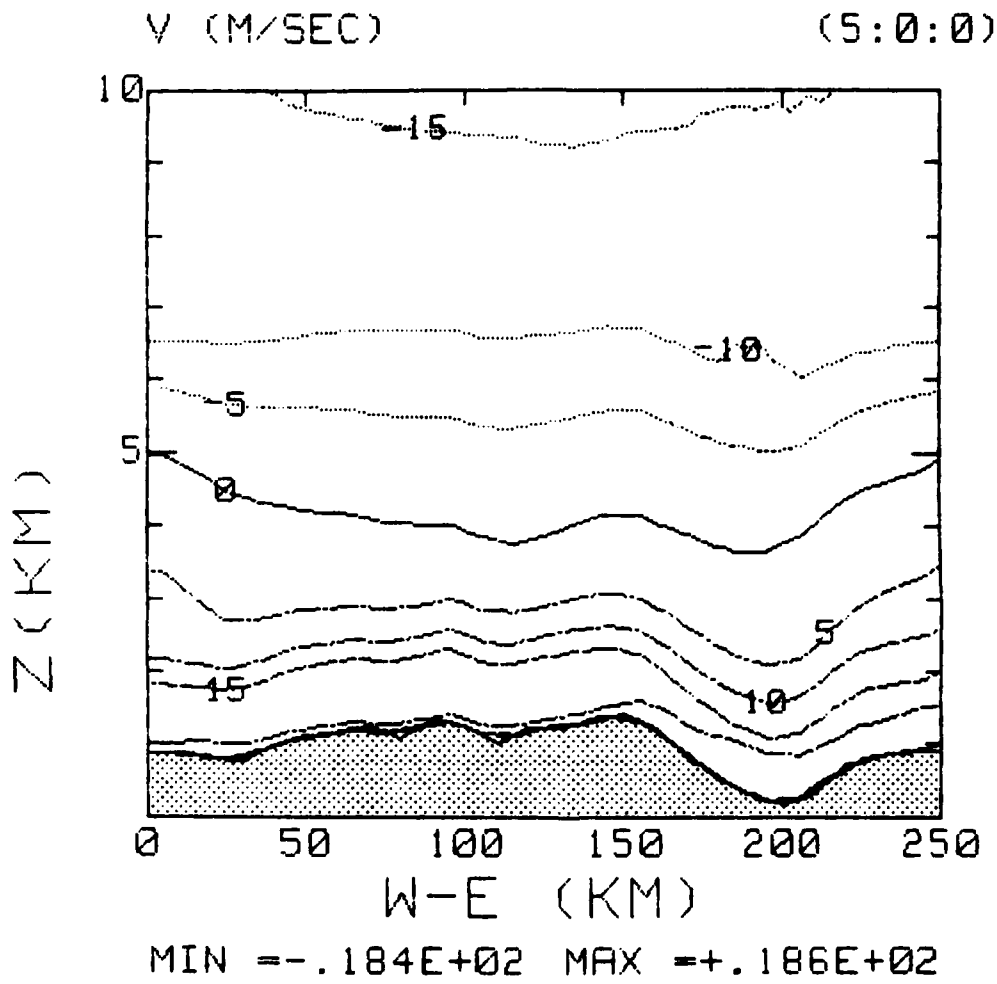


Figure 12.6  
Same as Figure 12.1 but after 5 hours.



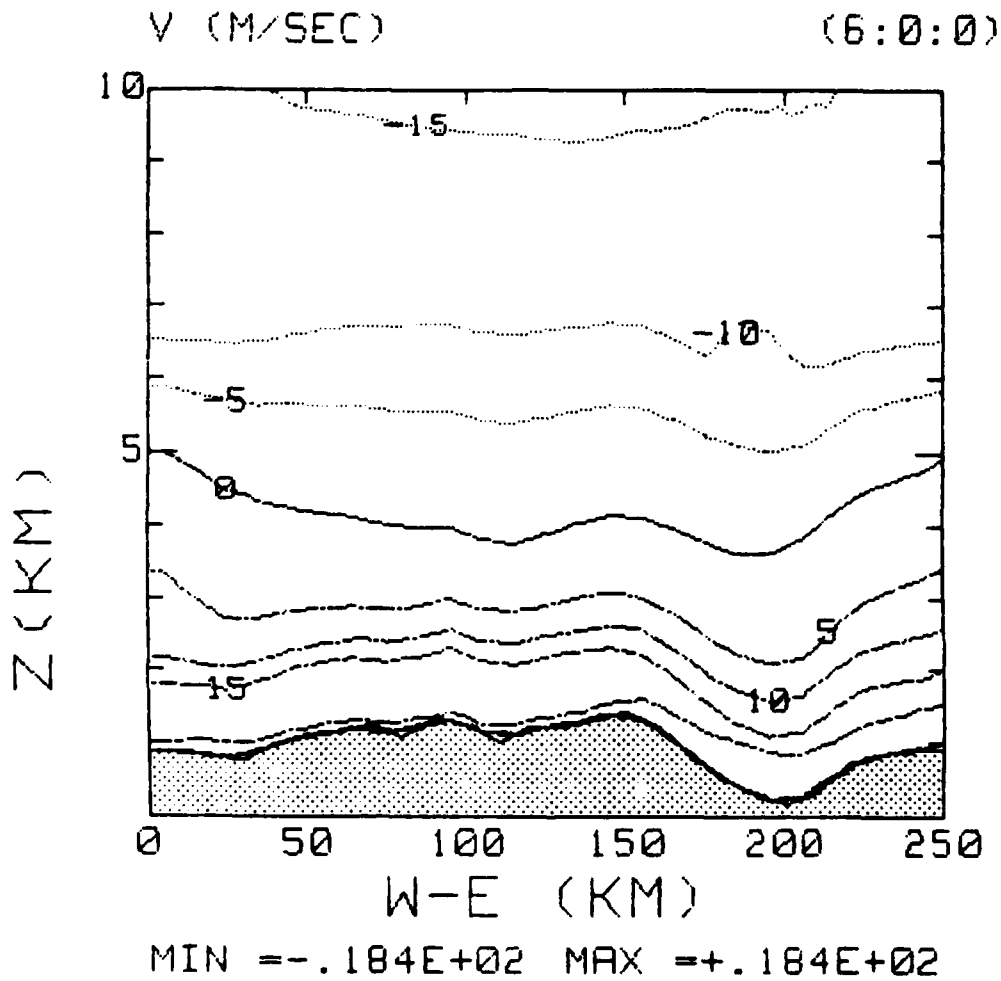


Figure 12.7  
Same as Figure 12.1 but after 6 hours.

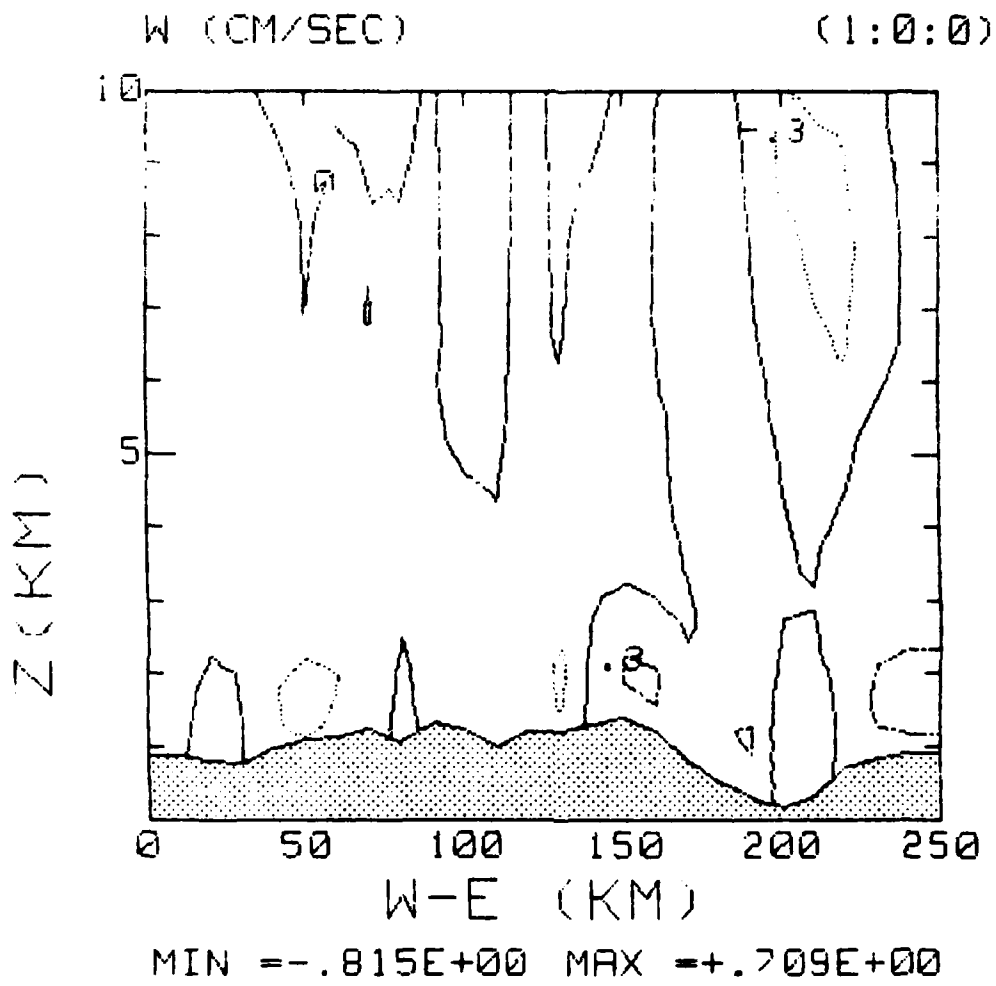


Figure 13.1  
West-East vertical cross section of W, 170 km  
from southern boundary after 1 hour.

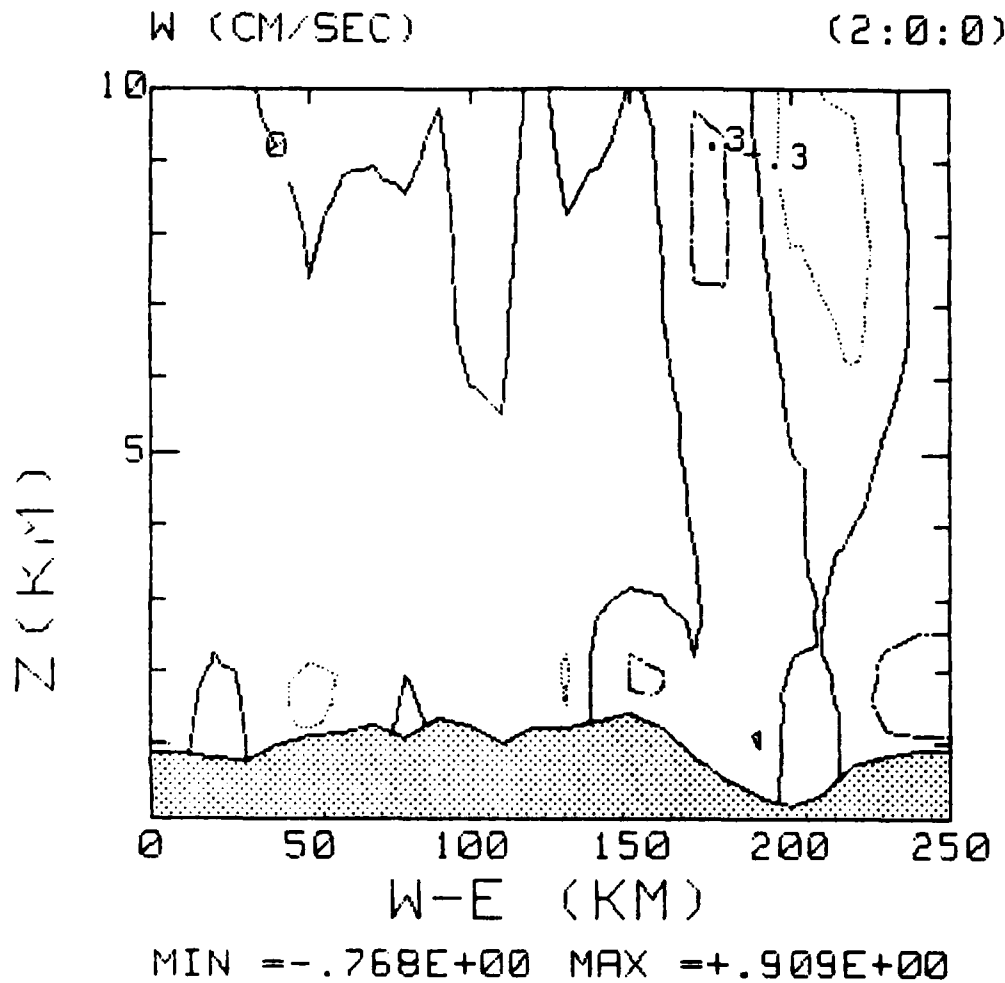


Figure 13.2  
Same as Figure 13.1 but after 2 hours.

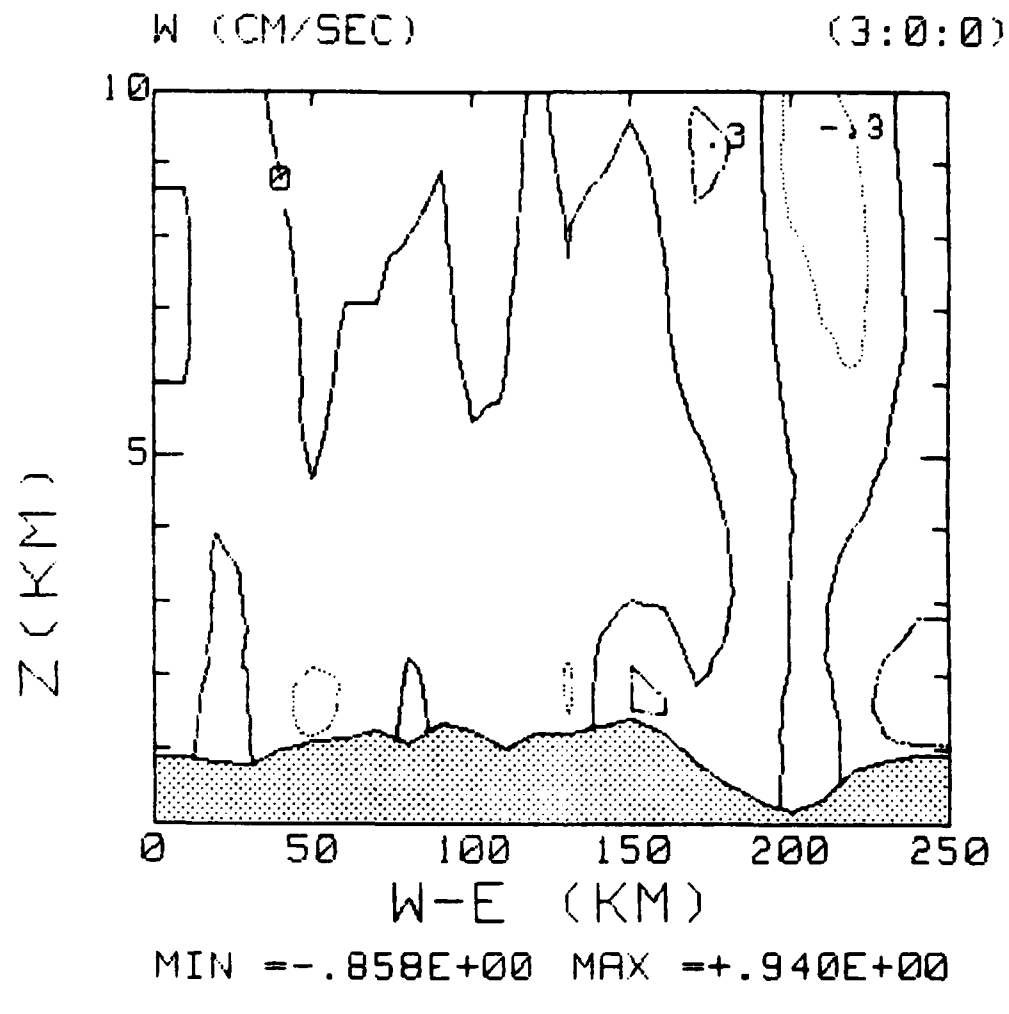


Figure 13.3  
Same as Figure 13.1 but after 3 hours.

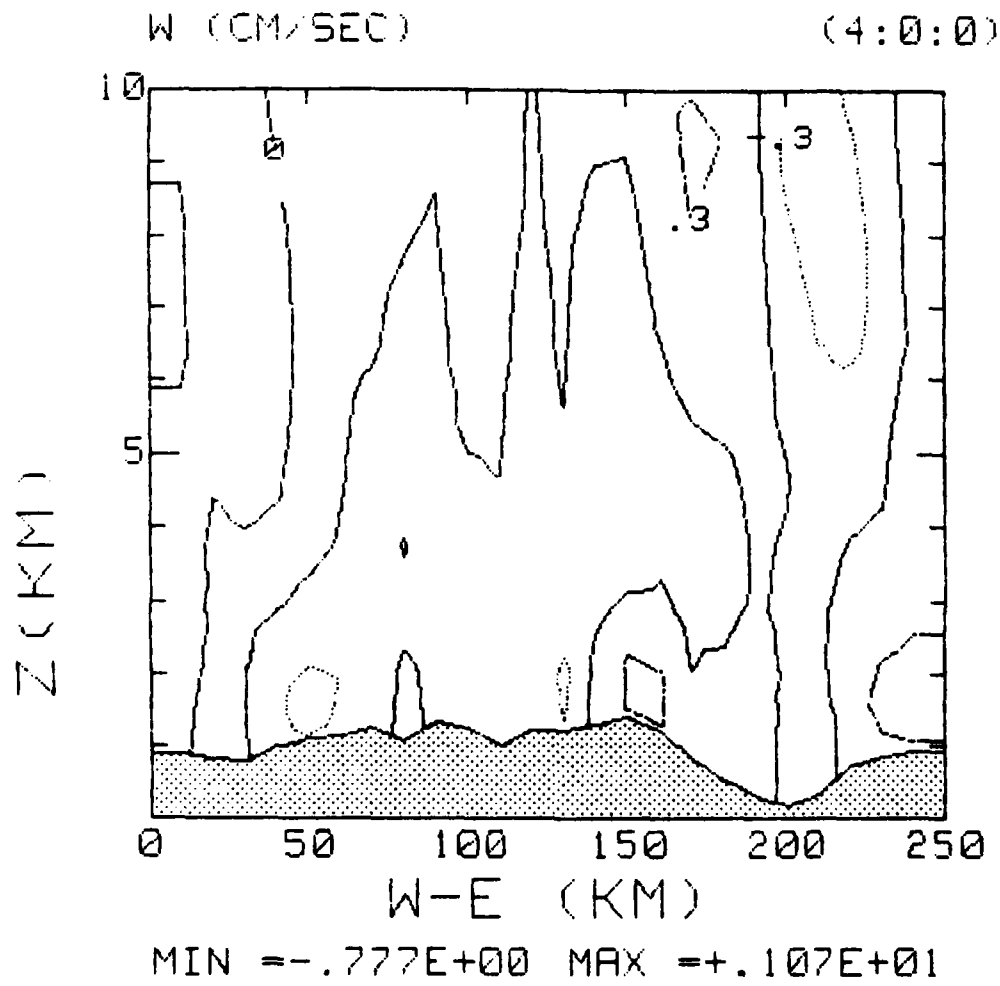


Figure 13.4  
Same as Figure 13.1 but after 4 hours.

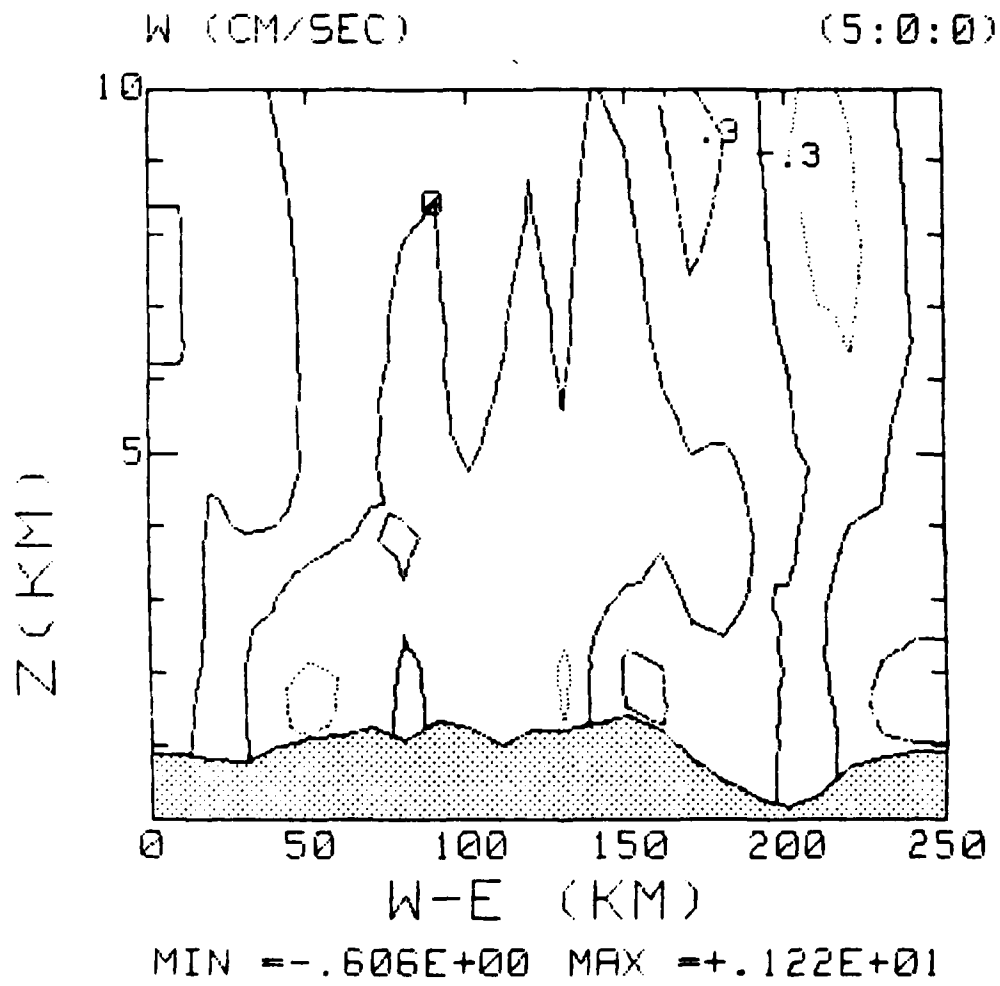


Figure 13.5  
Same as Figure 13.1 but after 5 hours.

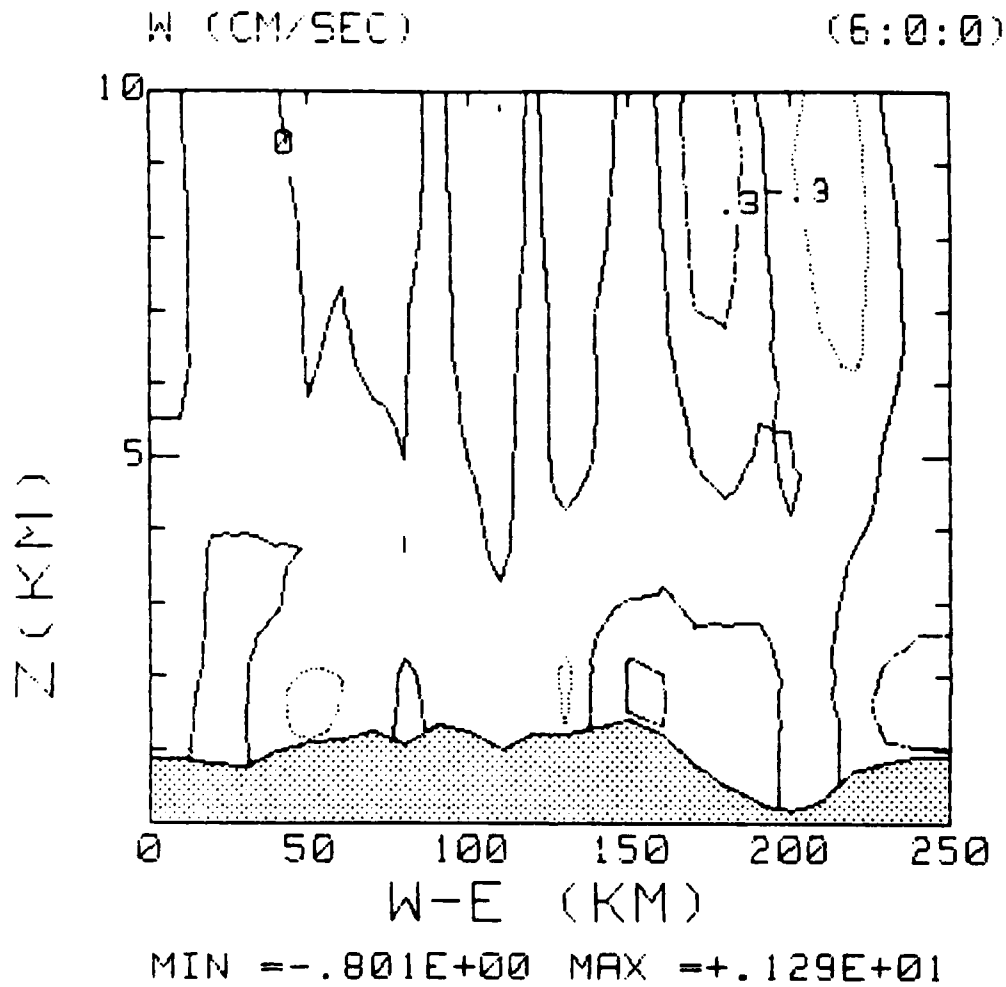


Figure 13.6  
Same as Figure 13.1 but after 6 hours.

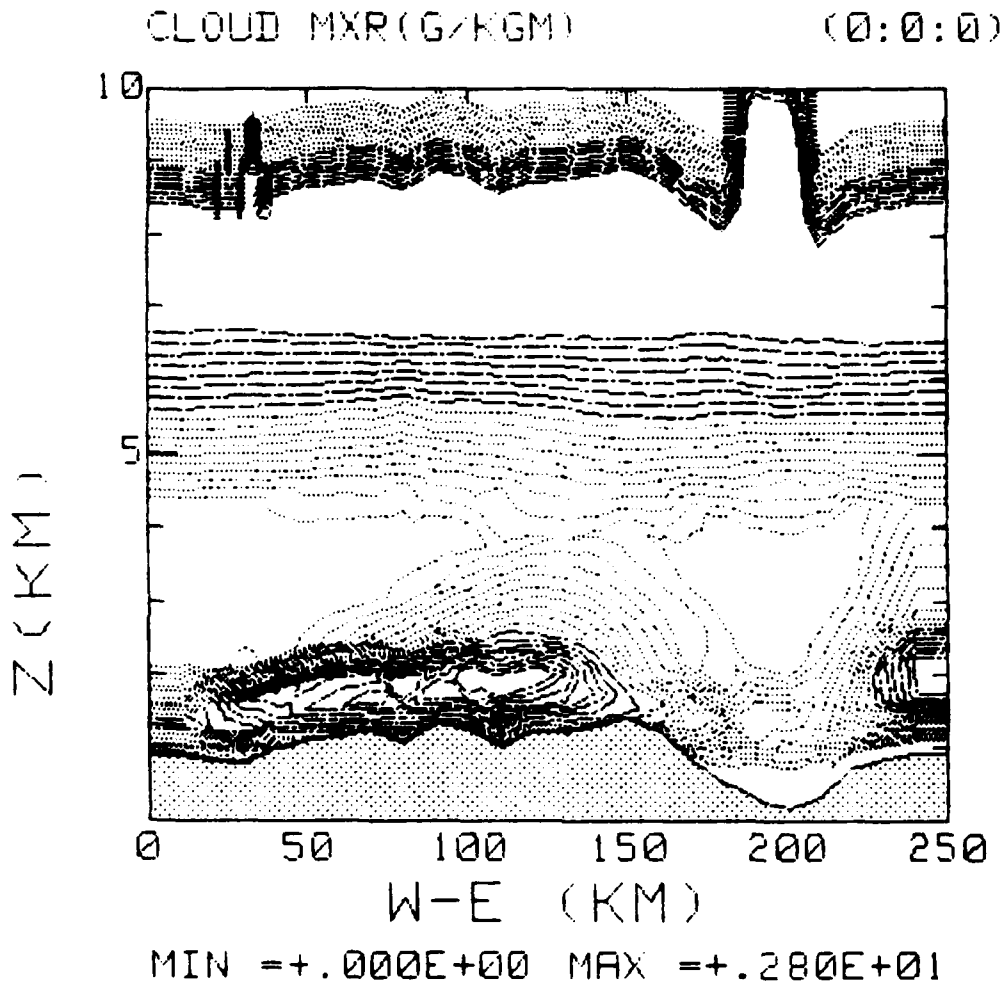


Figure 14.1  
West-East vertical cross section of cloud water  
mixing ratio, 170 km from southern boundary at  
time 0.



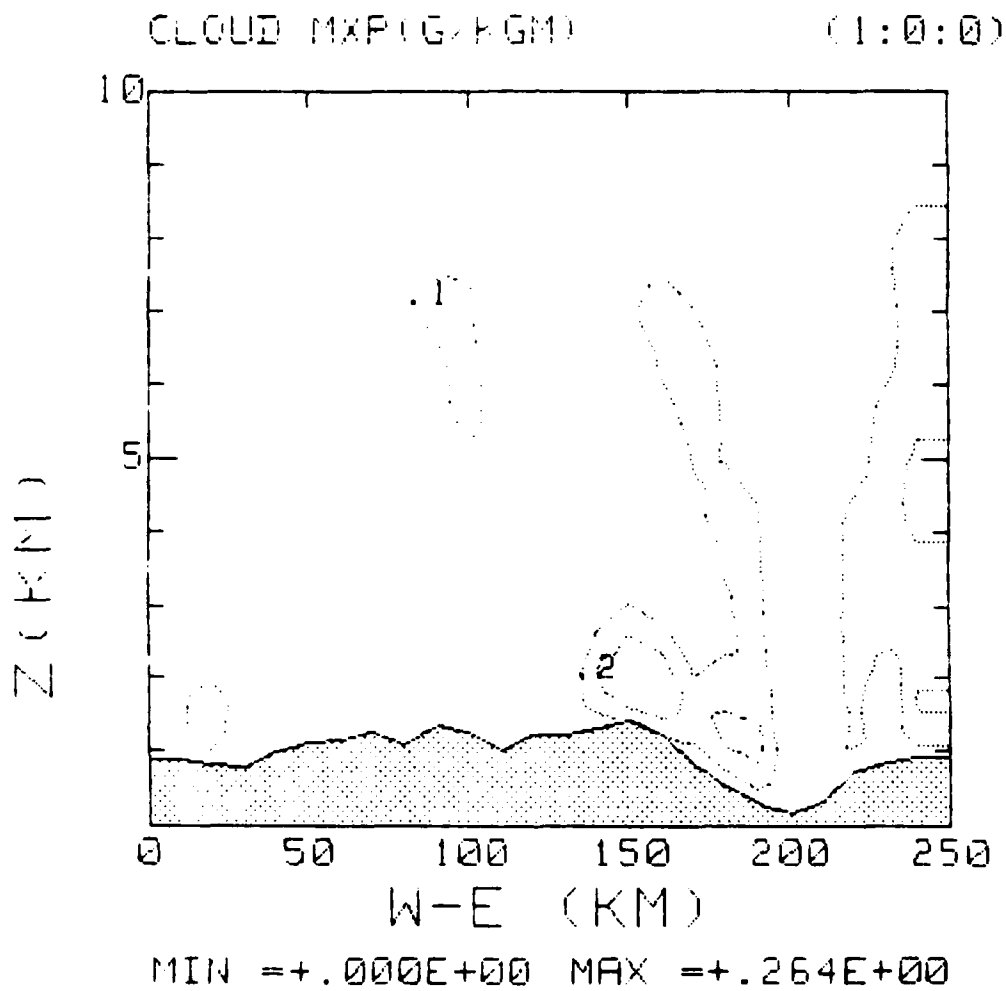


Figure 14.2  
Same as Figure 14.1 but after 1 hour.

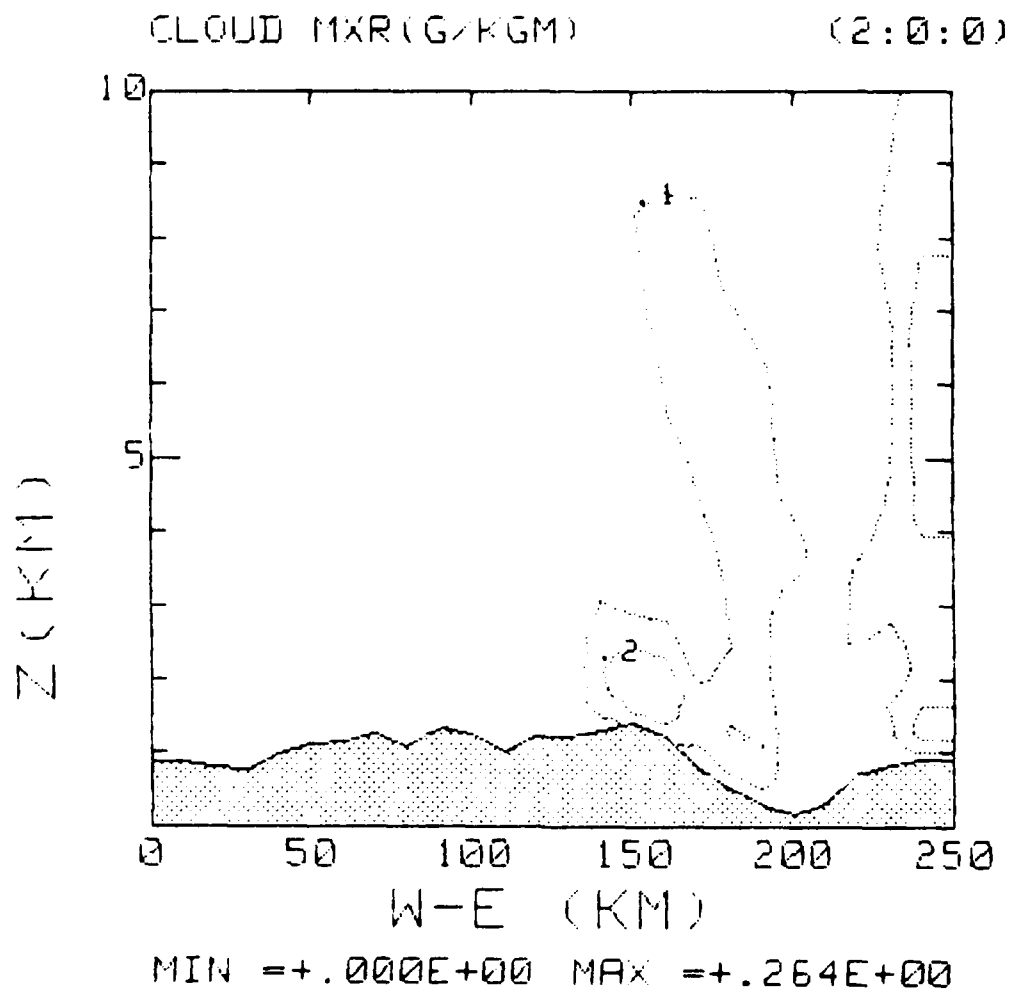


Figure 14.3  
Same as Figure 14.1 but after 2 hours.

AD-A164 468

A THREE-DIMENSIONAL MESOSCALE MODEL FOR THE SIMULATION  
OF CLOUDS PRECIPIT. (U) NATIONAL OCEANIC AND  
ATMOSPHERIC ADMINISTRATION BOULDER CO GE.

2/2

UNCLASSIFIED

E C NICKERSON 31 OCT 85 AFGL-TR-85-0307

F/G 4/2

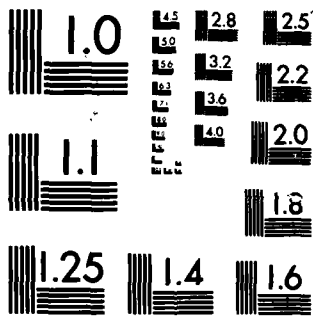
NL


END

FORM

100

100



MICROCOPY RESOLUTION TEST CHART  
NATIONAL BUREAU OF STANDARDS-1963-A

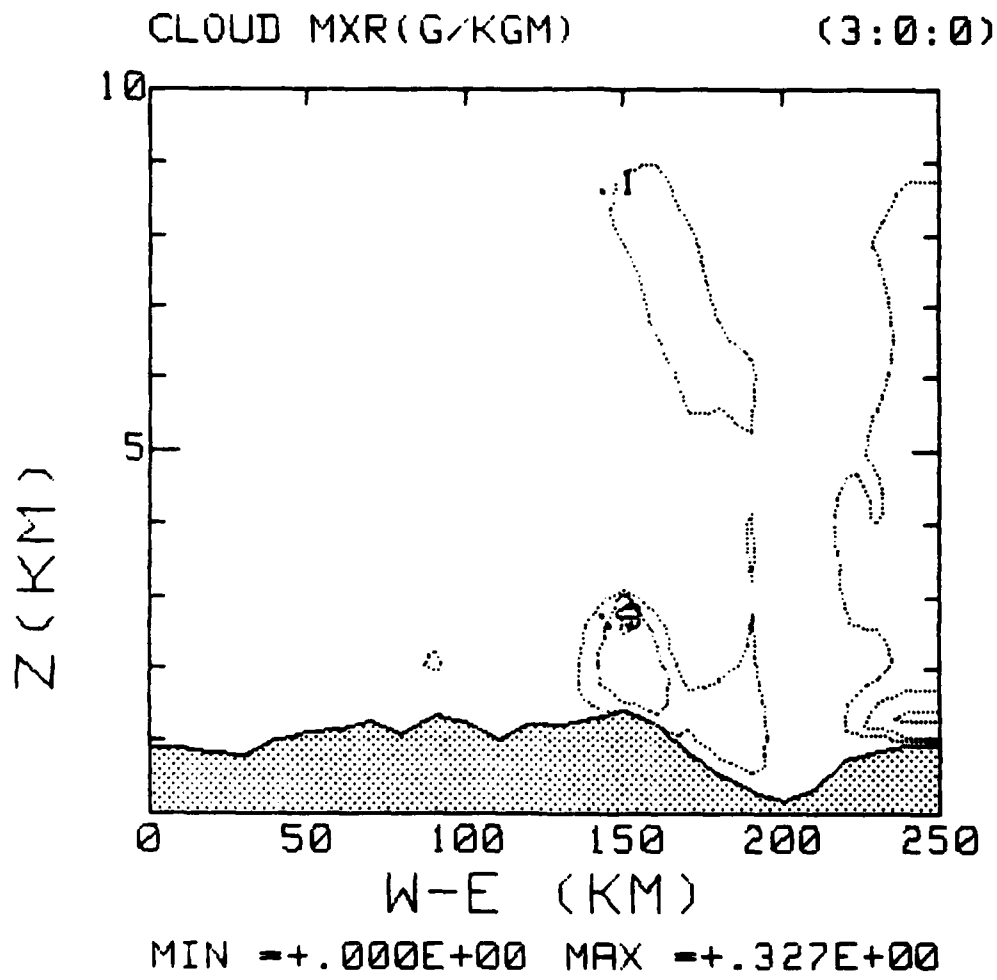


Figure 14.4  
Same as Figure 14.1 but after 3 hours.

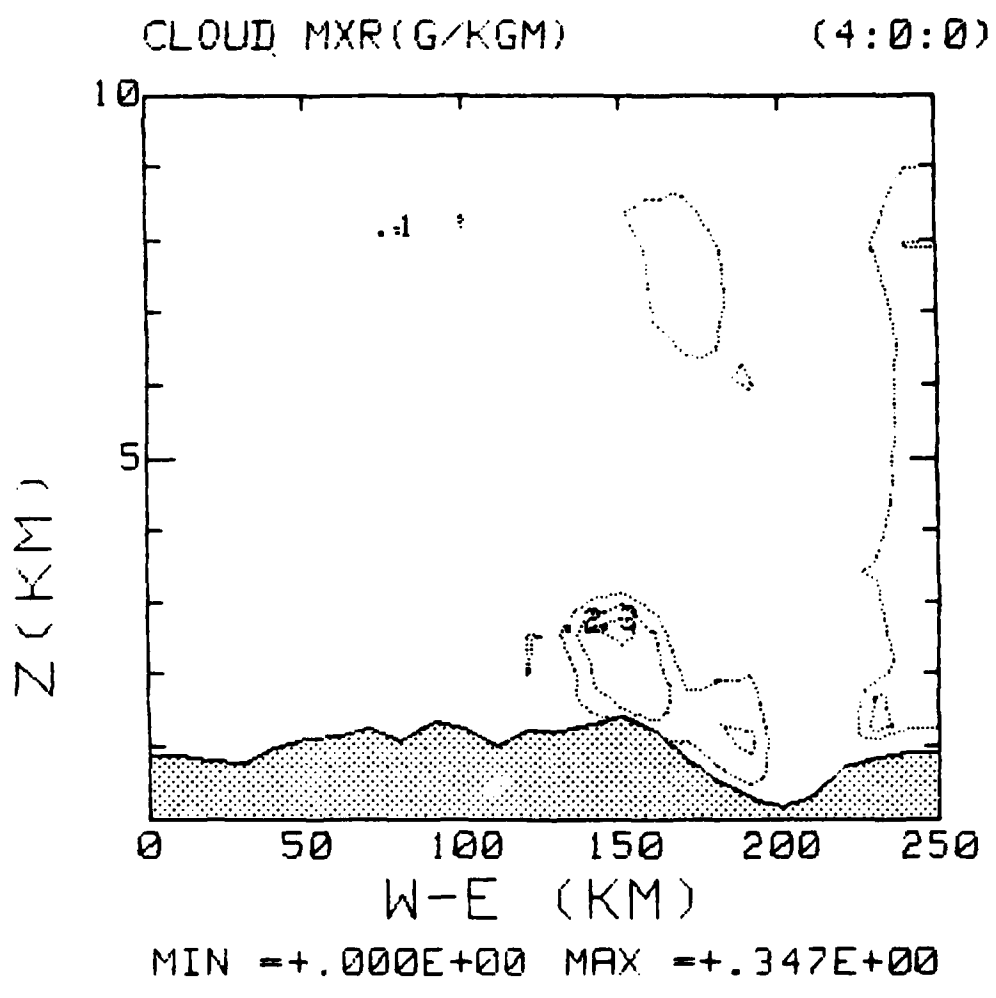


Figure 14.5  
Same as Figure 14.1 but after 4 hours.

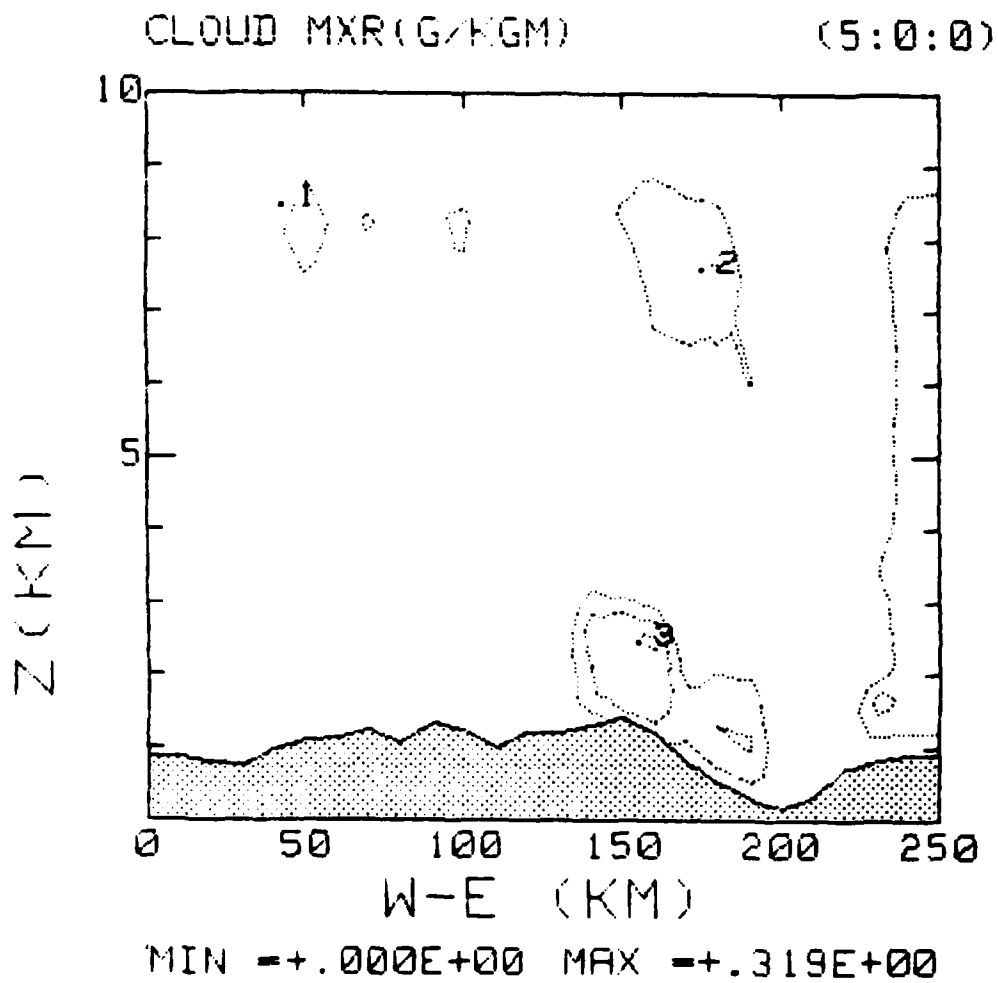


Figure 14.6  
Same as Figure 14.1 but after 5 hours.

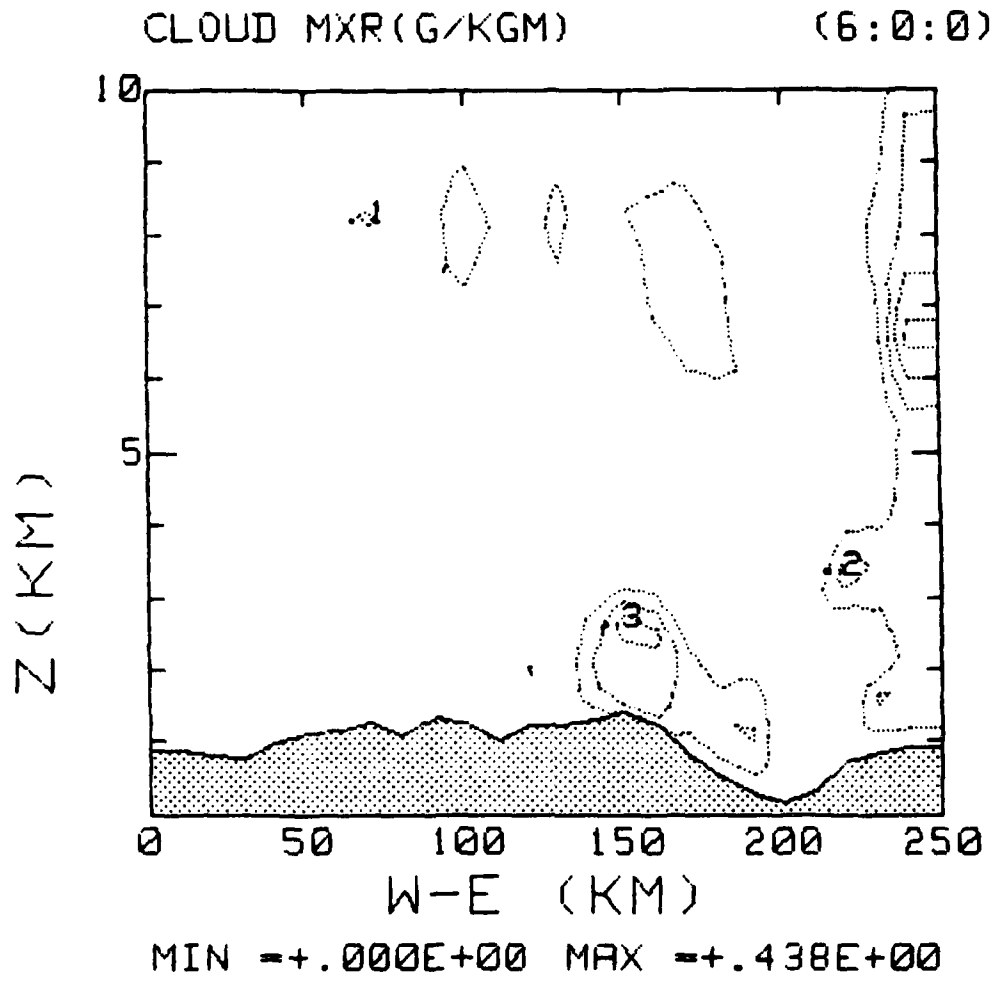


Figure 14.7  
Same as Figure 14.1 but after 6 hours.



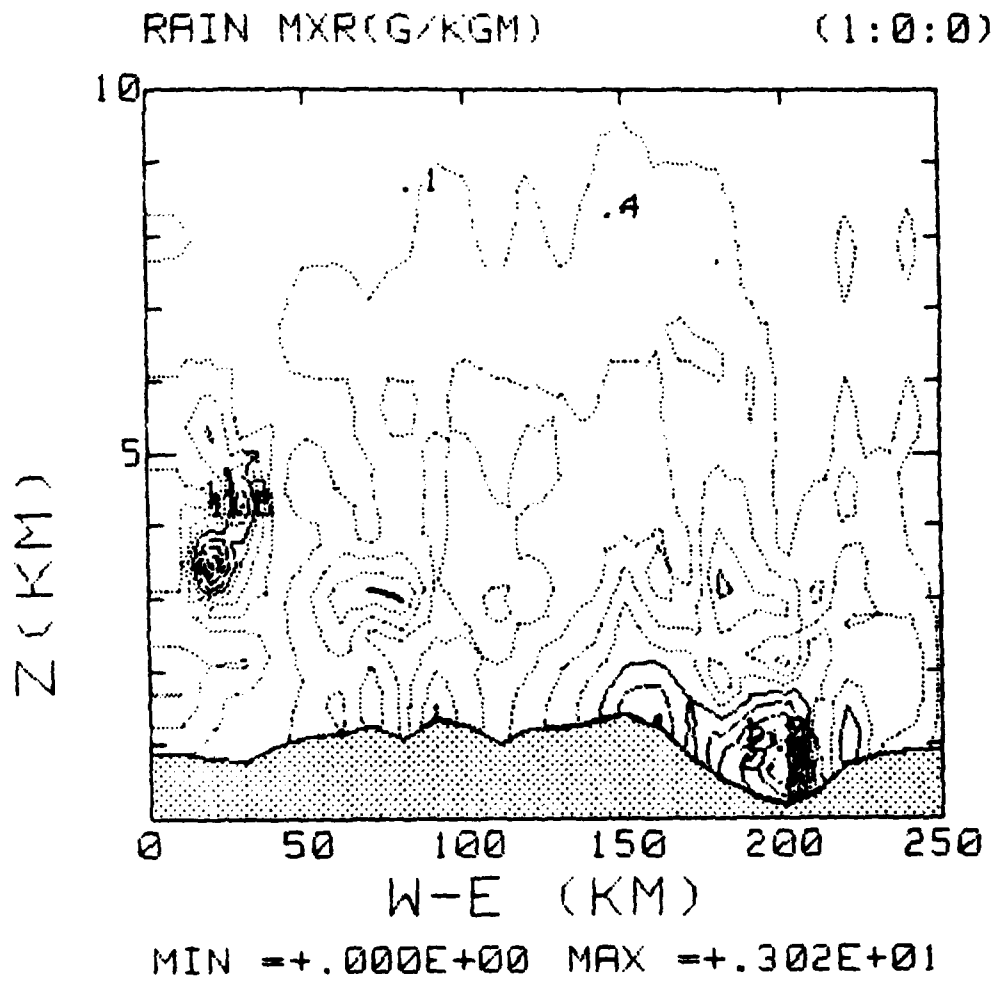


Figure 15.1  
West-East vertical cross section of rain water mixing ratio,  
170 km from southern boundary after 1 hour.

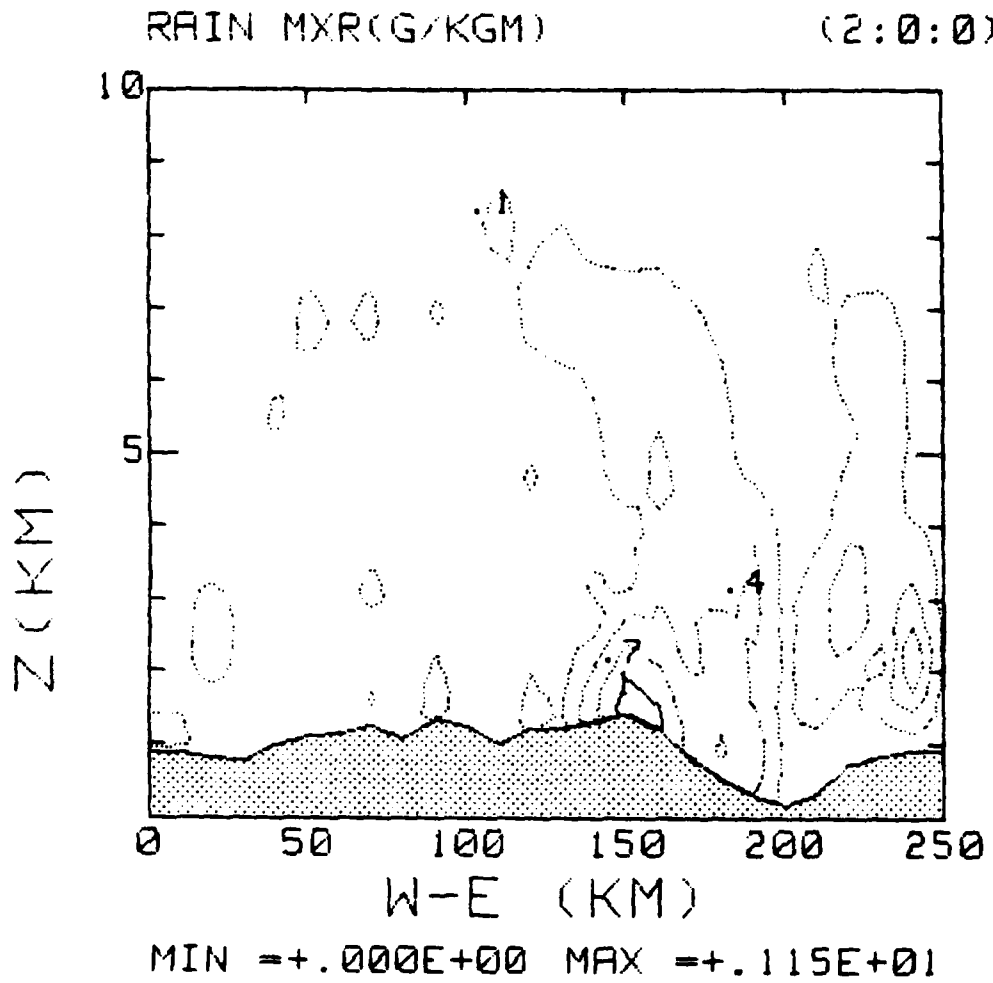


Figure 15.2  
Same as Figure 15.1 but after 2 hours.

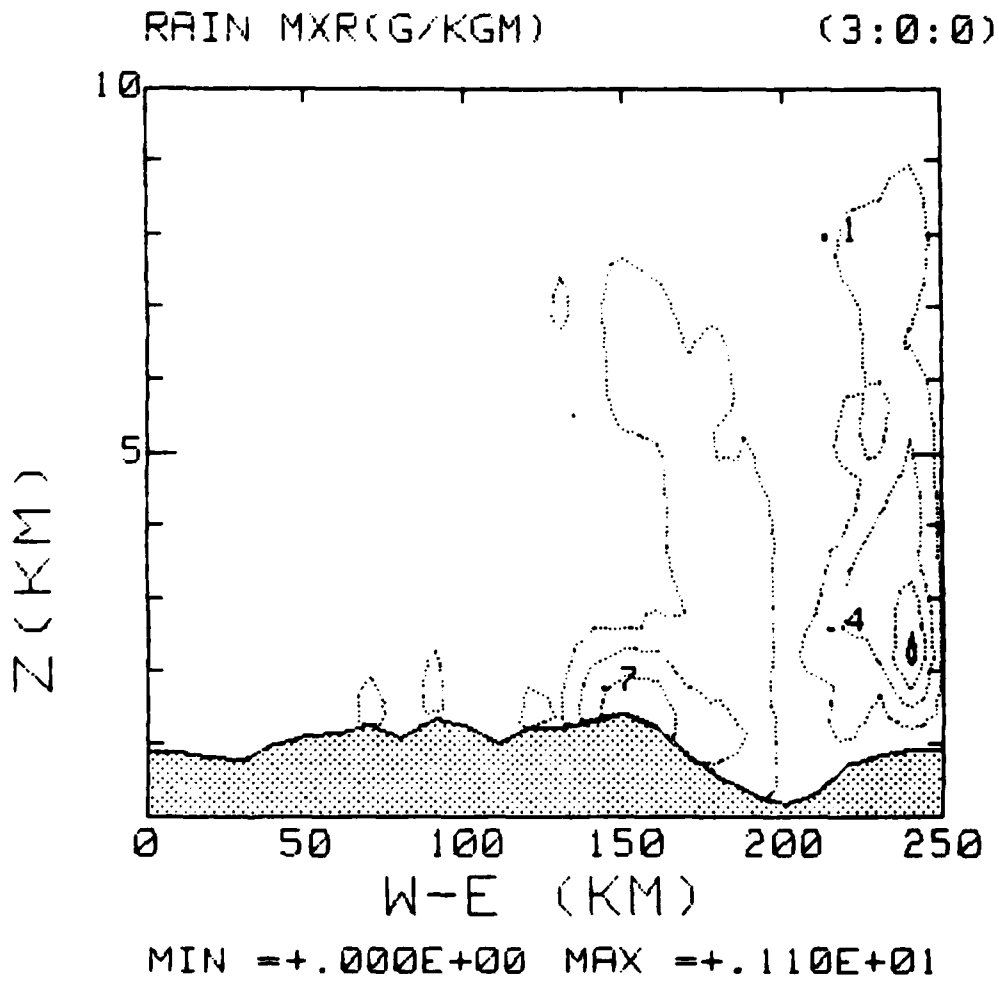


Figure 15.3  
Same as Figure 15.1 but after 3 hours.

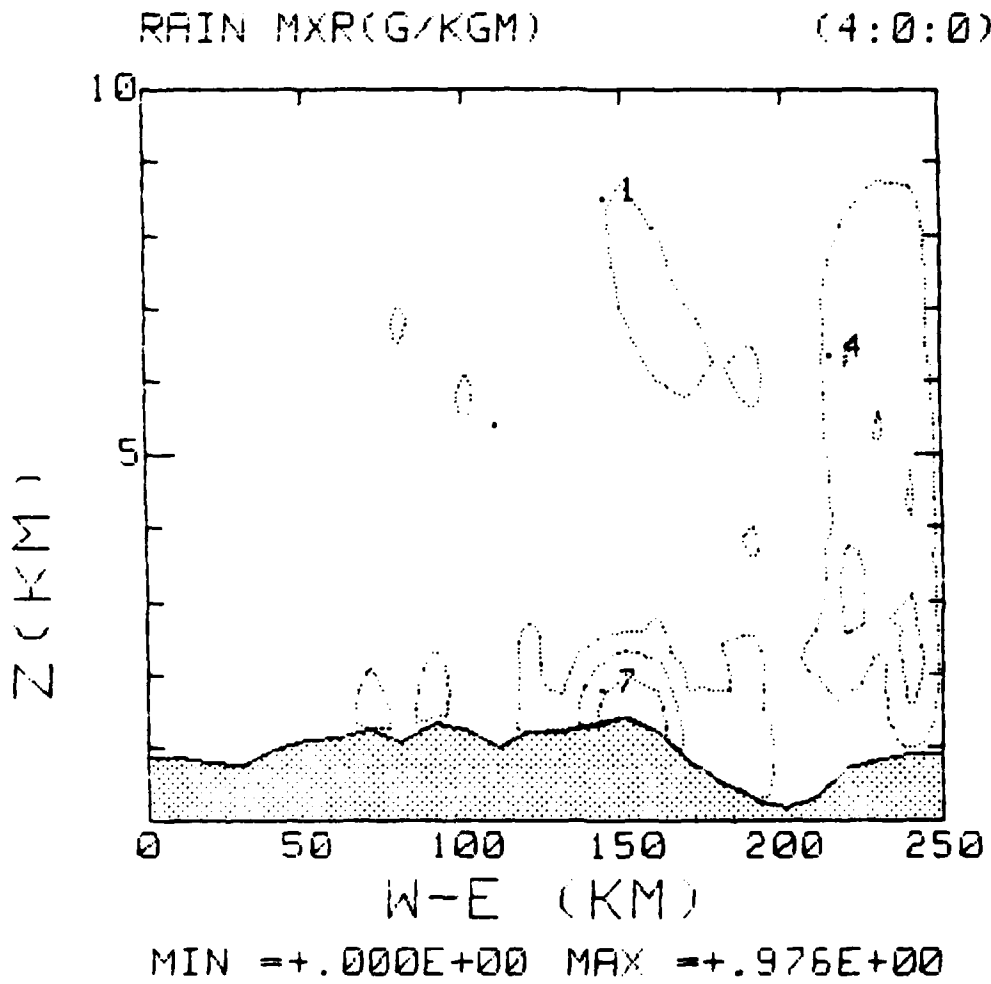


Figure 15.4  
Same as Figure 15.1 but after 4 hours.

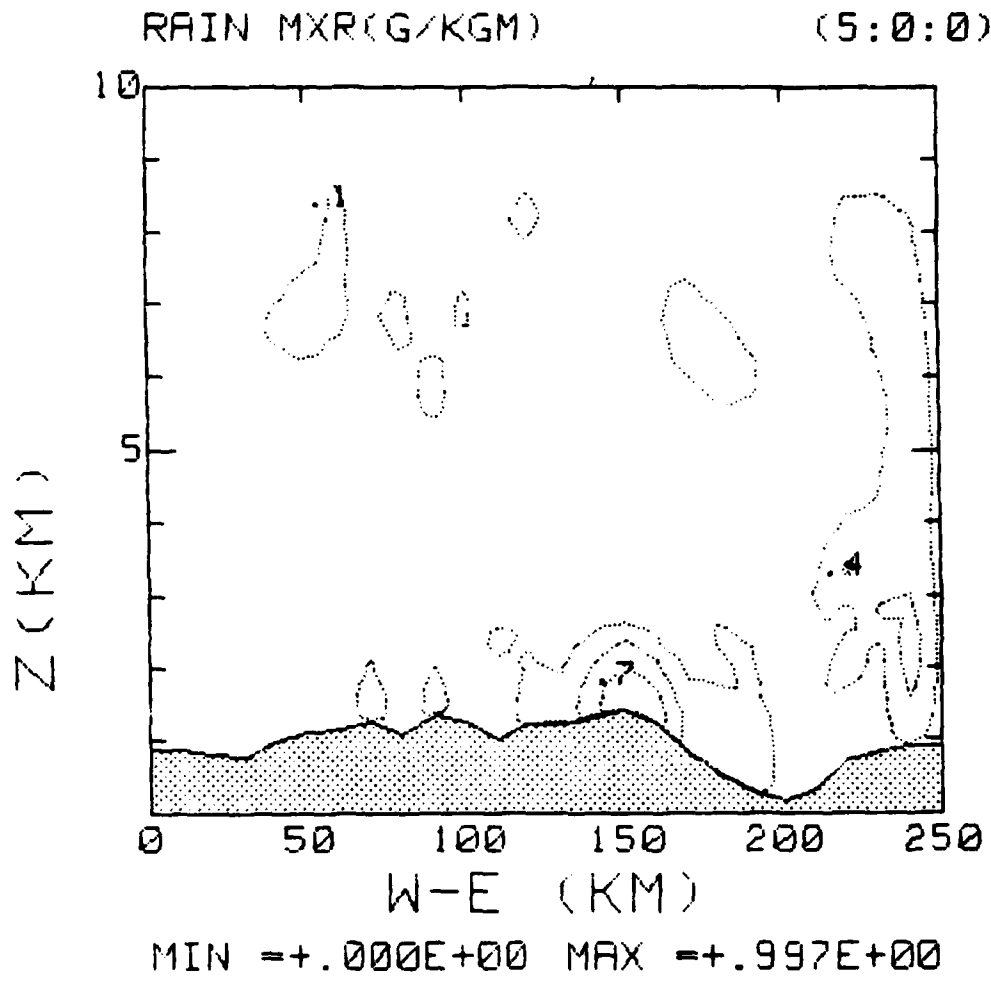


Figure 15.5  
Same as Figure 15.1 but after 5 hours.

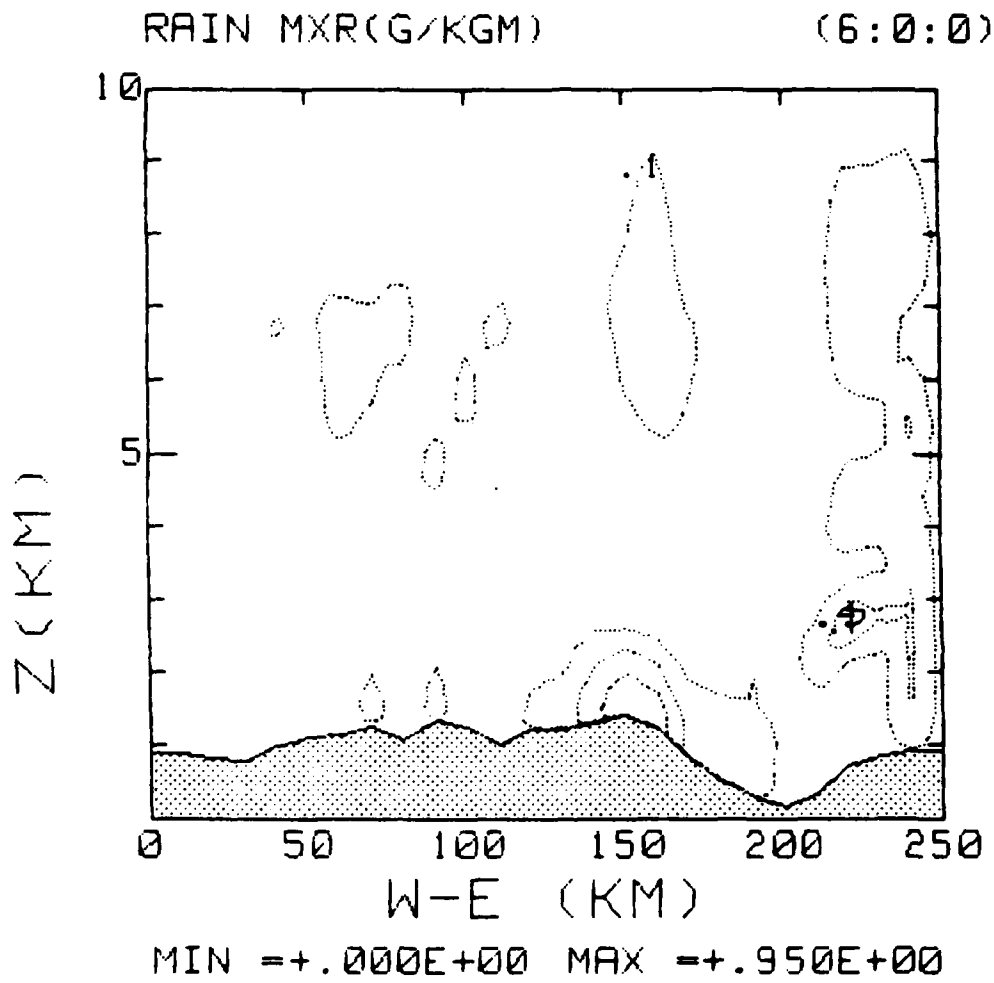


Figure 15.6  
Same as Figure 15.1 but after 6 hours.

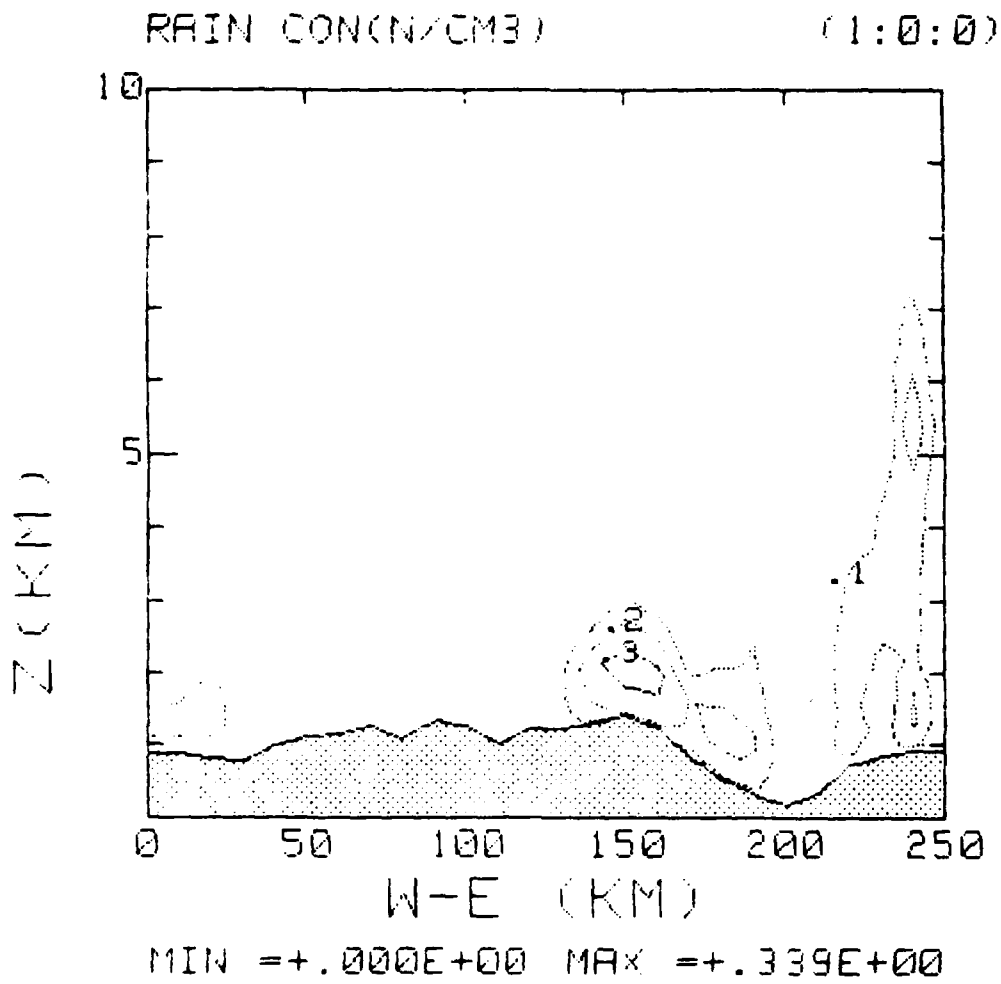


Figure 16.1  
West-East vertical cross section of rain concentration,  
170 km from southern boundary after 1 hour.

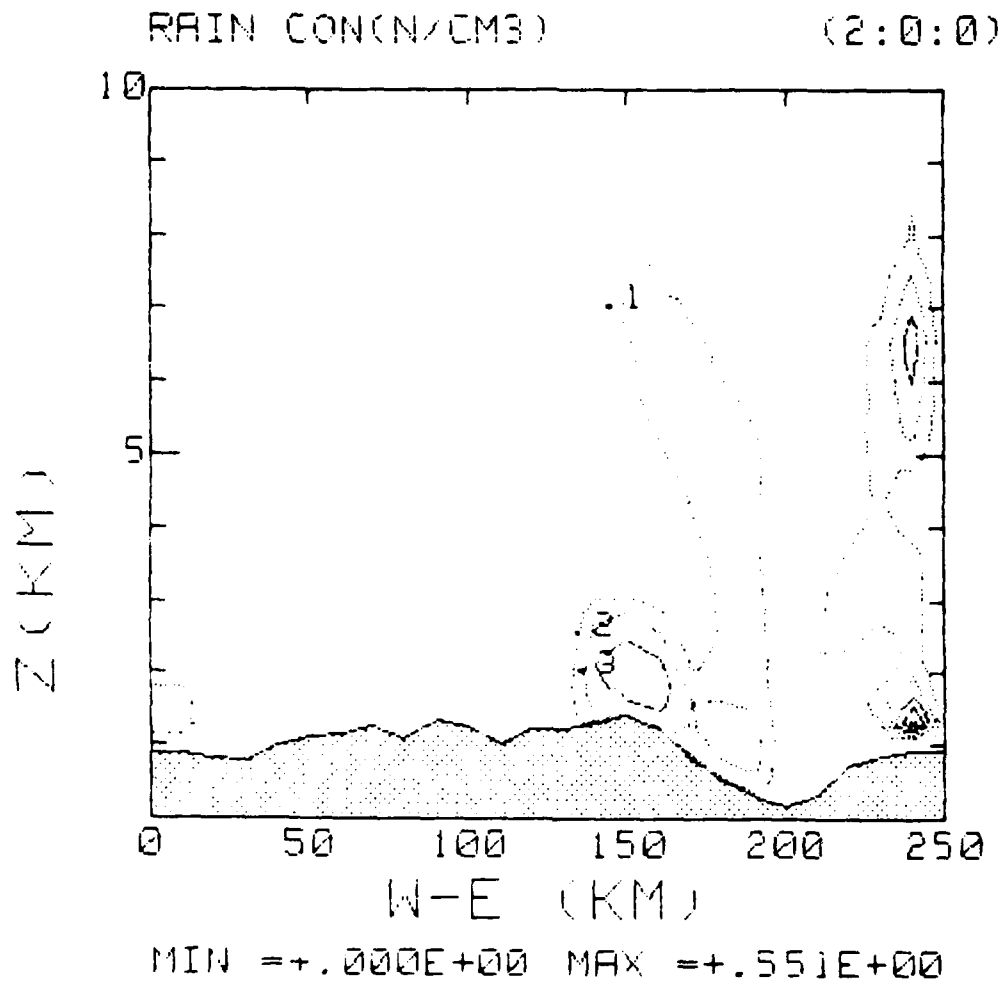


Figure 16.2  
Same as Figure 16.1 but after 2 hours.



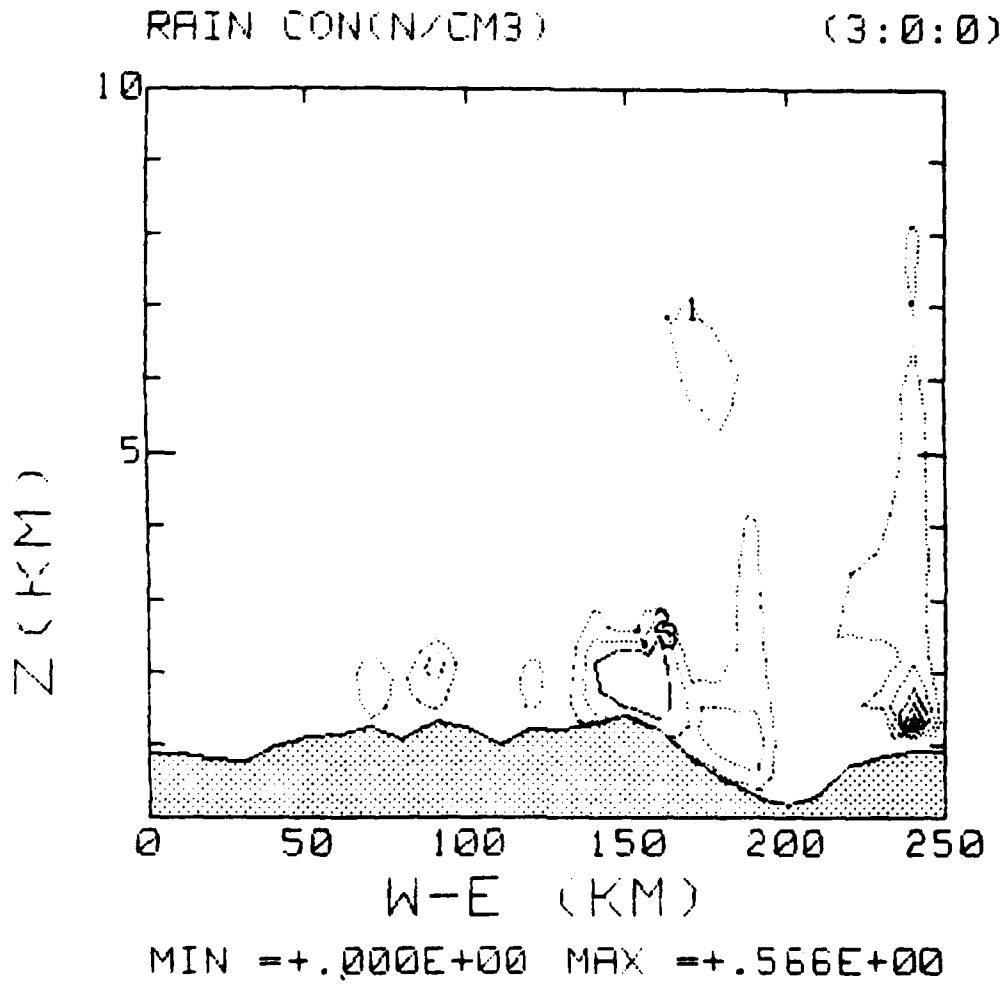


Figure 16.3  
Same as Figure 16.1 but after 3 hours.

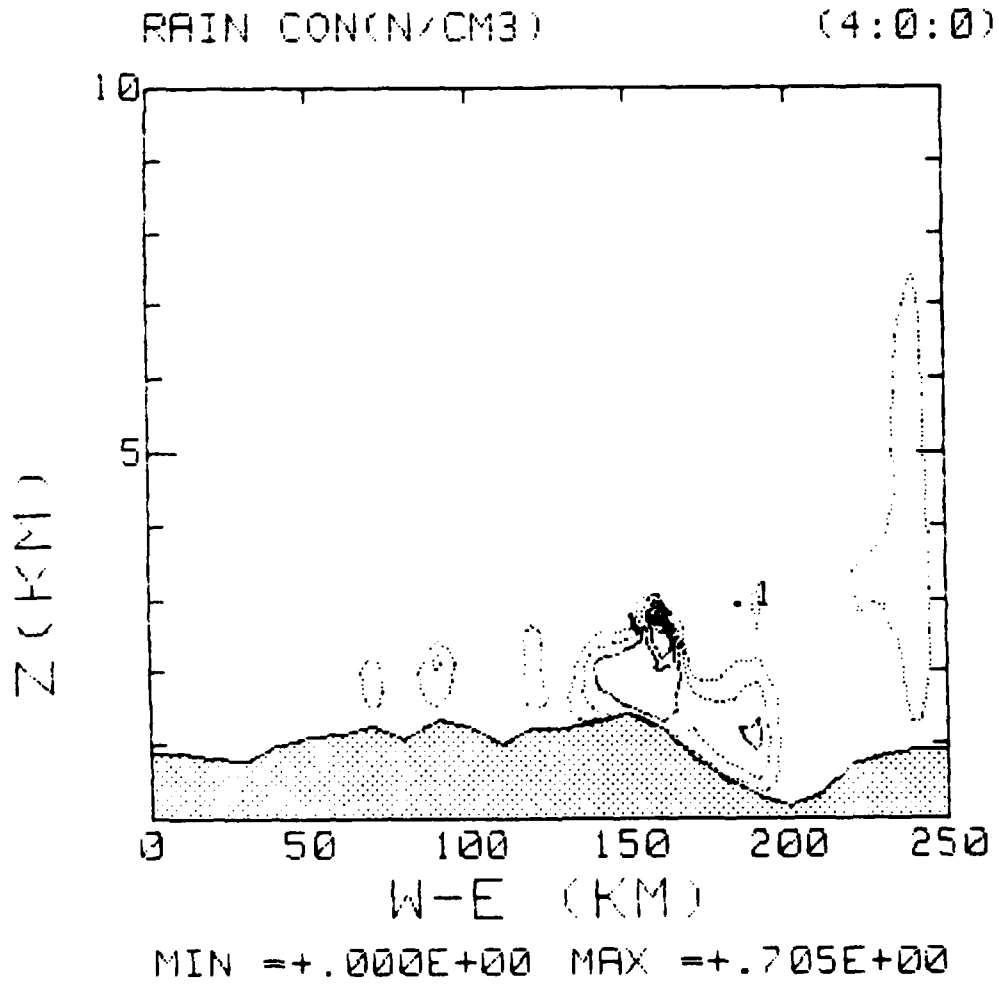


Figure 16.4  
Same as Figure 16.1 but after 4 hours.

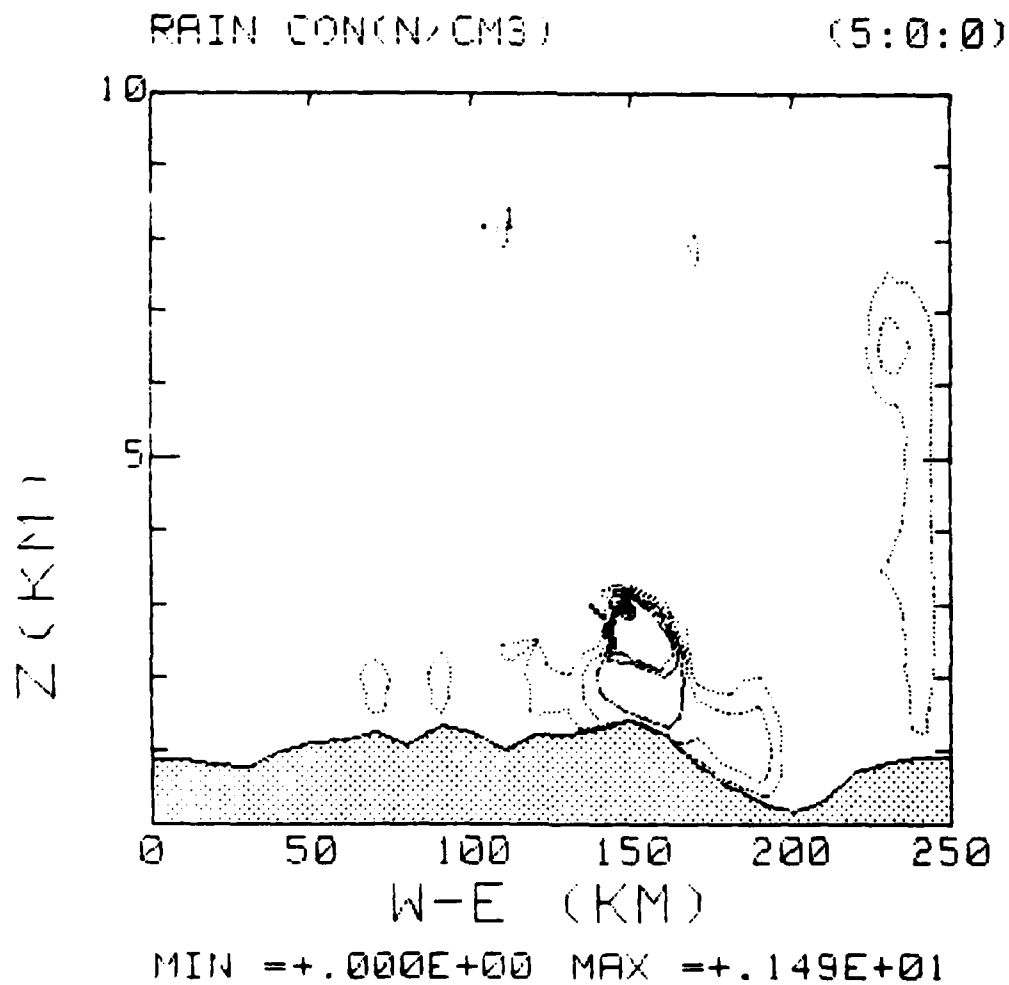


Figure 16.5  
Same as Figure 16.1 but after 5 hours.

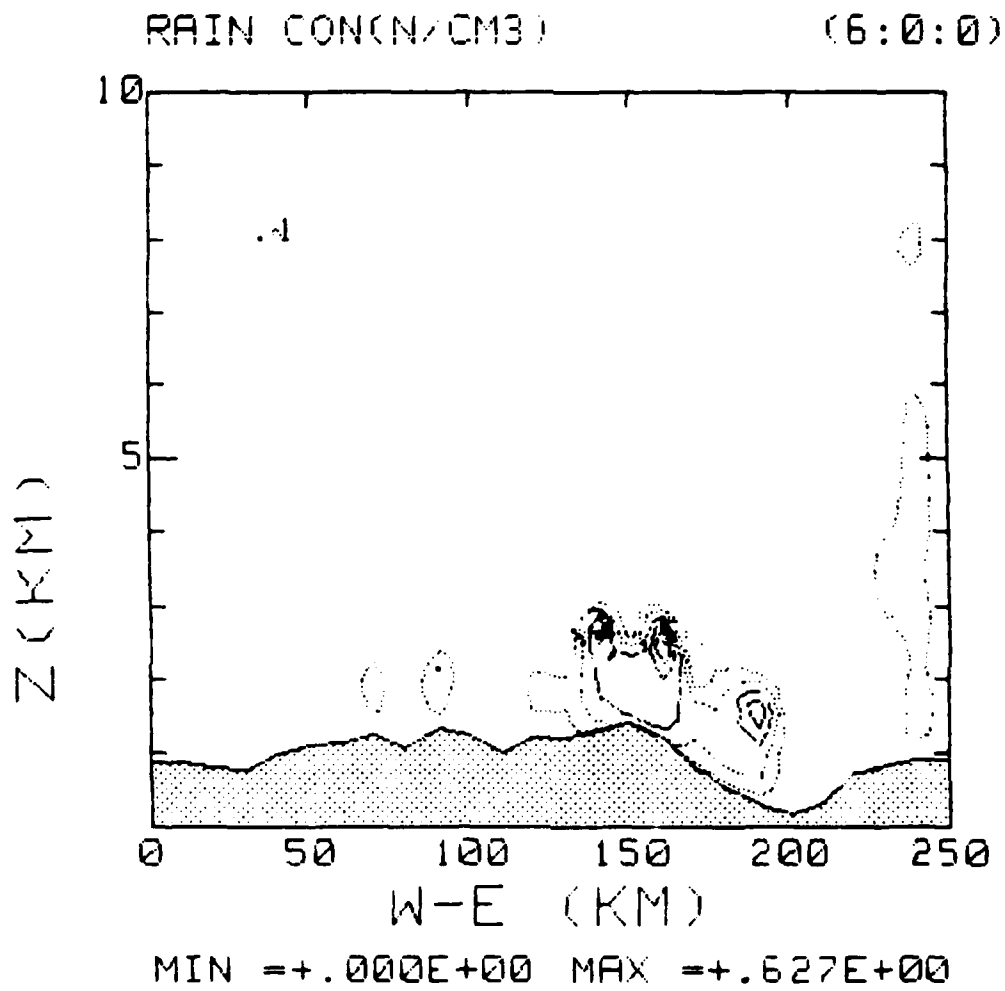


Figure 16.6  
Same as Figure 16.1 but after 6 hours.

DATE= 16 Oct 1985 TIME= 07:39:30  
The distance from the southern boundary in kilometers = 100

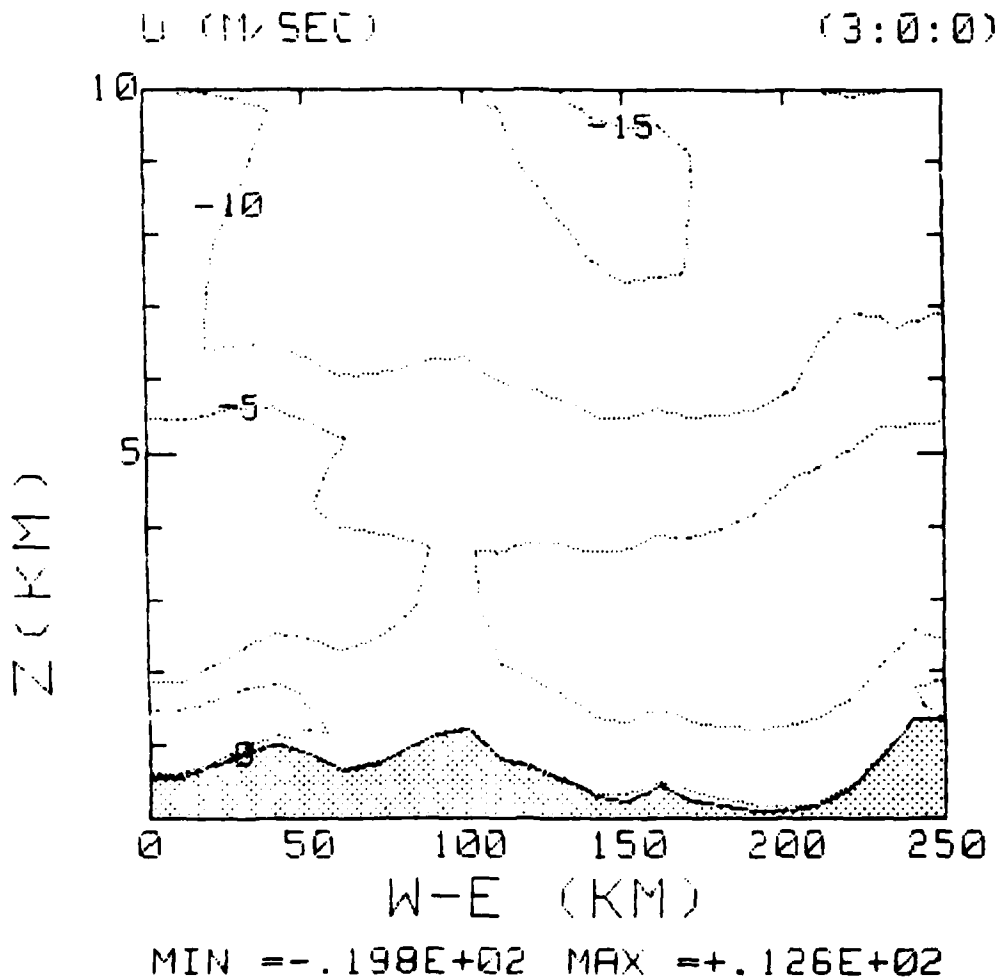


Figure 17.1  
West-East vertical cross section of U, 100 km from  
southern boundary after 3 hours.

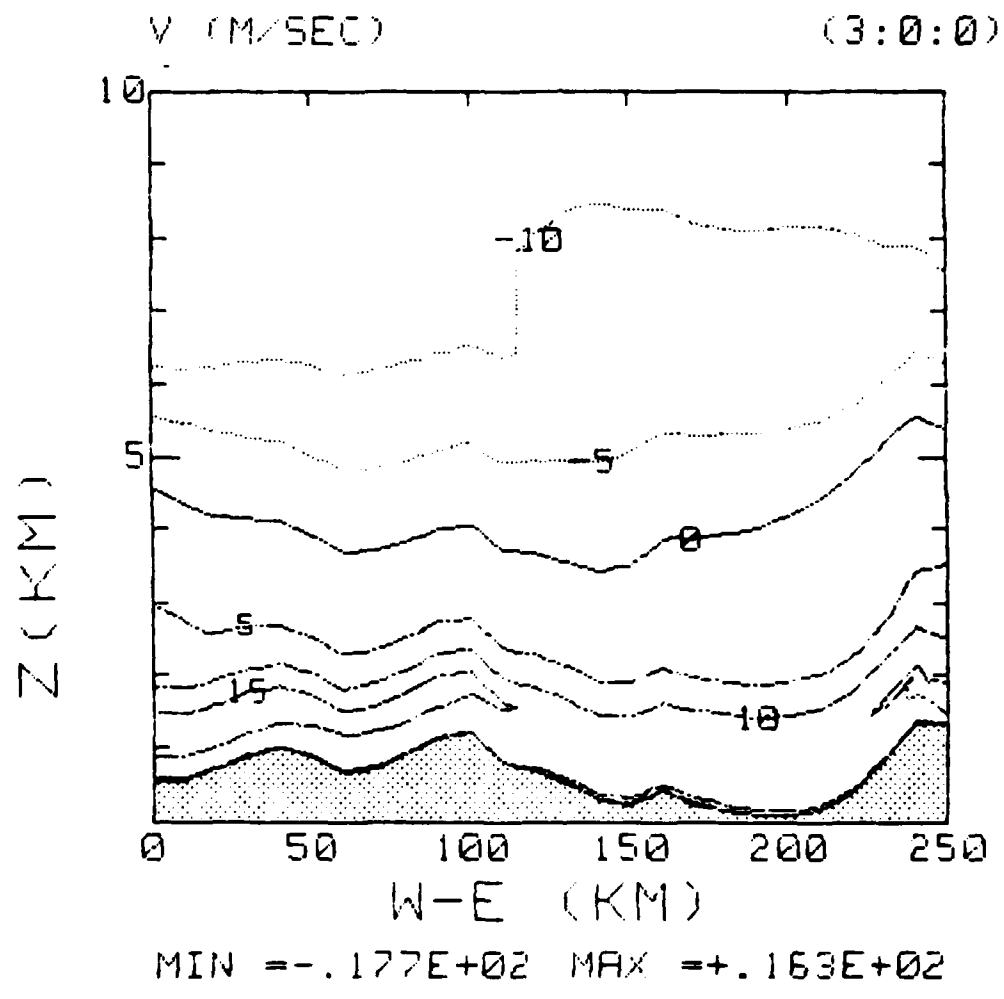


Figure 17.2  
Same as Figure 17.1 but for V.

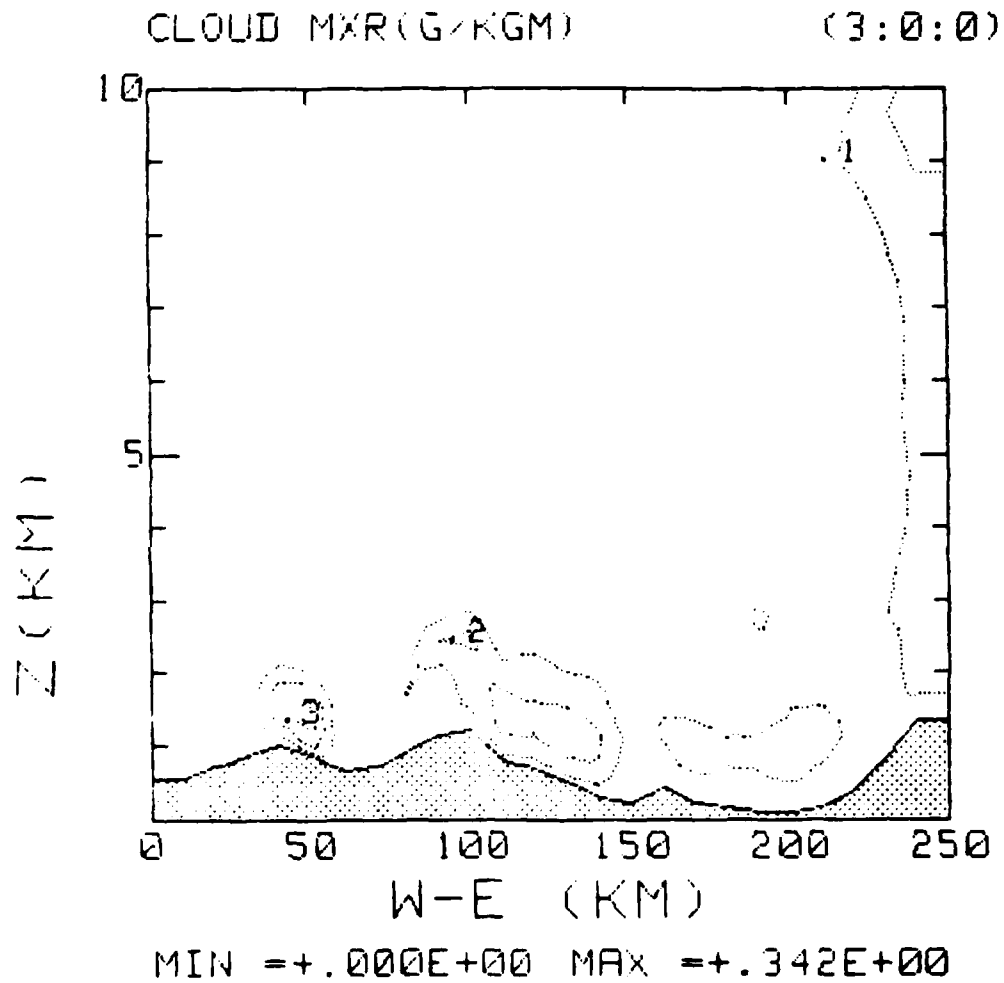


Figure 17.3  
Same as Figure 17.1 but for cloud water  
mixing ratio.

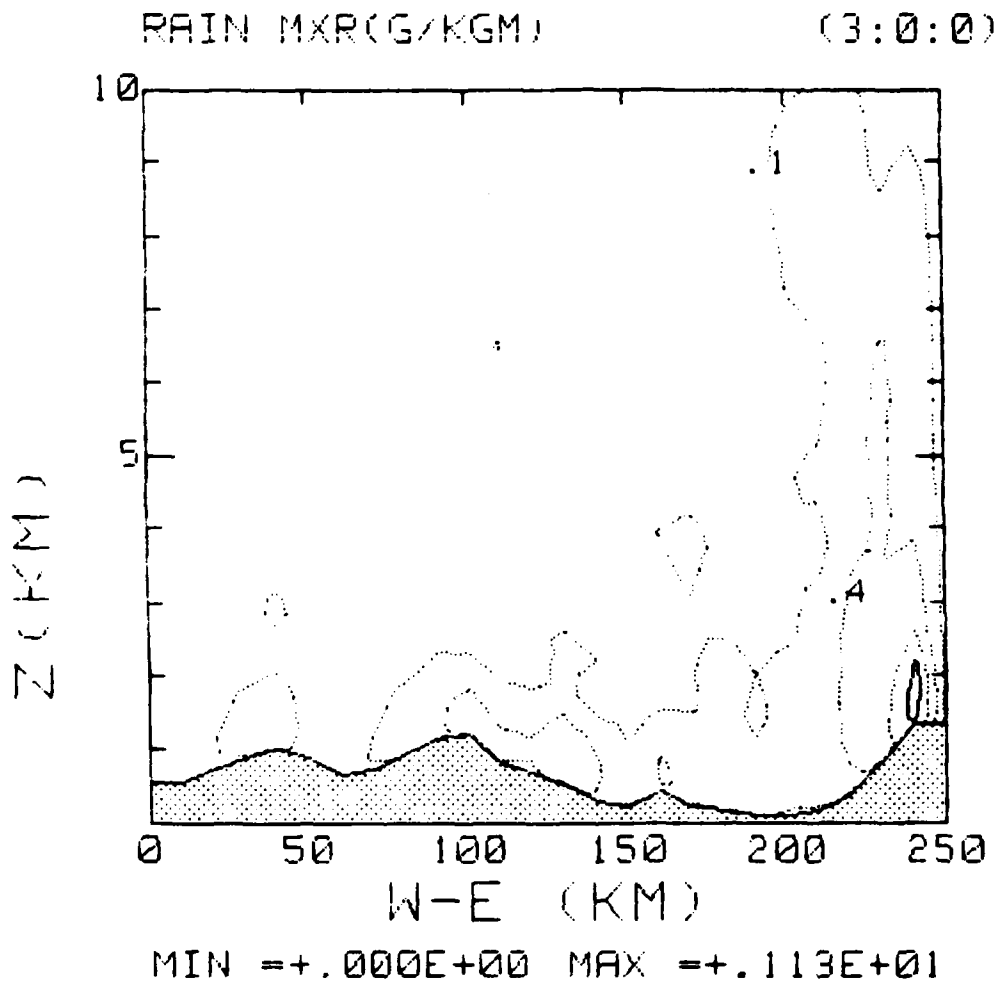


Figure 17.4  
Same as Figure 17.1 but for rain water mixing ratio.



. DATE= 16 Oct 1985 TIME= 07:57:30  
The distance from the southern boundary in kilometers = 150

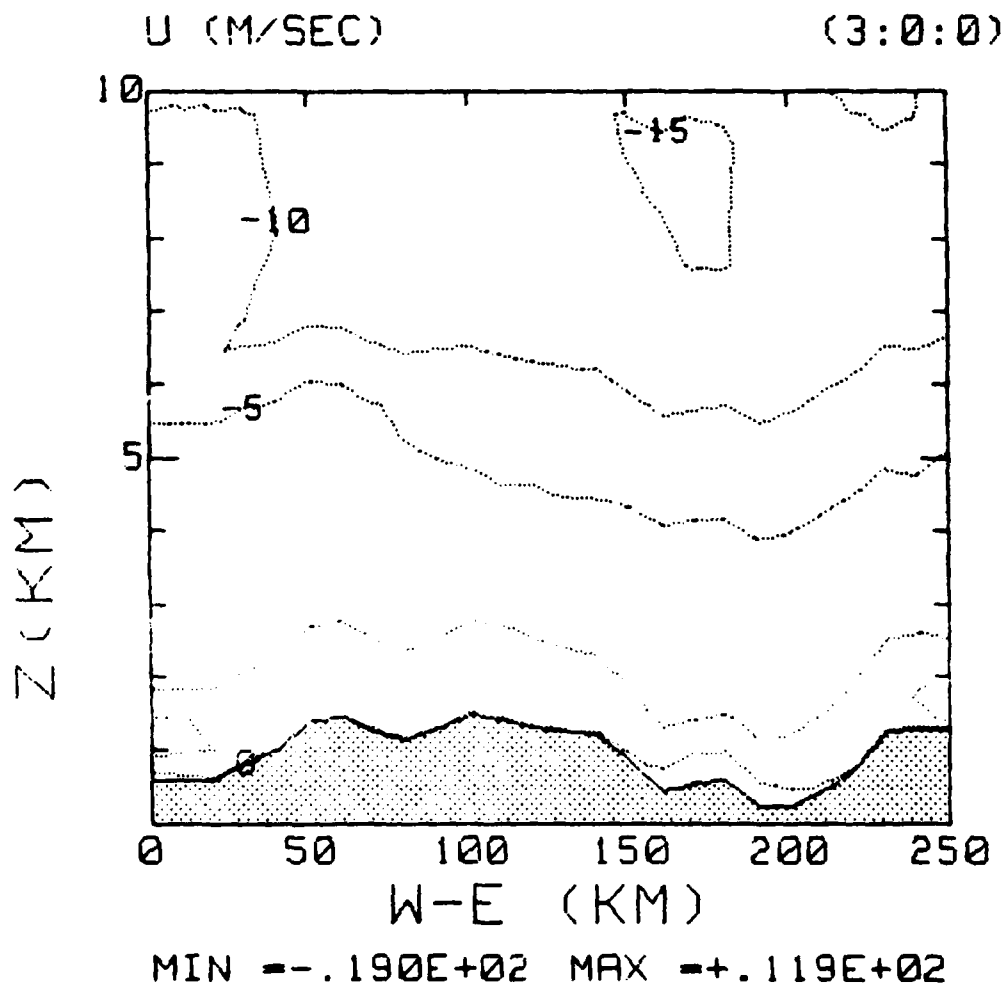


Figure 18.1  
West-East vertical cross section of U, 150 km  
from southern boundary after 3 hours.

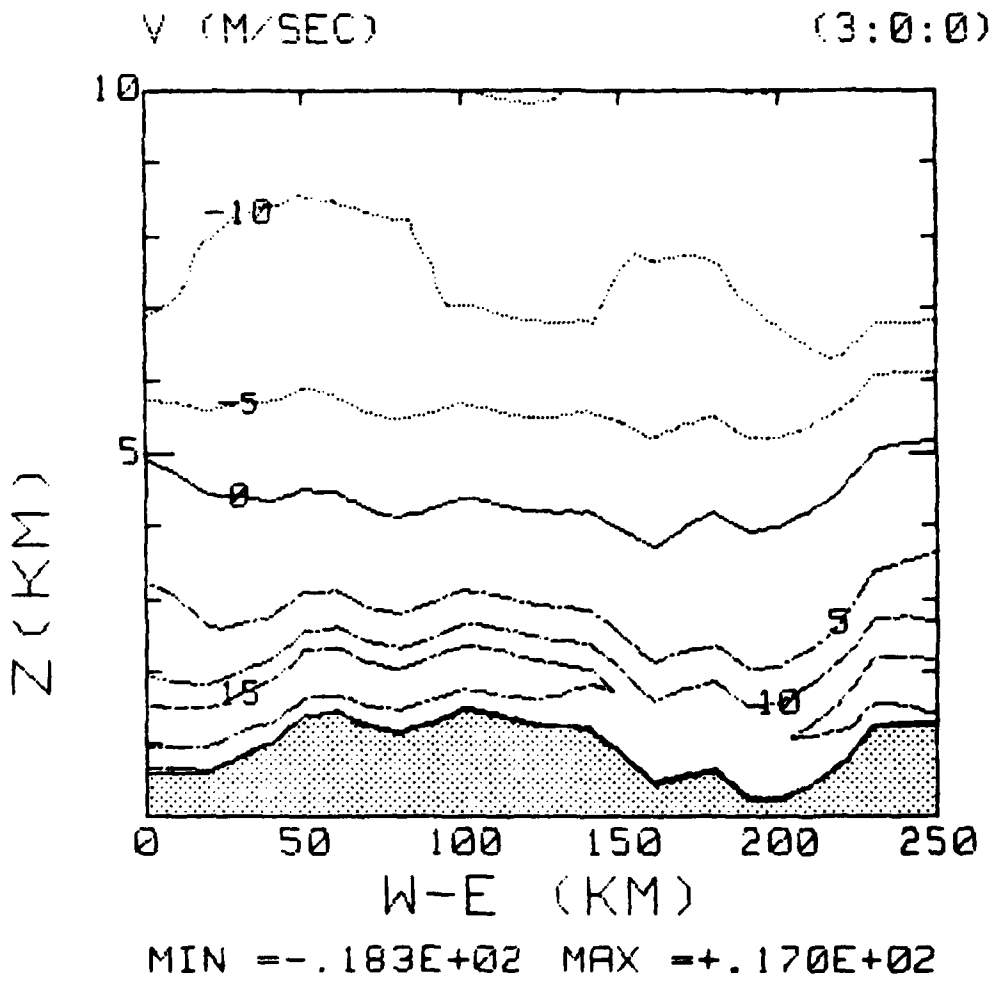


Figure 18.2  
Same as Figure 18.1 but for V.

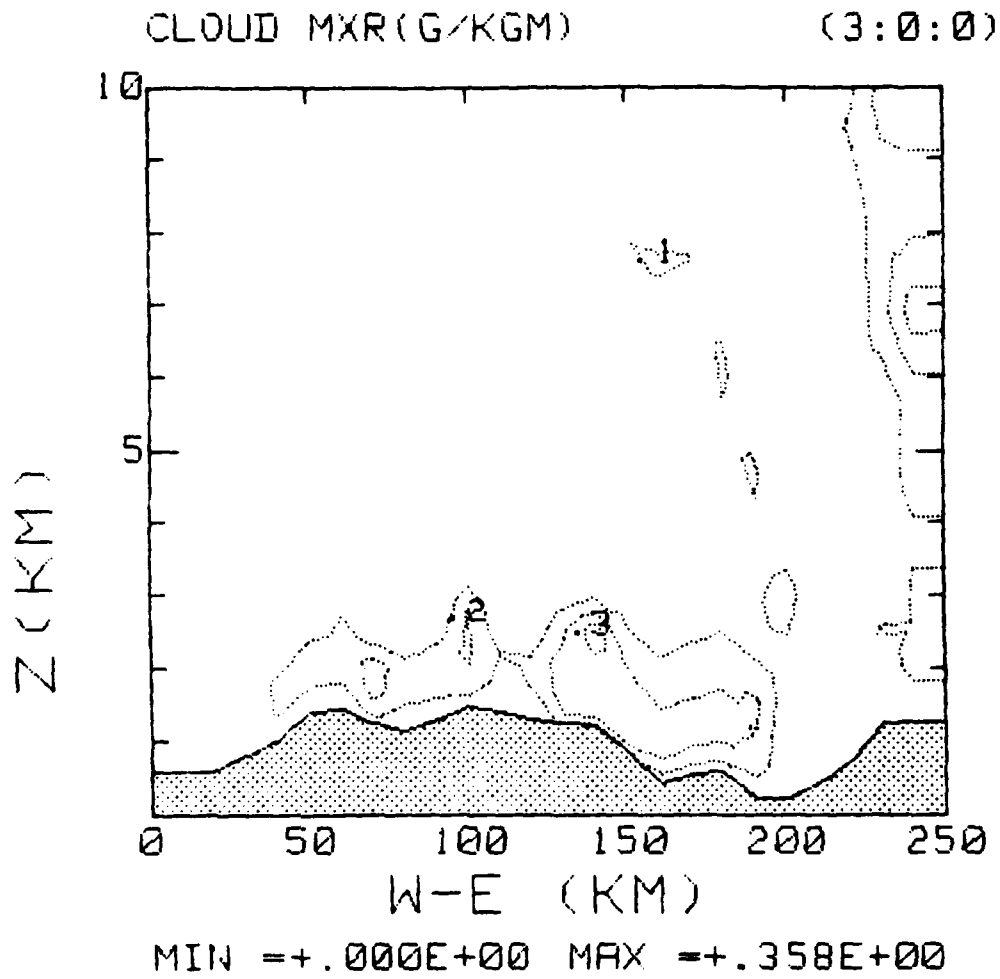


Figure 18.3  
Same as Figure 18.1 but for cloud water  
mixing ratio.

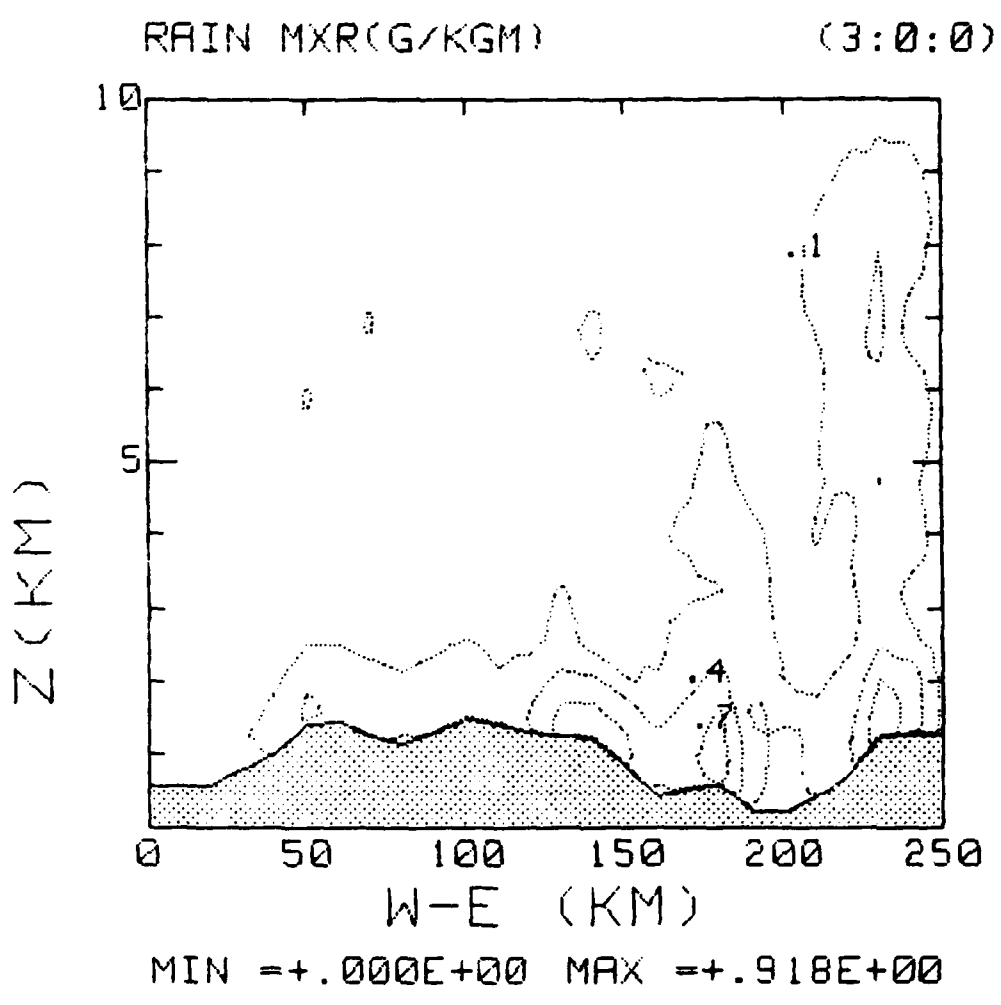


Figure 18.4  
Same as Figure 18.1 but for rain water  
mixing ratio.

The distance from the southern boundary in kilometers = 200

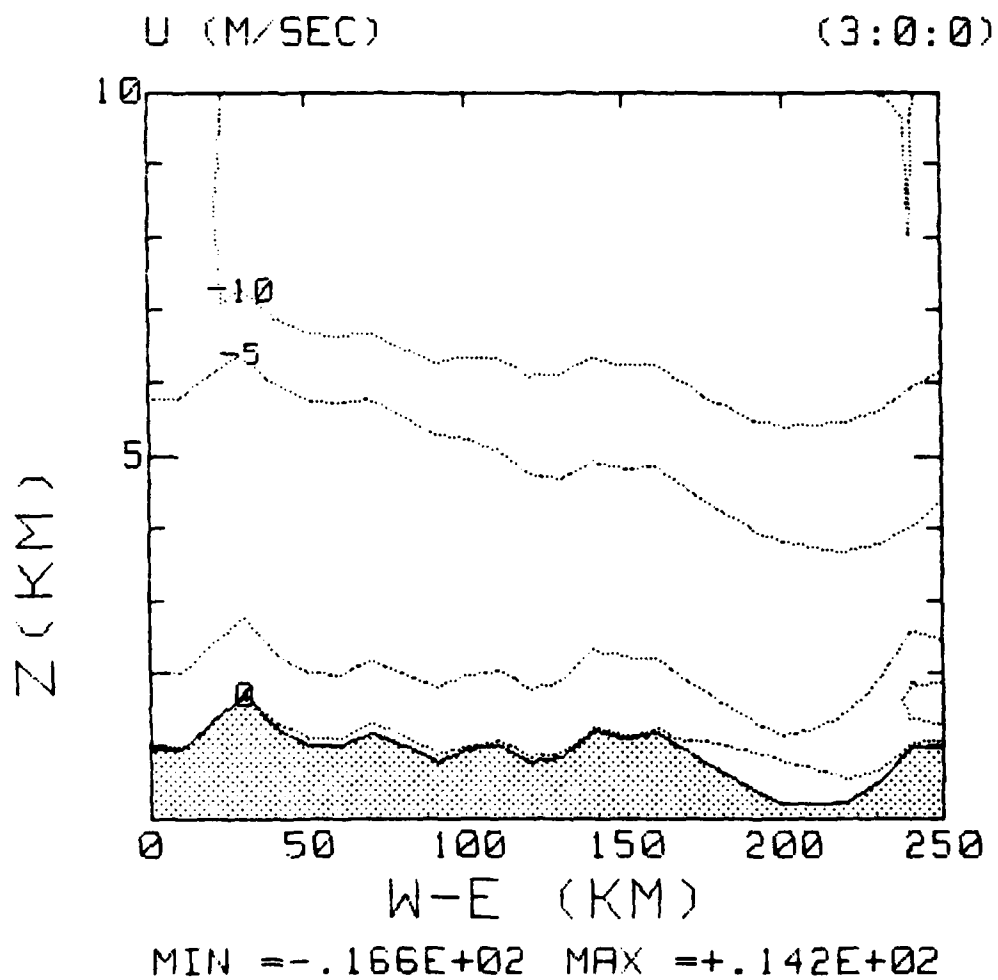


Figure 19.1  
West-East vertical cross section of U, 200 km  
from southern boundary after 3 hours.

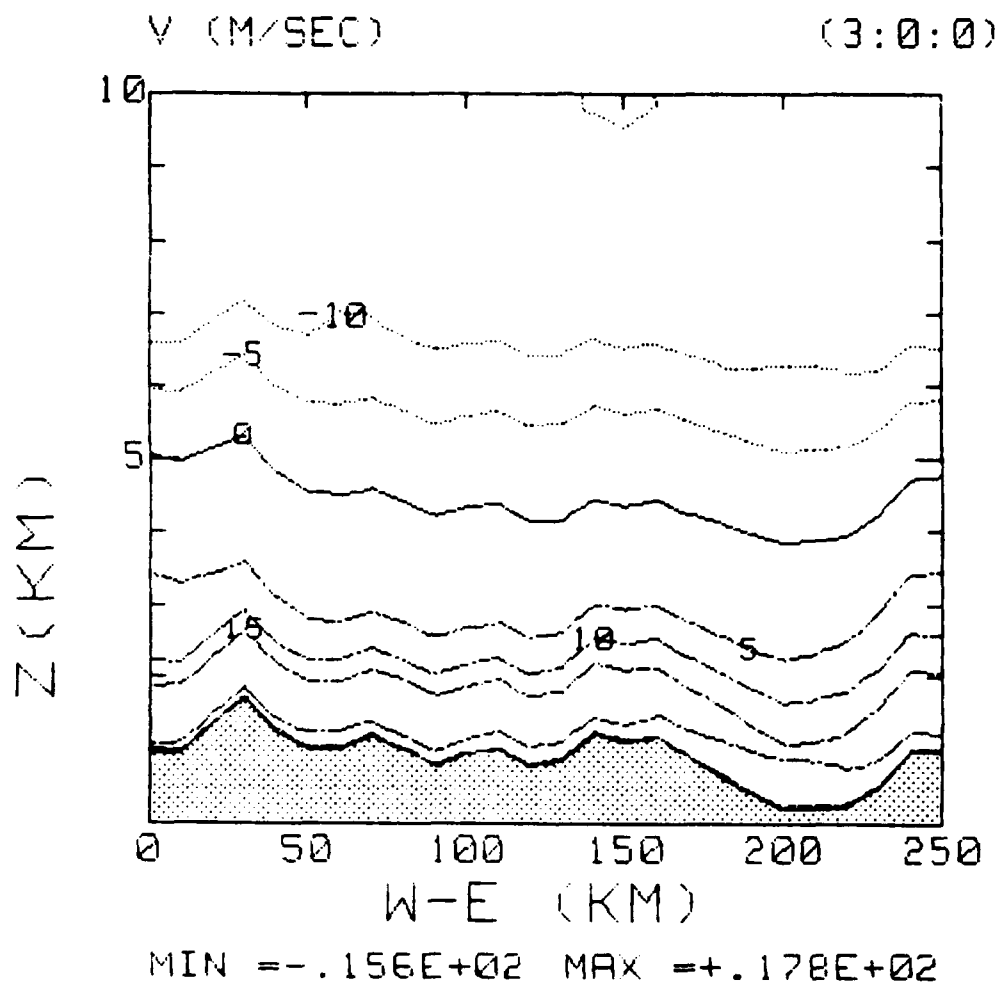


Figure 19.2  
Same as Figure 19.1 but for V.

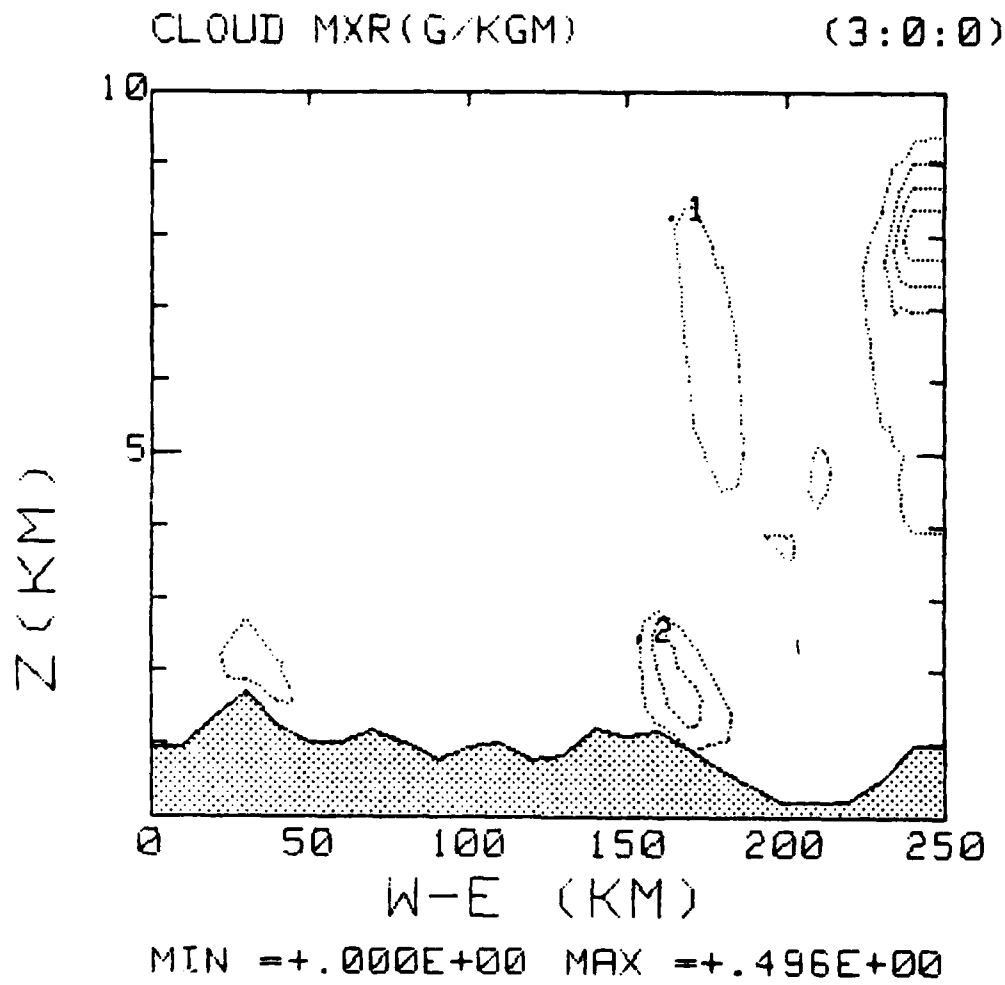


Figure 19.3  
Same as Figure 19.1 but for cloud water  
mixing ratio.

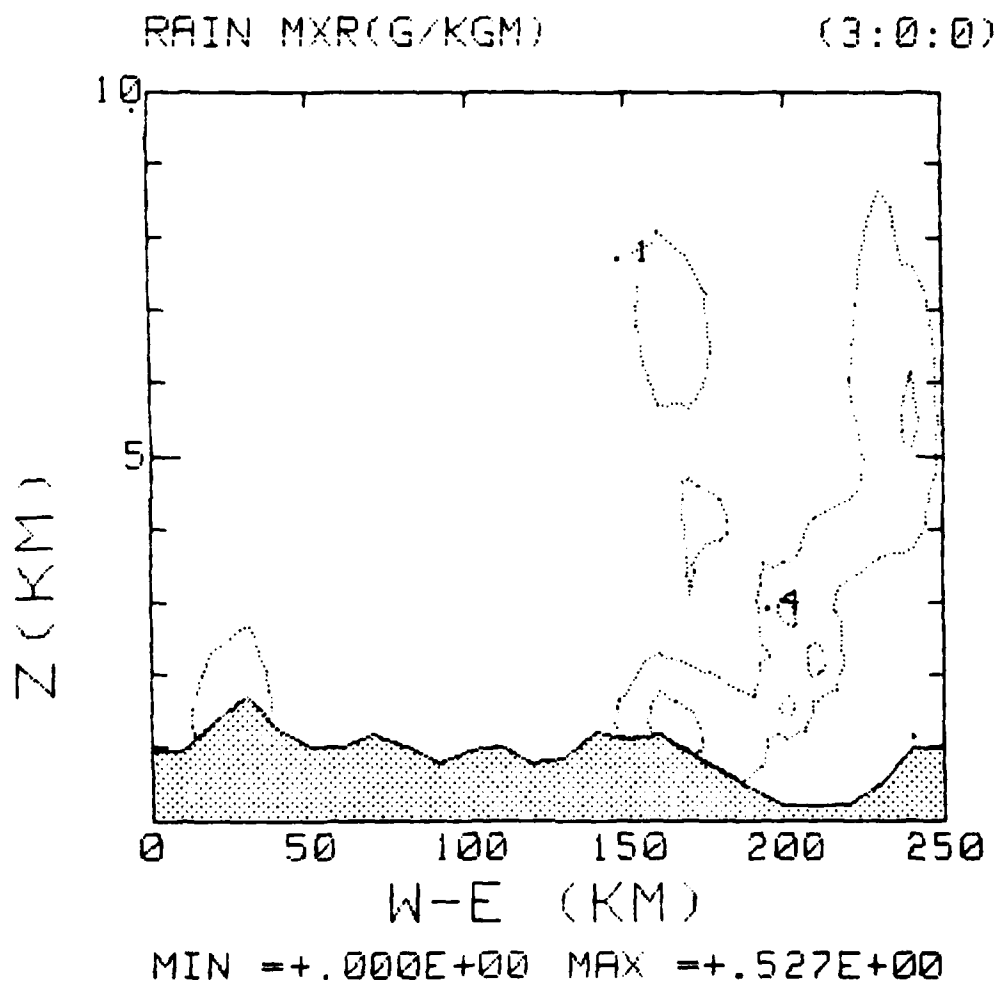


Figure 19.4  
Same as Figure 19.1 but for rain water  
mixing ratio.



Table 1  
Program flow Chart for the Medal Initialization Procedure

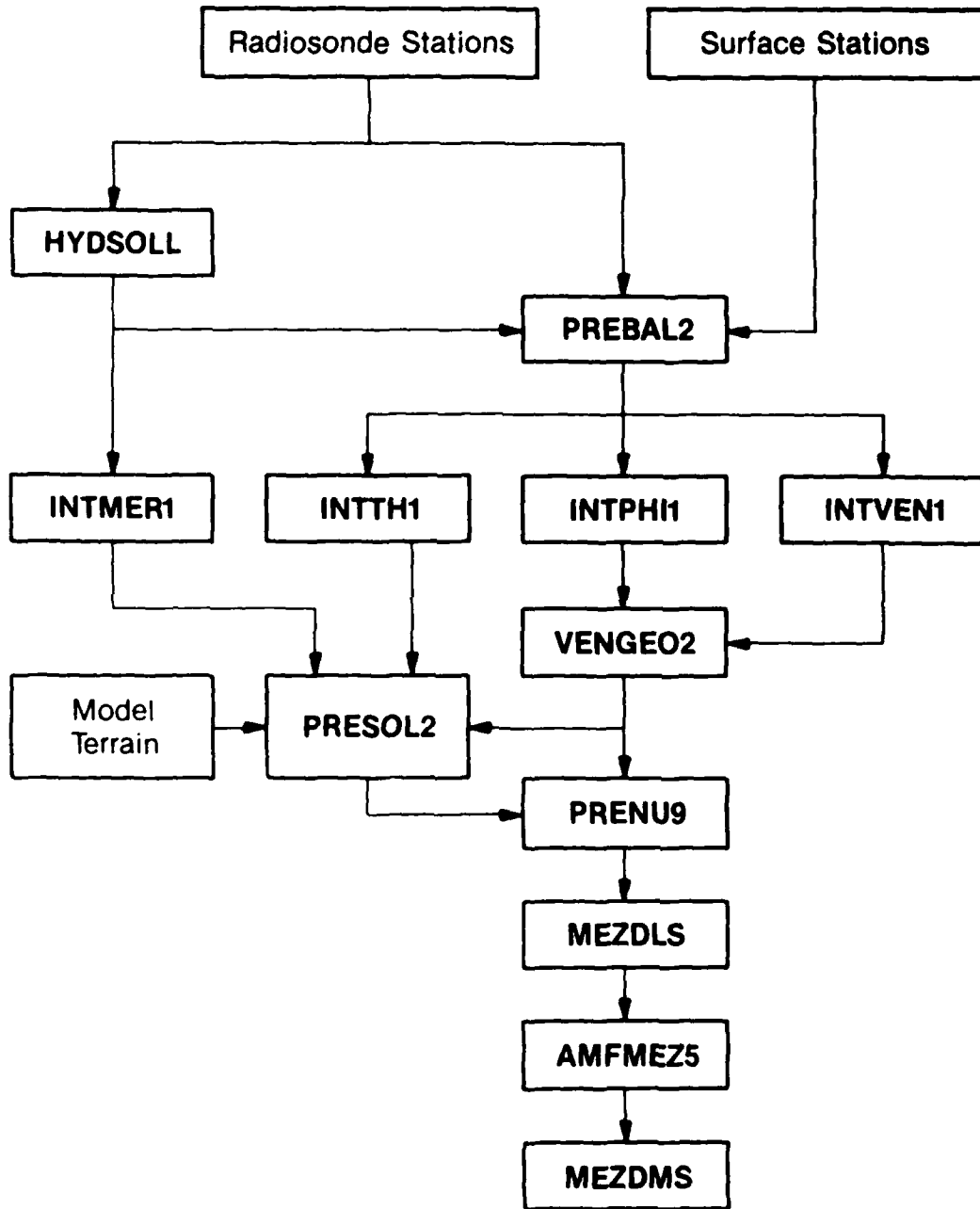


Table 2

Contents of Tape Number 9245

Format: 1600 bpi, ASCII, NL  
RECFM=FB  
RECORD LENGTH=80BLOCK SIZE=400

File Number	Program Name
1	CRAY01-MEZMODLS
2	CRAY01-MEZMODMS
3	DOM.AMFMEZ5
4	DOM.PRENU9
5	DOM.HYDSOL1
6	DOM.PRESOL2
7	DOM.PREBAL2
8	DOM.RW.INTBAR01
9	DOM.VENGE02
10	DOM.MASCRA3
11	DOM.MASMSC4
12	DOM.VENMSC4
13	DOM.VENCRA3
14	DOM.MASMSC7
15	DOM.VENMSC7
16	RWBA1
17	DOM.SOL29.V087600
18	DOM.SOL29.V087600
19	DOM.MER0129.5087600
20	DOM.EUROP1.M10
21	CEVEN
22	DOM.BAL29.T087600
23	DOM.BAL29.V087600
24	DOM.RW29.P987600
25	DOM.RW29.T087600
26	DOM.RW29.V087600
27	DOM.R20129.B087600
28	DOM.RW0129.C087600
29	DOM.R20129.R087600
30	DOM.SOLO129.S087600

Table 3

Contents of Tape Number 9223

Format: Same as tape number 9245  
File Number

Program Name

1	CRAY.MZ3DLS.OUT05
2	CRAY.MZ3DMS.OUT05
3	CRAY.AMA3DRR

Table 4

Contents of LANL Tape

File Number

Program Name

1	HYDSOL1
2	PREBAL2
3	INTMER1
4	INTTH1
5	INTPHI1
6	INTVEN1
7	VENGE02
8	PRESOL2
9	PRENU9
10	MEZDLS
11	AMFMEZ5
12	MEZDMS

Table 5

Initial Large-Scale Sounding

Pressure (mb)	U(m/sec)	V(m/sec)	T(deg C)	Qv(g/kgm)
0	12.0	4.4	-61.0	0.00
100	12.0	4.4	-61.0	0.00
200	12.0	4.4	-61.0	0.00
250	12.0	4.4	-55.7	0.01
300	12.0	4.4	-45.9	0.05
400	11.0	6.4	-18.7	0.44
500	3.1	17.6	-16.9	1.50
700	2.0	22.9	-1.8	4.00
850	-18.0	18.0	5.8	6.00
1000	-5.5	5.4	15.2	9.80

3. TASK II: Time Dependent Lateral Boundary Conditions

The problem of specifying lateral boundary conditions in the mesoscale model has been examined in some detail, as part of the general upgrading of the numerical procedures carried out under TASK III (see section 4 of this report). Unfortunately, however, the question of lateral boundary conditions, when viewed within the context of four-dimensional data assimilation, has not been solved. The enclosed conference paper by Marroquin and Brown (1985) clearly describes a fundamental difficulty in properly specifying mathematically correct lateral boundary conditions which are not changing in time. They conclude their paper with the following remarks.

"The gravity wave experiments reveal that there exists an incompatibility between the absorbing layer diffusion (second-order or Rayleigh) and the lateral radiation boundary formulation. This incompatibility is manifested in reflection of horizontally propagating gravity waves impinging upon the lateral boundaries in the absorbing layer region. Other authors have found the same difficulty (Van der Berg and Oerlemans, 1985). We have found that wave reflection is substantially reduced by using a single value of the phase velocity for the boundary computation. This value is the average of the phase velocities computed from the Orlanski formulation below the absorbing layer. Modelers should be aware of this problem that seems to be more prominent for short gravity waves."

Nevertheless, the real-data initialization procedure reported on under TASK I above, might be used on an ad-hoc basis: The meso-alpha code, MEZDLS, (see

Table 1) could be run either before or concurrently with the meso-beta code, MEZDMS. At every hour the results could be saved as input for the interpolation code, AMFMEZS. This new set of initial conditions generated from the meso-alpha model would then be incorporated into the meso-beta model using a weighting function which has the value of unity on the boundary, and which decreases to zero, four or five points into the model domain. The value on the boundary would then contain the large-scale initial conditions and the value some five points into the meso-beta model would contain the values predicted by that model. Those points in between would serve as a transition zone.

The need for additional theoretical studies of this problem cannot be overemphasized. Moreover, the presence of underlying terrain further complicates the situation. Vertical coordinate transformations such as the sigma-P system used in the present version of the model offer certain advantages, but they also add an extra degree of complexity to the problem.

#### 4. TASK III: Integration Procedures

A new version of the model has been developed in which the Shapiro filter has been eliminated and replaced with an explicit horizontal diffusion operator, and the TASU Matsuno time-integration procedure replaced by an Asselin filter. The new version of the model is described in the accompanying paper by Nickerson, et al., (1986) to be published by the Monthly Weather Review, February 1986. In order to implement the new scheme and verify that it worked properly, it was found necessary to conduct an extensive series of tests using a two-dimensional version of the model.

The new model code is contained in the third file on tape number 9223 previously given to AFGL. For integration periods of 3 to 6 hours over the Alsace terrain used in that three-dimensional simulation, the incompatibility problem between the upper wave absorbing layer and the lateral boundary condition did not seem to be especially serious. Nevertheless, such conclusions might not hold for other regions. Additional tests should be conducted using different initial conditions over the same terrain. However, what would contribute most to the development of a validated model is the specification of a set of well-posed three-dimensional numerical experiments, the results of which could be checked against independent predictions by either theory or laboratory experiment.

#### 5. TASK IV: Aerosol Model

Considerable progress has been made in the evaluation of the aerosol model. Although three-dimensional calculations using the aerosol model have been made by Chaumerliac et al., (1983), an extensive series of tests have just been completed using the new discretization schemes described above under TASK III. The new microphysical scheme of Richard, et al., (1984) now permits the aerosol model to include nucleation scavenging, a significant advancement over the previous version of the model.

An extensive series of tests have been carried out seeking to quantify the role of the various physical processes in the aerosol model. For example, the scavenging efficiencies of maritime and continental clouds are different. An article is presently in preparation for submission to the Journal of Geophysical Research.

Although the aerosol model has not been extended to include the larger size category appropriate for the treatment of dust particles, in principle that could be accomplished by adding another log-normal distribution similar to one presently used for the accumulation mode. In that regard, J. F. Mafouf, a student at the LAMP has completed a thesis containing a new formulation for the lower boundary conditions. The new PBL formulation includes a separate equation for the turbulent kinetic energy, and the treatment of vegetation and soil moisture. The ability to simulate the proper generating conditions for dust at the lower boundary then provides the opportunity for a realistic assessment of the resuspension and deposition of dust in the atmosphere. A copy of that thesis will be sent to AFGL when it becomes available.

## 6. CONCLUSIONS

A simulation of a heavy rainfall event has been carried out over southern France using 3-D Neph data supplied by AFGL to initialize a meso-alpha model. The model of Medal (1985) was run for a period of 3 hours, and the output from that simulation was subsequently interpolated to a meso-beta grid in order to provide balanced initial conditions for a regional scale model. An examination of the results shows that the meso-beta model is capable of simulating many features of an orographically forced precipitation event, including temporal and spatial information on the amount of liquid water present in the atmosphere, as well as the number concentration (and hence size distribution) of rain drops.

The model is capable of being relocated to other geographical areas for the purpose of simulating clouds, precipitation and airflow over complex



orography. Despite the presence of rather severe topographical conditions on the eastern boundary of the meso-beta model which included part of the Alps, no serious computational difficulties were encountered in either the meso-alpha or the meso-beta simulations.

#### 7. SUGGESTIONS FOR FURTHER WORK

In order to interface with other data sets and output from larger scale models such as the Air Force global model, it may be desirable to use a projection other than the Lambert projection used by Medal to calculate the map factor terms in the model equations. In addition, the initialization procedure should be modified to make it easier to move the model domain to a different geographical location.

At the present time, the model is not capable of utilizing all of the detailed moisture information contained in the 3-D Neph data sets. Simulations have shown that the mere inclusion of realistic initial moisture distributions will have little effect on the resultant simulations until a technique is developed to derive balanced motion and divergence fields which are consistent and compatible with the condensed water present in the air. Just as the meso-alpha model was used to provide balanced initial distributions of wind and moisture for the meso-beta model, a way must be developed to provide balanced initial conditions for the meso-alpha model using the output from a larger scale model as well as data from remote and in situ observing platforms.

## 8. ACKNOWLEDGMENTS

The completion of this work would not have been possible without the support and encouragement of D. Chisholm and D. Ridge of AFGL. The author would also like to acknowledge the important contributions of the staff of the LAMP, Clermont-Ferrand, France, including R. Soulage, P. Mascart, R. Rosset, J. Duron, L. Medal, E. Richard, N. Chaumerliac, J. P. Pinty, and J. F. Mafouf. The author also wishes to thank A. Marroquin of NOAA/CIRES for his important contributions. T. Yamada and S. Bunker of the Los Alamos National Laboratory made it possible for the calculations to be carried out at the Central Computing Facility of Los Alamos National Laboratory.

## 9. REFERENCES

- Anthes, R. A., and P. L. Haagenson, 1983: A comparative numerical simulation of the Sichuan flooding catastrophe (11-15 July 1981). Proc. First Sino-American Workshop on Mountain Meteorology, Beijing, AMS.
- Chaumerliac, N., E. C. Nickerson, and R. Rosset, 1983: A three-dimensional mesoscale numerical simulation of atmospheric cleansing during the 1982 Boulder Upslope Cloud Observation Experiment (BUCOE). Precipitation Scavenging, Dry Deposition, and Resuspension. Pruppacher et al., Eds., Elsevier Science Publ.
- Marroquin, A., and J. Brown, 1985: Response of an idealized atmosphere to parameterized heating. Proc. Second Conf. on Mesoscale Processes, 3-7 June, University Park, Penn.

Medal, D., 1985: Quatre procedures d'initialisation d'un modele mesoechelle: tests de sensibilite sur un episode typique d'averses Cevenoles.

Universite de Clermont II, Clermont-Ferrand, France.

Nickerson, E. C., and E. Richard, 1981: On the distribution and evolution of clouds and rain over the Vosges and Black Forest mountains: A three dimensional mesoscale simulation with parameterized microphysics, Fifth Conf. Numerical Weather Prediction, 2-6 November, Monterey, Calif.

Nickerson, E. C., D. Medal, E. Richard, and R. Rosset, 1984: Mesoscale numerical modeling of heavy precipitation events over mountainous terrain. AGU, 5 December, San Francisco, Calif.

Nickerson, E. C., E. Richard, R. Rosset, and D. R. Smith, 1986: The numerical simulation of clouds, rain, and airflow over the Vosges and Black Forest mountains: A meso-beta model with parameterized microphysics. To appear in Monthly Weather Review, Feb. 1986.

Perkey, D. J., 1979: Impact of moisture on regional-scale numerical model simulations. Proc. of the Intern. Workshop on Atmospheric Water Vapor, 11-13 September, Vail, Colo.

Richard, E., J. P. Pinty, and N. Chaumerliac, 1984: Modelisation numerique a mesoechelle: microphysique des nuages chauds. Note no. 71 de l'I.O.P.G., Universite de Clermont II, Clermont-Ferrand, France.

Van der Berg, L. C. J., and J. Oerlemans, 1985: Simulation of the sea-breeze front with a model of moist convection. Tellus, 38a:30-40.

**END**

**FILMED**

**386**

**DTIC**